Spring 1-1-2010

From regulation to pathogenesis: employing fluorescent tools to study calcium

Janet Elaine McCombs
University of Colorado at Boulder, jemccombs2003@yahoo.com

From regulation to pathogenesis: employing fluorescent tools to study calcium

by

Janet Elaine McCombs

B.S., Biochemistry, University of Wisconsin-Madison, 2003

A thesis submitted to the

Faculty of the Graduate School of the

University of Colorado in partial fulfillment

of the requirement for the degree of

Doctor of Philosophy

Department of Chemistry and Biochemistry

2010

This thesis entitled:

From regulation to pathogenesis: employing fluorescent tools to study calcium

written by Janet Elaine McCombs
has been approved for the Department of Chemistry and Biochemistry

_____

Amy E. Palmer, Ph.D. (Principal Advisor)

_____

Marcelo C. Sousa, Ph.D.

_____

Natalie G. Ahn, Ph.D.

_____

Xuedong Liu, Ph.D.

_____

Gia Voeltz, Ph.D.

Date: _____

The final copy of this thesis has been examined by the signatories, and we find that both the content and the form meet acceptable presentation standards of scholarly work in the above mentioned discipline.

McCombs, Janet Elaine (Ph.D., Biochemistry)

From regulation to pathogenesis: employing fluorescent tools to study calcium

Thesis directed by Assistant Professor Amy E. Palmer

Ca^{2+} is a ubiquitous and highly regulated signaling second messenger in cells, involved in a number of processes and pathways. Due to the complexity of Ca^{2+} signaling and its organization within a cell, it is inherently difficult to study. A number of fluorescent tools have been developed throughout the years in order to overcome these complications. Such probes allow for imaging of rapid Ca^{2+} transients in real-time at the single cell level, enabling the separation of the spatio-temporal aspects of Ca^{2+} signals. As Ca^{2+} is essential to cellular regulation and function, it is unsurprising Ca^{2+} homeostasis is often altered in disease. In the studies herein, we examined Ca^{2+} as it pertains to pathogenesis in order to further current understandings about how its dysregulation leads to disease progression . By employing a specifically targeted Ca^{2+} sensor, we monitored changes in intracellular store levels and release caused by mutations in the Alzheimer's disease related protein presenilin-1. Our results suggest mutations have differential effects on cellular Ca^{2+} homeostasis and stress the importance of directly investigating compartmentalized Ca^{2+} as opposed to inferring intracellular levels based on release into the cytosol. In addition, Ca^{2+} transients caused by bacterial infection of host cells were studied to determine molecular mechanisms involved in *Salmonella*-induced Ca^{2+} fluxes, providing insights into how bacteria modulate Ca^{2+} pathways to facilitate their survival. Finally, in order to characterize Ca^{2+} regulation in mitochondria, we used a mitochondrial targeted Ca^{2+} sensor to determine the involvement of a newly identified protein in Ca^{2+} uptake into the organelle. The use of fluorescent tools to study Ca^{2+} sheds light on effects of disease on Ca^{2+} regulation and homeostasis, providing mechanistic details that may lead to therapeutics.

Acknowledgements

I would like to acknowledge all who have inspired me most in science, especially my parents, whose own interests in the subject sparked mine at a young age. I would especially like to give my appreciation to my advisor, Dr. Amy Palmer, whose excitement for science is contagious and just what I needed to keep going. Without her support and encouragement, none of this would have been possible.

Many thanks to everyone else who encouraged me as I worked toward my Ph.D. Specifically, my parents Bill and Terry, my sister Carolyn, my brother-in-law Rob, and my niece Amelia for always supporting me. In addition, I want to acknowledge my friends and confidantes, especially fellow scientists Meghana, Michelle, and Martha. Finally, to the entire Palmer lab, past and present, thank you for being both inspiration and distraction in exactly the right quantities.

Table of Contents **Page Number**

Table of Contents **Page Number**

List of Tables **Page Number**

Chapter 1: Introduction

Chapter 4: The protein *MICU1* regulates mitochondrial Ca^{2+} uptake

List of Figures **Page Number**

Chapter 1: Introduction

Chapter 2: Using a genetically targeted sensor to investigate the role of presenilin-1 in ER Ca^{2+} levels and dynamics

Chapter 3: *Salmonella* invasion induces a Ca^{2+} influx through TRPM7 channels dependent on SopB phosphatase activity

List of Figures **Page Number**

Chapter 1:

Introduction

1.1 Introduction

Ca^{2+} is one of the most versatile and ubiquitous intracellular signaling second messengers; because of this, it is also perhaps one of the most complex. Multiple pathways and cellular functions are regulated by Ca^{2+} through the tightly coordinated action of a variety of Ca^{2+}-related proteins. These proteins allow Ca^{2+} signals to vary in speed, amplitude, location, and timing, facilitating a defined pattern in the Ca^{2+} signal, which can then activate a specific downstream pathway[1,2]. The resulting array of Ca^{2+} signals enables spatio-temporal control of a diverse number of critical process, including fertilization, proliferation, gene transcription, exocytosis, and apoptosis[3]. Given the inherent complexity of Ca^{2+} signaling systems, it can be difficult to understand how one ion can control such a vast number of cellular processes.

In order to regulate Ca^{2+} signaling, the cell expresses a so-called "Ca^{2+} signaling toolkit" comprised of a complex system of buffers, effectors, pumps, and exchangers[1]. Berridge and coworkers use this term to describe the proteins responsible for shaping Ca^{2+} transients in a signaling event. The versatility of Ca^{2+} signaling is expanded by the fact that multiple isoforms for each component exist and the composition of the toolkit is unique for different cell types. This diversity between various cell types makes the study of Ca^{2+} even more enigmatic and illustrates unique attributes of the Ca^{2+} signaling system.

1.2 The organization and function of cellular Ca^{2+}

1.2.1 Distribution of Ca^{2+} and the Ca^{2+}-related proteins

Ca^{2+} is organized into a number of intracellular compartments, leading to heterogeneity in its overall distribution. Within the cytosol, Ca^{2+} concentrations are maintained at ~100 nM, despite extracellular levels reaching 1 – 2 mM. In addition, stores of Ca^{2+} contained within the endoplasmic reticulum (ER) are almost 1000 fold cytosolic levels at about 100 μM[5]. This

compartmentalization enables the structuring of Ca^{2+} signals by components of the Ca^{2+} signaling toolkit. For example, in order to maintain cellular homeostasis, the concentration of cytosolic Ca^{2+} is kept at a fairly constant level. Therefore, upon a rise in intracellular Ca^{2+}, excess Ca^{2+} is rapidly removed by the various Ca^{2+} related proteins, buffers, and organelles in the cell[1,3] as discussed below and depicted in **Figure 1.1**. This causes a shaping of the Ca^{2+} transients, which results in the production of Ca^{2+} signals and activation of downstream pathways. Without the existence of this rigid organization of Ca^{2+} and its signaling components, the phenomenon of Ca^{2+} signaling would not be possible.

A number of factors function together to ensure the constant regulation of cytosolic Ca^{2+}. Maintenance of the steep gradient of Ca^{2+} across the plasma membrane is accomplished through the action of several pumps and tightly gated channels, prohibiting free diffusion of Ca^{2+} into the cell[5]. Regulated influx of Ca^{2+} is instead made possible by activation of one of several membrane channels, including voltage-operated channels (VOCs), which are found in excitable cells such as neurons, receptor-operated channels (ROCs), transient receptor potential (TRP) channels, second messenger operated channels (SMOCs), and store-operated channels (SOCs)[3]. **Table 1.1** lists examples of various channels that fall into each of these classes, highlighting the repertoire of Ca^{2+} channels available in the toolkit. The distribution of these channels varies from cell-to-cell, with each cell expressing multiple types[1]. This allows for diversity in the Ca^{2+} signals produced, which are specific to the needs of the cell. Upon a rise in intracellular Ca^{2+} levels, such as that occurring in a signaling event, Ca^{2+} is actively removed from the cytosol through the work of the plasma membrane Ca^{2+} ATPase (PMCA)[3], a high affinity pump with a low conductance for Ca^{2+}. This pump is activated by modest increases in Ca^{2+}, ensuring its timely removal to maintain the concentration of Ca^{2+}. Cytosolic concentrations are further impacted by

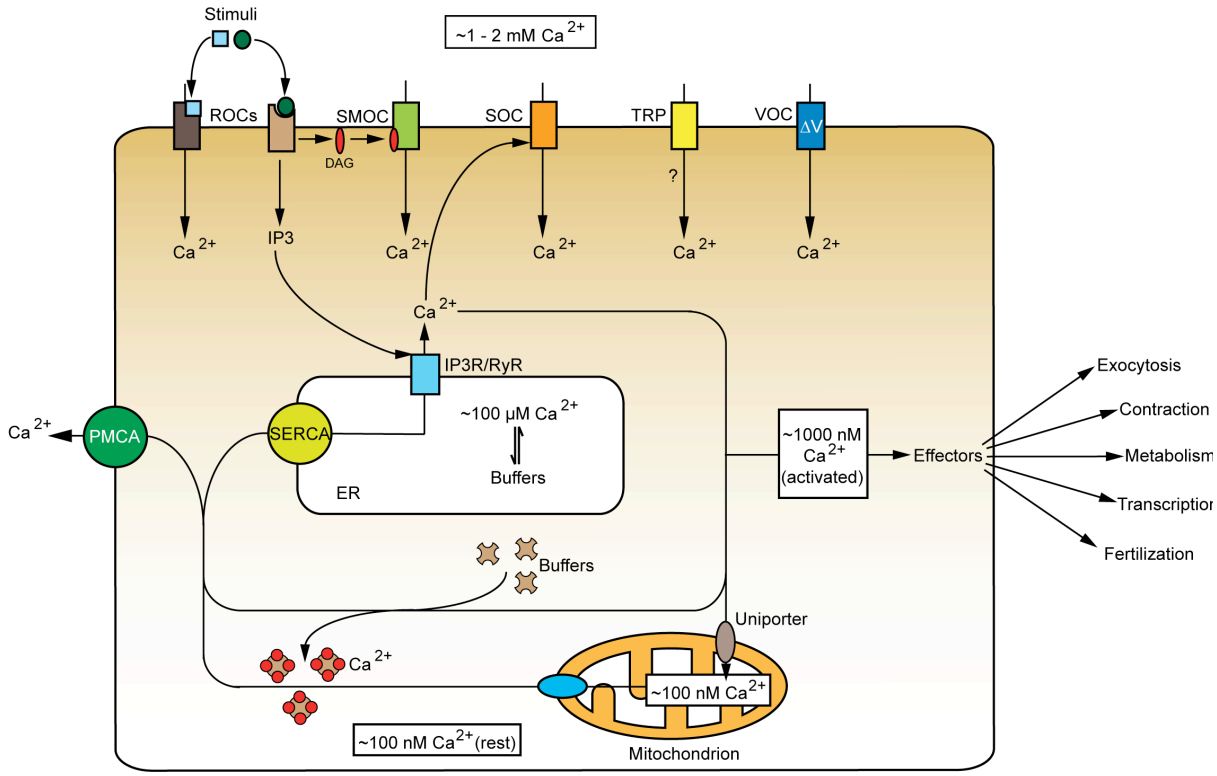

Figure 1.1 Complexity and organization of the Ca^{2+} signaling toolkit. Ca^{2+} influx into a cell is regulated by a number of membrane channels, including the ROCs, where a stimulus binds to either activate influx or mobilize signaling second messengers to elicit release from internal stores; SMOCs, which are bound by intracellular second messengers to activate Ca^{2+} influx; SOCs, which are activated upon increases in intracellular Ca^{2+} resulting from release from cell stores; TRP channels, which can be activated by a variety of methods; and VOCs, which induce an influx upon depolarization of the membrane and are found in excitable cells. Release from internal stores generally occurs through the RyRs or IP_3Rs, stimulated most often by either Ca^{2+} or IP_3. Upon increases in cytosolic Ca^{2+}, effectors are mobilized to activate a number of downstream processes. Buffers bind excess cytosolic Ca^{2+}, and levels in the cytosol are quickly returned to ~100 nM through the activation of PMCA and SERCA pumps in the plasma membrane and ER, respectively. Mitochondria also take up excess cytosolic Ca^{2+} though it is removed after a signaling event to return levels to resting states. Adapted from Berridge, *et al*. (2000 and 2003)[1,3].

Table 1.1 Plasma membrane Ca^{2+} channels

Channel Type	Examples	Tissue distribution
VOC	Ca_v1 family	
	L-type	Skeletal muscle, heart, CNS*, endocrine cells, retina
	Ca_v2 family	
	P/Q-type, N-type, R-type	CNS, neuromuscular junction
	Ca_v3 family	
	T-type	CNS, heart, smooth muscle, liver, kidney
ROC	Cysteine-loop receptors	
	nAChRs†, 5-HT3‡, GABA§, GlycRs[a]	Brain, muscle, immune cells
	Glutamate receptors	
	AMPA[b], NMDA[c], Kainate	Brain
	P2X	
	P2X1-7	Ubiquitous
SMOC	Cyclic nucleotide-gated channels (CNGC)	
	CNGA1-4, CNGB1, CNGB3	Sensory cells, brain, testis, kidney
	Arachidonic acid-regulated Ca^{2+} channels	Parotid and pancreatic acinar cells
SOC	Ca^{2+} release-activated Ca^{2+} channel	T-lymphocytes
TRP[d]	TRPC1 – 7	Smooth muscle, brain, heart, CNS, blood, kidney, lung
	TRPV1 – 6	Brain, CNS, bladder, kidney, liver, heart
	TRPM1 – 8	Eye, melanocytes, brain, smooth muscle, liver, lungs, kidney, heart

* CNS, central nervous system.
† nAChR, nicotinic acetylcholine receptor
‡ 5-HT3, 5-Hydroxytryptamine 3
§ GABA, γ-Aminobutyric acid
[a] GlycR, Glycine receptor
[b] AMPA, α-Amino-3-hydroxy-5-methylisoxazole-4-propionic acid
[c] NMDA, *N*-Methyl-D-aspartate
[d] Some TRP channels are also proposed to function as SOCs or SMOCs.

the presence of Ca^{2+} buffers such as calbindin D-28 and calretinin[3]. Located within the cytosol, they regulate the effective concentration of Ca^{2+} at any given moment. These buffers can bind Ca^{2+} once it enters the cell, masking the actual rise in Ca^{2+}. Also present in the cytosol are effectors, which bind Ca^{2+} in order to activate Ca^{2+} sensitive pathways. For example, the two effectors calmodulin (CaM) and Troponin C are both regulators of muscle contraction upon binding of Ca^{2+} [3].

In addition to being pumped out of the cell through the PMCA, cytosolic Ca^{2+} can be shuttled into intracellular organelles. As stated above, the majority of cellular Ca^{2+} is stored within the ER, often referred to as the central storehouse for Ca^{2+} within the cell[5]. In muscle cells, a somewhat similar structure called the sarcoplasmic reticulum (SR) exists and functions in much the same way. The ER is a continuous network of tubules extending from the nuclear membrane. The pumping of Ca^{2+} into the ER occurs through the sarco/endoplasmic reticulum Ca^{2+} ATPase (SERCA), the only pump present in the membrane of this organelle. There are three known SERCA genes, each capable of being expressed as a number of isoforms[5]. As with the plasma membrane channels, their distribution throughout an organism is cell-type specific, adding to the molecular heterogeneity and thus complexity of Ca^{2+} signaling in cells. Release of Ca^{2+} from the ER is a tightly regulated process. Ca^{2+} usually exits the ER through one of two channels, each with three isoforms: the inositol-1,4,5-trisphosphate receptors (IP_3R) or Ryanodine receptors (RyR), the best-characterized channels in the ER[6,7]. RyRs are activated by Ca^{2+} and are mostly found in smooth muscle, skeletal muscle and brain tissue, with a low concentration being ubiquitously expressed throughout an organism. On the other hand, IP_3Rs are distributed throughout all tissue in the body, and can be activated by either Ca^{2+} or IP_3. Both channels can be formed by homotetramers of the isoforms, whereas the IP_3R can be a

heterotetramer as well. In addition, these two channels are generally activated independently of each other, allowing for even greater diversity in the formation of Ca^{2+} signals. While most of the Ca^{2+} released from the ER is done so in a tightly regulated manner, there exists a "leak" of Ca^{2+} such that inhibition of the SERCA allows a rapid rise in cytosolic Ca^{2+} followed by clearance, presumably by the PMCA[8]. Though the molecular mechanism of the leak is still unknown, several studies have attributed it to one of the Ca^{2+} channels in the ER membrane[9-12]. Ca^{2+} concentrations within the lumen of the ER are maintained by the presence of buffers including calnexin, calreticulin, and calsequestrin[3]. These buffers help preserve high levels of Ca^{2+} in the organelle, and increase the total amount of the ion that can be stored there and thus released in a signaling event.

In addition to the ER, Ca^{2+} can also be sequestered into mitochondria, Golgi, or other membrane-bound vesicles[5]. The role of mitochondria in Ca^{2+} homeostasis is less well characterized than that of the ER, but mitochondria rapidly take up excess cytosolic Ca^{2+} through a poorly understood Ca^{2+} uniporter[13,14]. Though the resting level of mitochondrial Ca^{2+} is equivalent to that of the cytosol at ~100 nM, upon uptake of Ca^{2+}, these levels can reach over 10 μM[5]. Efflux of Ca^{2+} is facilitated by one of two exchangers, and generally occurs shortly after elevation of Ca^{2+} in the matrix[5]. Less is known about the overall handling of Ca^{2+} by Golgi or endocytic compartments. The Golgi extends from the ER, and like the ER, SERCA pumps mediate Ca^{2+} uptake into both the *cis*- and intermediate Golgi compartments[5]. In the *trans*-Golgi, however, an alternate pump, termed the secretory pathway Ca^{2+}-ATPase (SPCA), is responsible for Ca^{2+} uptake[15-17]. This pump is able to transport both Ca^{2+} and Mn^{2+} equally, and is present in all of the Golgi compartments, being coexpressed with SERCA in the *cis*- and intermediate

Golgi. Though Ca^{2+} sequestration by Golgi appears to be important for signaling, the exact nature of the Ca^{2+} fluctuations in these compartments remains elusive.

1.2.2 Ca^{2+} signaling dynamics and functions

The cellular organization of Ca^{2+} and the components of the Ca^{2+} signaling toolkit are essential in creating and shaping Ca^{2+} transients within the cell. The resulting signals regulate a number of processes in a time and space dependent manner, ensuring proper cellular functioning. Because of this, the expression of the toolkit varies between cell types, and even changes upon differentiation. In neurons, for example, fast Ca^{2+} transients are necessary at the synaptic junctions in order to regulate neurotransmitter release; therefore, these cells express channels and buffers with faster kinetics. However, during cell proliferation, slower signals regulate progression through the cell cycle, and thus components with slower kinetics may be expressed for this process[3]. Given the complexity of Ca^{2+} organization and plethora of pathways modulated by Ca^{2+}, the study of Ca^{2+} signaling can be an arduous task.

Signaling events are generally initiated by influx of Ca^{2+} across the electrochemical gradient of the plasma membrane, which is regulated by the various channels expressed there. Influx of Ca^{2+} from extracellular sources can be initiated by multiple factors, such as membrane stretch and intracellular second messengers in the case of TRP channels, ligands binding to the ROCs, depolarization for the VOCs, and depletion of intracellular stores for the SOCs[1,3] (**Figure 1.1**). Once inside the cell, several pathways lead to Ca^{2+} activation of a number of processes. Entry through membrane channels allows for localized pools of Ca^{2+} at the sub-plasma membrane, termed microdomains[5]. These microdomains are key regulators of intracellular Ca^{2+} signaling, including initiation of exocytosis in neurotransmitter release[18], inactivation of membrane Ca^{2+} channels[19-22], or even gating channel opening[23]. Another interesting process

found to be influenced by sub-plasma membrane microdomains is that of cAMP response element binding (CREB) protein phosphorylation, an example that illustrates the extent of the control Ca^{2+} microdomains have over cellular processes[24-26]. Phosphorylation of CREB occurs in the nucleus but has been found to be caused by local rises in Ca^{2+} at the mouth of membrane VOC channels. It was determined this concentrated pool of Ca^{2+} pool was able to activate the mitogen activated protein kinase pathway which led to CREB phosphorylation.

Ca^{2+} influx through membrane channels or stimulus binding to receptors on the cell surface can also lead to activation of an intracellular signaling cascade that produces signaling second messengers such as IP_3, diacylglycerol (DAG), or even Ca^{2+} itself. These factors function to regulate release of Ca^{2+} from internal stores in the ER through the channels in the ER membrane, of which the IP_3R and RyRs have been most thoroughly studied[6,7]. For example, stimulation of a membrane ROC, such as a P2X receptor, activates phospholipase C (PLC) which in turn generates IP_3 and DAG. While DAG goes on to activate Ca^{2+}-dependent protein kinase C (PKC) in other Ca^{2+}-related processes, IP_3 is able to sensitize IP_3R in the ER to open and allow release of a small amount of Ca^{2+}, initiating a signaling event[3] (**Figure 1.2**). Similarly, Ca^{2+} signaling is induced through RyRs by multiple mechanisms, and release is generally stimulated by Ca^{2+}, with other factors facilitating receptor sensitivity to the ion[1]. This efflux of Ca^{2+} is generally issued in a "puff" (or a "spark" in the case of RyRs), a small, localized release around the channel or clusters of channels[27-30]. After the initial Ca^{2+} release from ER, subsequent release of Ca^{2+} through these channels is regulated by Ca^{2+} itself, in a process termed Ca^{2+} induced Ca^{2+} release (CICR)[1,3]. Through CICR, a puff can initiate release from channels in close proximity, leading to continuation of IP_3R activation and opening, causing a Ca^{2+} wave, a global signaling event. In the same way small amounts of Ca^{2+} can activate the IP_3R, too much Ca^{2+}

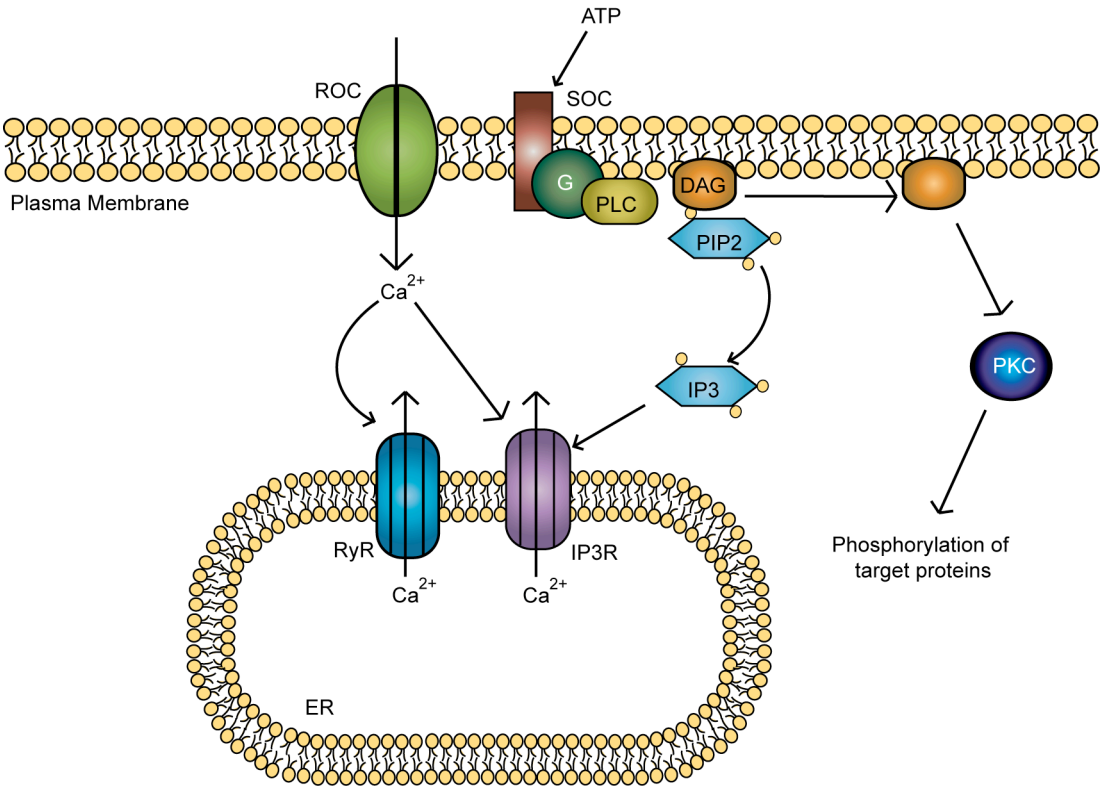

Figure 1.2 Ca^{2+} signaling. Ca^{2+} release through the RyR and IP3R is generally gated by Ca^{2+} and IP_3. In the case of ROCs, Ca^{2+} influx is stimulated by an outside ligand that can then initiate release of Ca^{2+} from internal stores from both channels. In addition, interaction of an SOC with ATP activates phospholipase C (PLC) initiating a signaling cascade that produces IP_3. By binding to IP_3R, Ca^{2+} is released through the channel and is sensitized to changes in Ca^{2+}, causing activation or inhibition of Ca^{2+} release. Production of the byproduct DAG allows for activation of PKC and phosphorylation a variety of protein targets, depending on the pathway.

inhibits Ca^{2+} release, ceasing the Ca^{2+} response. In addition, Ca^{2+} can sensitize the IP_3R from the lumen of the ER through the buffers calnexin and calreticulin[3].

Release of Ca^{2+} from the ER is shaped by the abundance of Ca^{2+} related proteins within the cell, including the pumps, buffers, and channels in the plasma membrane and ER[1,3]. These cellular components are responsible for structuring the excess Ca^{2+} present in the cytosol into a defined pattern to signal a specific downstream event. Often, the patterns of Ca^{2+} transients are seen as oscillations. Oscillations are able to vary in frequency, amplitude, duration, and number, and these variations are what define which pathways are activated during a signaling event. For example, in a study on the transcription factors NF-κB and NF-AT, slower periods of oscillation specifically activated NF-κB, while a faster frequency of oscillation enabled activation of both transcription factors[31]. In order to decode oscillations, cells employ the action of such proteins as Ca^{2+}/CaM-dependent protein kinase II (CaMKII)[32,33]. The frequency of the Ca^{2+} oscillation affects the extent of autophosphorylation of CaMKII, enabling the enzyme to "read out" frequency of the signal, which then regulates specific proteins that can be activated by the enzyme[33]. In addition, the availability of multiple splice variants of CaMKII expands the number of processes that can be regulated by this protein through Ca^{2+} oscillations[32].

Though not technically part of the signaling toolkit, mitochondria are also essential in shaping Ca^{2+} transients in the cytosol[34,35]. Mitochondria depend on Ca^{2+} to regulate multiple processes, including respiration and apoptosis[36-39]. The distribution of mitochondria throughout the cell puts them in close proximity to both the ER and the plasma membrane. In this way, mitochondria are believed to directly interact with the ER, such that Ca^{2+} signals emerging from the ER can quickly be diffused into the mitochondrial matrix through the uniporter[40-42]. This so-called tethering of the two organelles buffers the Ca^{2+} in the mitochondria and cytosol, regulating

the Ca^{2+} concentrations in each compartment[43]. A number of proteins have been identified that are responsible for interactions between the ER and mitochondria, among which is the IP_3R[44,45]. Through this tethering, mitochondria are able to participate in Ca^{2+} signaling by shaping cytosolic Ca^{2+} transients. Mitochondria can also sense and take up Ca^{2+} microdomains at the plasma membrane, regulating the amount of Ca^{2+} present in the microdomain, and controlling its effect on downstream processes[41,46].

1.3 Studying Ca^{2+} signaling dynamics in live cells using fluorescent tools

Given the complexity of cellular Ca^{2+} signaling, it has been a challenge to study Ca^{2+} transients in live cells or organisms in a way that fully illustrates the spatio-temporal patterning of activation and release. Therefore, due to the importance of Ca^{2+} signaling for a cell's proper functioning, many tools have been developed in order to better understand its dynamics in live cells. In general, these tools utilize fluorescent properties of proteins or small molecules in such a way that binding of Ca^{2+} alters their fluorescent properties, offering a readout of Ca^{2+} fluctuations. These tools have enabled the study of transients in real-time, within separate signaling compartments, microdomains, and organelles, and help determine the origin and cause of Ca^{2+} responses in cells. In the past several decades, fluorescent tools for studying Ca^{2+} have increased our understanding of this signaling ion by a great deal.

To date, fluorescent tools to study Ca^{2+} fall into three main categories. First, there are small molecule dyes, which are Ca^{2+} reactive small molecules having fluorescent properties. Second, genetically encoded sensors have been developed that are transfected into cells and expressed by the cell's own transcription machinery. Finally, there is a hybrid of these two techniques, which aims to address the weaknesses of each. Different applications dictate which

of these tools is the most beneficial and when used in combination, fluorescent tools to study Ca^{2+} can enable dissection of complex Ca^{2+} signaling pathways.

1.3.1 Small molecule dyes to study Ca^{2+}

Small molecule Ca^{2+} indicators have been available for a number of decades. They were developed based on the tetracarboxylate structure of 1,2-Bis(2-aminophenoxy)ethane-N,N,N′,N′-tetraacetic acid tetrakis (BAPTA), a Ca^{2+} chelator. This generation of indicators engineered in the 1980s was designed to be more selective for Ca^{2+} over Mg^{2+} and 30 – 40 times brighter than previously available probes[47-49]. Despite being built around the structure of a Ca^{2+} chelator, the small molecule Ca^{2+} indicators appear to cause minimal buffering in cells when loaded at low enough concentrations. Buffering is most problematic for dyes with higher affinities, such as Fura-2 and CalciumGreen, though a number of derivatives exist for each of these that exhibit lower affinities and thus enable researchers to avoid buffering issues altogether[50]. The small molecule Ca^{2+} indicators can be divided into two main classes: the ratiometric probes, which include Fura-2, Indo-1 and derivatives[48], and the intensity based probes, which include Rhod-2, Fluo-3 and Fluo-4, CalciumGreen and derivatives[49]. The ratiometric dyes exhibit a change in emission or excitation upon binding of Ca^{2+}, such that ratioing the intensity in one channel over the other can be converted into a Ca^{2+} concentration. An advantage of this method is that it accounts for uneven staining, varying thicknesses of cells, photobleaching, and leakage of the probe from cells when interpreting a Ca^{2+} readout[48]. In an alternate approach for examining Ca^{2+} dynamics, the class of intensity-based probes changes its maximum fluorescent readout upon binding of Ca^{2+} during transients[49]. While these probes can be calibrated using known amounts of Ca^{2+}, this can be inherently difficult in live cells. Intensity based dyes are also less quantitative than the ratiometric dyes, but this caveat can be overcome by dual staining of a cell with both a

ratiometric and intensity based indicator, such as fura red and Fluo-3[51-54]. However, an issue with this method is buffering risks increase as the fura red concentration must be over three times that of the Fluo-3 in order to have an accurate Ca^{2+} output, potentially causing an overload of Ca^{2+} binding molecules in the cell[53].

Since intracellular Ca^{2+} stores are an essential part of Ca^{2+} signaling, measuring dynamics in these locales is important to gain full understanding of observed signals. To this end, lower affinity small molecule probes have been utilized for loading into mitochondria[50,55-60] and ER[50,61,62]. Unfortunately, the methods to load these dyes into intracellular compartments are inexact, as they rely on charge or higher temperatures for organelle sequestration. For example, Rhod-2 is a multivalent cation, which enables it to be sequestered into mitochondria when loaded into a cell[59]. In addition, Fura-2 can be loaded into the ER when incubated above physiological temperature[63]. Though measurements of mitochondrial Ca^{2+} have been "faithfully" reported using Rhod-2[56-58], this method for measuring organellar Ca^{2+} is potentially subject to artifacts of non-specific loading, such that the exact compartment of Ca^{2+} being measured can remain ambiguous.

Despite the inability to measure intracellular stores of Ca^{2+} in a spatially defined manner, small molecule probes for Ca^{2+} maintain many strengths. For one, their fast kinetics allow measurements of cytosolic Ca^{2+} transients that occur on a timescale of milliseconds to seconds. This enables the researcher to capture cellular Ca^{2+} signals in real time, providing a more accurate measure of the exact nature of the Ca^{2+} response. Therefore, these sensors are more appropriate for measuring Ca^{2+} transients where timing is a critical factor. In addition, small molecule indicators exhibit a large dynamic range, as measured by the ratio in fluorescence intensity at maximum Ca^{2+} bound over intensity in a Ca^{2+} depleted state, and high sensitivity.

Thus, when signal-to-noise is expected to be a limiting factor, these sensors are the ideal choice. Loading of the small molecule dyes is a relatively easy process as well, as they are generally provided as membrane permeable acetomethoxy (AM)-esters, such that upon being taken up into the cell, intracellular esterases cleave the AM-ester, thus retaining the dyes within the cell. However, because of the challenge in targeting small molecule indicators to the ER, mitochondria, membrane microdomains, or channels, a number of genetically encoded sensors have been developed to examine subcellular Ca^{2+} levels and dynamics.

1.3.2 Genetically encoded Ca^{2+} sensors

Throughout the years, a number of genetically encoded Ca^{2+} indicators (GECIs) have been developed in order to examine the intracellular compartmentalization of Ca^{2+}. These sensors generally fall into one of several classes, including bioluminescent probes based on aequorins[64,65], single fluorescent protein (FP) based sensors[66-73], and fluorescence resonance energy transfer (FRET)-based sensors[74-82] (**Figure 1.3**). The design of GECIs utilizes the fluorescence properties of one or two FPs and the Ca^{2+} binding abilities of some Ca^{2+}-related protein or domain. These two pieces are fused together in such a way that upon Ca^{2+} binding of the Ca^{2+}-related protein, modulation in the fluorescence of the FP occurs. Both the FRET-based and single FP-based sensors employ this design, while aequorins contain their own Ca^{2+} binding domains and thus are not engineered in the same way.

Among the first genetically encodable Ca^{2+} indicators made widely available, aequorins were derived from the jellyfish *Aequore forskålea* and have been used to study cellular Ca^{2+} since the late 1960s[64,65]. These bioluminescent probes are inherently different than the FP-based sensors as light is generated by a chemical reaction that requires reconstitution of the apoaequorin protein with the luminophore coelenterazine. Upon binding at least two Ca^{2+} ions

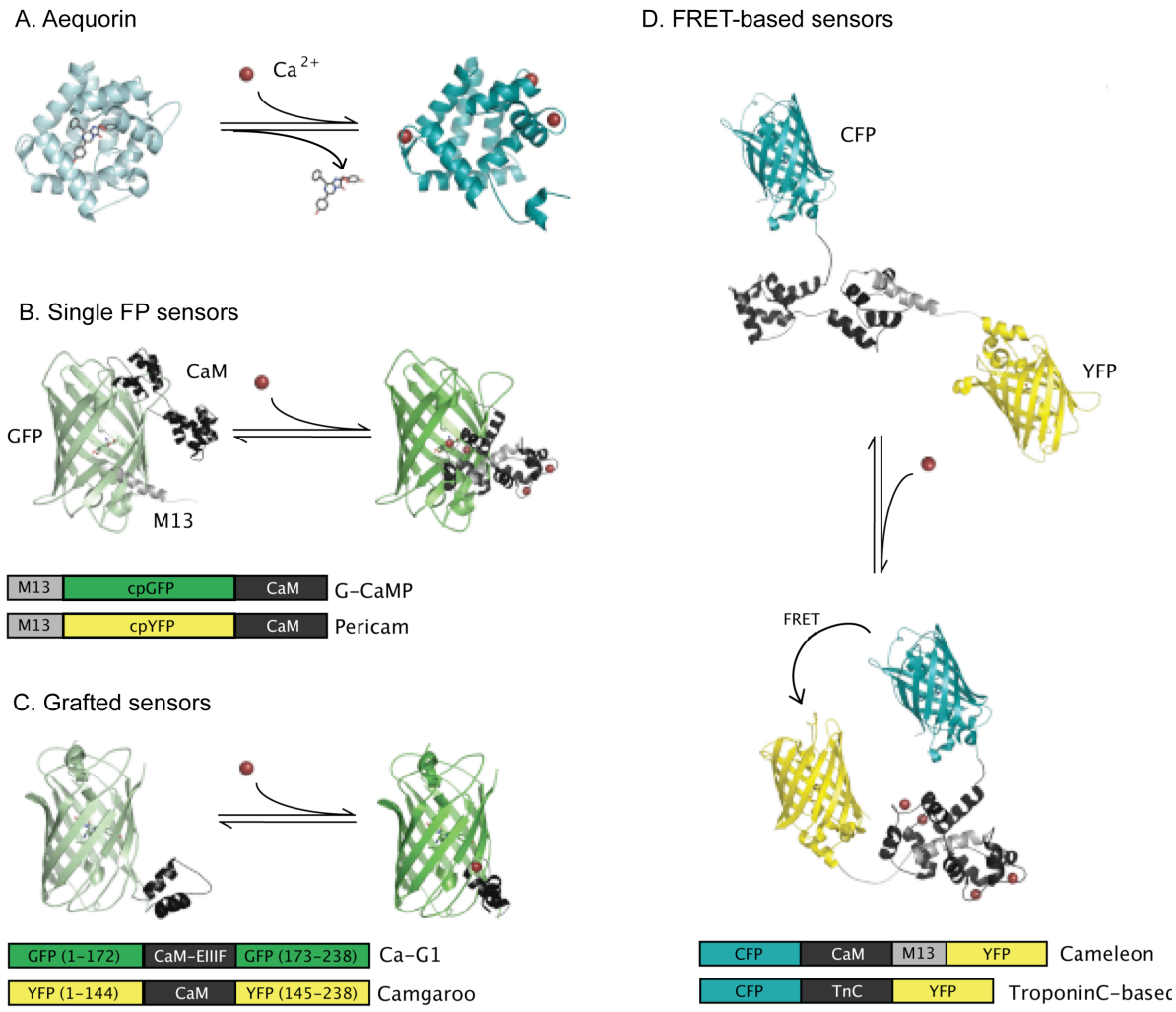

Figure 1.3 Models of the three classes of GECIs. (A) The aequorin photoprotein is shown in complex with coelenterazine. Upon binding of Ca^{2+}, the aequorin undergoes a conformational change, releasing coelenteramide and emitting blue light. (B) Single FP sensors employing the Ca^{2+}-responsive element CaM and a CaM binding peptide attached to a circularly permutated FP. On binding Ca^{2+}, CaM executes a conformational change, interacting with the peptide and altering the protonation state of the chromophore, thus changing the fluorescence intensity of the protein. (C) Grafted sensors utilizing EF-hands or portions of CaM inserted into a fluorescent protein. Binding of Ca^{2+} causes a change in protein conformation and a shift in the protonation state of the chromophore. (D) FRET-based sensors having a Ca^{2+} binding domain located between two fluorescent proteins. As Ca^{2+} binds, the Ca^{2+} binding domain undergoes a conformational change, interacting with its binding peptide. This brings the two FPs closer together, increasing the efficiency of FRET. Below each model are maps for the various available families of GECIs. Reproduced from McCombs and Palmer, 2008[4].

(out of three Ca^{2+}-binding sites), the coelenterazine is oxidized to coelenteramide, causing emission of blue light[64] (**Figure 1.3A**). Because aequorin is genetically encodable, these probes have been directly targeted to organelles such as the ER[83-87], Golgi[88], and mitochondria[40-42,89,90]; however, in order to measure Ca^{2+} dynamics in these locales, cellular stores must first be depleted for reconstitution with coelenterazine before being re-filled, which may lead to artificial readouts of Ca^{2+} homeostasis in the cell[64]. In addition, luminescence is weaker than fluorescence, resulting in a signal that is not strong enough to allow for single cell imaging, and instead only populations of cells can be examined for Ca^{2+} transients. Therefore, development of less perturbing methods that could also be used to image single cells was necessary to more thoroughly examine Ca^{2+} organization and signaling.

Several single FP sensors exist, and were developed after it was discovered that the β-barrel of GFP allows for insertion of a protein fragment or peptide without destroying the protein's fluorescence, provided a proper insertion is carefully chosen[66]. Examples of single FP-based sensors include camgaroos[66,67], G-CaMPs[68,69,73], pericams[70], "Case" sensors[71], and the grafted EF-hands[72] (**Figure 1.3B** and **C**). The Ca^{2+} responsive element CaM, or portions thereof, is inserted into the FP, such that Ca^{2+} binding alters the protonation state, and hence spectral properties of the chromophore. With the exception of the camgaroos, the 26 residue M13 peptide from skeletal muscle myosin light chain kinase (referred to as M13) is also inserted into the protein, enhancing the conformational change of CaM upon Ca^{2+} binding. Though some versions of the pericams are ratiometric, for the most part single FP probes are intensity based, and thus are not as quantitative as the available ratiometric sensors.

Much like the single-FP sensors, the initial FRET-based sensors were based on CaM and M13[74,75] (**Figure 1.3D**). These sensors, dubbed cameleons, utilize the endogenous Ca^{2+} effector

protein to induce a conformational change between CaM and M13 upon binding of 4 Ca^{2+} ions. This conformational change induces the two FPs at the N- and C-terminus (cyan FP and yellow FP, respectively) to undergo FRET. These probes have been optimized throughout the past decade and a half, through changes in the FPs as well as mutations in the Ca^{2+} binding motifs[67,76,78-80,91]. Changing the YFP improved problems with quenching and pH sensitivity, and even increased the dynamic range in some cases[67,91]. In addition, the "design" series of cameleons mutated both CaM and M13 to create a number of sensors with different affinities that were less likely to interact with endogenous proteins[78,79]. Therefore, these cameleons are minimally perturbing to the cellular environment, decreasing buffering effects. In an additional effort to curb buffering problems of the cameleons, a group of FRET sensors based on Troponin C, a protein found only in skeletal and cardiac muscle tissues, have been made and so far are found to not perturb intracellular Ca^{2+} systems to any measurable extent[80,82,92].

GECIs offer many advantages in examining Ca^{2+} transients within the cell. Since they are genetically encoded, they can be localized to specific regions of the cell, making the study of organellar Ca^{2+} and microdomains more feasible. Localization of GECIs is made possible by adding a signal sequence to the indicator. Sensors have been targeted to the plasma membrane, ER, mitochondria, nucleus, and Golgi using this method. They can also be genetically fused to a protein of interest and therefore are able to measure Ca^{2+} in micro-domains in the immediate vicinity of a given protein or even at the mouth of a channel. This has many advantages when looking at sources of Ca^{2+} in signaling as well as effects of altering aspects of the Ca^{2+} signaling machinery. For long-term experiments, GECIs can be maintained within cells over days to weeks, if stably incorporated, enabling extended time-lapse experiments where small molecule indicators would slowly leak out, or be extruded, from the cell. Incorporation of GECIs into

plasmids containing an inducible promoter allows for control over concentration of GECIs within the cell. This can be important, as overexpression of the GECI has been found to negatively affect available Ca^{2+} pools, perturbing the environment and thus skewing results for measurements of Ca^{2+} dynamics. GECIs can also be used in non-vertebrate but genetically tractable organisms, which do not permit the use of small molecule indicators. Finally, an emerging advantage to the use of GECIs is that they can be used in cell- or tissue-specific expression in transgenic or virally transduced organisms. This is perhaps one of the least explored but more interesting applications of the GECIs, given the ability to monitor Ca^{2+} transients in live organisms or whole tissues can expand current understandings of Ca^{2+} signaling systems as they relate to entire organisms.

1.3.3 Choosing the appropriate sensor to best examine Ca^{2+} transients

With the proliferation of GECIs in recent years, a big challenge for researchers is choosing the most appropriate sensor for a given application. The simple truth is that different applications will likely require different sensors. Overall, sensors differ in how they sense Ca^{2+} (FRET vs. modulation of single FP properties), the dynamic range (minimum to maximum signal), the affinity for Ca^{2+} (K_d), the rate at which they respond to changes in Ca^{2+}, the pKa, and brightness. In choosing which sensor to use, researchers must compare and contrast each of these features. For example, ratiometric indicators are often preferable to intensity-based indicators as they are more quantitative, more easily interpreted, and less subject to artifacts and pH interference. However, ratiometric indicators typically require more sophisticated instrumentation to collect multiple parameters. In addition, for the FRET-based sensors, those that incorporate a circularly permuted (cp) version of the acceptor fluorescent protein generally exhibit greater ratiometric sensitivity and expanded dynamic ranges[78,80,91]. However, sensors

with cpVenus do not express well in the ER and Golgi and therefore cp variants may not be appropriate for some localized sensors. Choosing a sensor with an appropriate affinity is particularly important for measuring Ca^{2+} in different subcellular domains. While measuring Ca^{2+} in the cytoplasm requires a high affinity indicator, the ER requires a low affinity indicator. For some applications, the most important criterion may be to choose a sensor with the fastest response kinetics, in which case GCaMP2.0 or a small molecule indicator (if no genetic targeting is required) may be the most appropriate. Overall, the plethora of available sensors makes it possible to study almost any aspect of Ca^{2+} signaling, broadening our current understandings of this complex and highly regulated system.

1.4 Ca^{2+} dysregulation in disease and pathogenesis

Because Ca^{2+} is such an important signaling second messenger in cells, it is no surprise that it is often found to be dysregulated in disease. As Ca^{2+} signaling is such a highly regulated process, alterations in its homeostasis can have a profound effect on downstream signaling pathways. In addition, if pump or channel density in membranes is not maintained, dysregulation in signal propagation can occur. A number of studies have established Ca^{2+} dyshomeostasis in disease, including those into neurodegenerative disorders and bacterial pathogenesis. To fully examine the effects in Ca^{2+} regulation in these diseases and processes, the employment of fluorescent tools is extremely useful. Much can be determined using such tools to elucidate pathways involved in pathogeneses.

1.4.1 Ca^{2+} dysregulation in neurodegeneration and aging

Ca^{2+} is essential to regulation of neuronal signaling and function, facilitating spatio-temporal control of rapid electrochemical signals. It is responsible for mediating neurotransmitter release from presynaptic terminals and is critical for responses of the postsynaptic neuron[93-95].

Unsurprisingly, upon neurodegeneration brought on by disease or aging, neurons are impaired in their ability to control Ca^{2+} fluxes and recover from Ca^{2+} loads during signaling processes. Therefore, Ca^{2+} has been implicated in disease progression, and many studies have looked into how this cellular second messenger is dysregulated in pathogenesis in order to uncover mechanism of disease onset, as well as potentially identify targets for therapeutics.

The process of neurodegeneration in diseases such as Alzheimer's disease (AD), Parkinson's disease (PD), and Huntington's disease (HD), generally elicits a dyshomeostasis in neuronal Ca^{2+} regulation. In AD, for example, neurofibrillary tangles in neuronal cells are associated with increases in free and buffer-bound Ca^{2+} concentrations[96,97]. In addition, overload of cellular Ca^{2+} causes death of neurons, leading to disease progression in both PD and HD. The mechanisms leading to cell death varies for each of these cases. In PD, excitotoxicity and overproduction of nitric-oxide are to blame[98-100], while in HD, antiapoptotic proteins are underexpressed[101], or mitochondria become overloaded with Ca^{2+} in a signaling event[102]. Despite multiple pathways to neuronal death in disease, it is apparent Ca^{2+} signaling is to blame for inducing the cytotoxicity.

A number of disease related proteins have been shown to contribute to dysregulation in cellular Ca^{2+} seen in neurodegenerative disorders. The AD-related protein presenilin-1 (PS1) has been shown to contribute to altered ER signaling through membrane channels and changes in ER Ca^{2+} homeostasis[12,103-110]. An interesting example is that mutations in PS1 appear to increase RyR levels, altering their distribution in ER membranes and increasing vulnerability of neurons to cell death[111]. In addition, mutations in the PD-related protein α-synuclein increase the ion permeability of membranes[112,113] and in HD, repeats of the trinucleotide CAG in the huntingtin gene leads to changes in Ca^{2+} regulation such that release from intracellular stores is altered[114].

By studying mutations in these disease-associated proteins, much can be learned about disease progression, potentially enabling identification of mechanisms of onset for pathogenesis.

1.4.2 Ca^{2+} dysregulation in bacterial pathogenesis

To date, a number of reports have found alterations in cellular Ca^{2+} homeostasis during bacterial pathogenesis. However, little has been done to characterize the molecular mechanisms underlying this Ca^{2+} dysregulation. Therefore, it remains enigmatic as to how or why bacteria modulate Ca^{2+} signaling during infection of host cells. However, it seems apparent that pathogenic microorganisms utilize Ca^{2+} to set up their intracellular niches in order to create an environment in which they can replicate.

Bacterial enterotoxins, found in strains of *E. coli* (STa) and *Vibrio cholerae* (NAG-ST) induce an upregulation in cyclic nucleotide production and deregulation of chloride channels in host cells in order to stimulate fluid secretion in the intestinal lumen[115,116]. These toxin-mediated effects have consistently been found to be dependent on increases in cytosolic Ca^{2+} concentrations[117,118]. For example, STa triggers a rise in intracellular Ca^{2+}, which in turn increases cGMP levels, activating the cGMP-dependent protein kinase C (PKC) required for stimulation of membrane-bound guanylyl cyclases[117]. However, the mechanism for the Ca^{2+}-induced rise in cGMP remains unclear. In addition, the *E. coli* heat labile toxin and Anthrax edema factor increase cAMP levels, causing a rise in Ca^{2+} and activation of PKC, which stimulates toxin adenylcyclase activity[119,120]. Therefore, for infection by these pathogens, the enterotoxins produce a rise in intracellular Ca^{2+} leading to protein kinase activation and regulation of cyclic nucleotide concentrations, allowing interference of intracellular signaling and functions.

Though the exact mechanisms remain unexplored, it seems clear pathogens are able to exert a spatio-temporal control over regulation of Ca^{2+} signaling within a host cell. Invasion by pathogens that employ the type III secretion system (TTSS) for host cell infection are an excellent example of this. The TTSS is a macromolecular complex resembling a syringe that is used to inject protein effectors into the cell. These effectors hijack a number of host cell signaling pathways in order to induce infection. In the case of *Salmonella* and *Shigella*, effectors elicit a rearrangement in the cytoskeletal structure of cells leading to membrane ruffles and ultimately the encapsulation of bacteria[121,122]. Both pathogens cause a rise in the intracellular Ca^{2+} concentrations upon invasion initiation in a manner dependent on effector secretion[123-126], and in the case of *Salmonella*, internalization of bacteria was shown to be dependent on the Ca^{2+} increase [125]. Another pathogen utilizing the TTSS is enteropathogenic *E. coli* (EPEC). While effectors are secreted through TTSS similar to *Salmonella* and *Shigella*, instead of membrane ruffles, EPEC induce actin pedestals upon infection, which are actin-rich extensions of the membrane occurring upon contact between the bacteria and host cell membrane. Whether an increase in Ca^{2+} is required for the cytoskeletal reorganization seen during infection is still unclear[127,128], though some studies have suggested an involvement of Ca^{2+} in association with the scaffolding protein IQGAP1 along with Rac1 and Cdc42 to induce pedestal formation[129]. Further characterization into the processes of bacterial invasion and Ca^{2+} signaling are necessary in order to understand this highly complex interaction between the two pathways.

1.5 References

1 Berridge, M. J., Lipp, P. & Bootman, M. D. The versatility and universality of calcium signalling. *Nat Rev Mol Cell Biol* **1**, 11-21, (2000).

2 Carafoli, E., Santella, L., Branca, D. & Brini, M. Generation, control, and processing of cellular calcium signals. *Crit Rev Biochem Mol Biol* **36**, 107-260, (2001).

3 Berridge, M. J., Bootman, M. D. & Roderick, H. L. Calcium signalling: dynamics, homeostasis and remodelling. *Nat Rev Mol Cell Biol* **4**, 517-529, (2003).

4 McCombs, J. E. & Palmer, A. E. Measuring calcium dynamics in living cells with genetically encodable calcium indicators. *Methods* **46**, 152-159, (2008).

5 Rizzuto, R. & Pozzan, T. Microdomains of intracellular Ca^{2+}: molecular determinants and functional consequences. *Physiol Rev* **86**, 369-408, (2006).

6 Berridge, M. J. Inositol trisphosphate and calcium signalling. *Nature* **361**, 315-325, (1993).

7 Clapham, D. E. Calcium signaling. *Cell* **80**, 259-268, (1995).

8 Camello, C., Lomax, R., Petersen, O. H. & Tepikin, A. V. Calcium leak from intracellular stores--the enigma of calcium signalling. *Cell Calcium* **32**, 355-361, (2002).

9 Masuno, M. N., Pessah, I. N., Olmstead, M. M. & Molinski, T. F. Simplified cyclic analogues of bastadin-5. Structure-activity relationships for modulation of the RyR1/FKBP12 Ca^{2+} channel complex. *J Med Chem* **49**, 4497-4511, (2006).

10 Pessah, I. N. *et al.* Bastadins relate ryanodine-sensitive and -insensitive Ca^{2+} efflux pathways in skeletal SR and BC3H1 cells. *Am J Physiol* **272**, C601-614, (1997).

11 Yang, T. *et al.* Elevated resting [$Ca(^{2+})$](i) in myotubes expressing malignant hyperthermia RyR1 cDNAs is partially restored by modulation of passive calcium leak from the SR. *Am J Physiol Cell Physiol* **292**, C1591-1598, (2007).

12 Cheung, K. H. *et al.* Mechanism of Ca^{2+} disruption in Alzheimer's disease by presenilin regulation of InsP3 receptor channel gating. *Neuron* **58**, 871-883, (2008).

13 Deluca, H. F. & Engstrom, G. W. Calcium uptake by rat kidney mitochondria. *Proc Natl Acad Sci U S A* **47**, 1744-1750, (1961).

14 Vasington, F. D. & Murphy, J. V. Ca ion uptake by rat kidney mitochondria and its dependence on respiration and phosphorylation. *J Biol Chem* **237**, 2670-2677, (1962).

15 Wuytack, F., Raeymaekers, L. & Missiaen, L. PMR1/SPCA Ca^{2+} pumps and the role of the Golgi apparatus as a Ca^{2+} store. *Pflugers Arch* **446**, 148-153, (2003).

16 Gunteski-Hamblin, A. M., Clarke, D. M. & Shull, G. E. Molecular cloning and tissue distribution of alternatively spliced mRNAs encoding possible mammalian homologues of the yeast secretory pathway calcium pump. *Biochemistry* **31**, 7600-7608, (1992).

17 Rudolph, H. K. *et al.* The yeast secretory pathway is perturbed by mutations in PMR1, a member of a Ca^{2+} ATPase family. *Cell* **58**, 133-145, (1989).

18 Augustine, G. J. & Neher, E. Neuronal Ca^{2+} signalling takes the local route. *Curr Opin Neurobiol* **2**, 302-307, (1992).

19 Anderson, M. E. Ca^{2+}-dependent regulation of cardiac L-type Ca^{2+} channels: is a unifying mechanism at hand? *J Mol Cell Cardiol* **33**, 639-650, (2001).

20 Findlay, I. Physiological modulation of inactivation in L-type Ca^{2+} channels: one switch. *J Physiol* **554**, 275-283, (2004).

21 Lee, A. *et al.* Differential modulation of Ca(v)2.1 channels by calmodulin and Ca^{2+}-binding protein 1. *Nat Neurosci* **5**, 210-217, (2002).

22 Soldatov, N. M. Ca^{2+} channel moving tail: link between Ca^{2+}-induced inactivation and Ca^{2+} signal transduction. *Trends Pharmacol Sci* **24**, 167-171, (2003).

23 Li, H. S. & Montell, C. TRP and the PDZ protein, INAD, form the core complex required for retention of the signalplex in Drosophila photoreceptor cells. *J Cell Biol* **150**, 1411-1422, (2000).

24 Dolmetsch, R. E., Pajvani, U., Fife, K., Spotts, J. M. & Greenberg, M. E. Signaling to the nucleus by an L-type calcium channel-calmodulin complex through the MAP kinase pathway. *Science* **294**, 333-339, (2001).

25 Kornhauser, J. M. *et al.* CREB transcriptional activity in neurons is regulated by multiple, calcium-specific phosphorylation events. *Neuron* **34**, 221-233, (2002).

26 Deisseroth, K., Bito, H. & Tsien, R. W. Signaling from synapse to nucleus: postsynaptic CREB phosphorylation during multiple forms of hippocampal synaptic plasticity. *Neuron* **16**, 89-101, (1996).

27 Yao, Y., Choi, J. & Parker, I. Quantal puffs of intracellular Ca^{2+} evoked by inositol trisphosphate in Xenopus oocytes. *J Physiol* **482 (Pt 3)**, 533-553, (1995).

28 Bootman, M., Niggli, E., Berridge, M. & Lipp, P. Imaging the hierarchical Ca^{2+} signalling system in HeLa cells. *J Physiol* **499 (Pt 2)**, 307-314, (1997).

29 Reber, B. F. & Schindelholz, B. Detection of a trigger zone of bradykinin-induced fast calcium waves in PC12 neurites. *Pflugers Arch* **432**, 893-903, (1996).

30 Koizumi, S. *et al.* Characterization of elementary Ca^{2+} release signals in NGF-differentiated PC12 cells and hippocampal neurons. *Neuron* **22**, 125-137, (1999).

31 Lewis, R. S. Calcium oscillations in T-cells: mechanisms and consequences for gene expression. *Biochem Soc Trans* **31**, 925-929, (2003).

32 Bayer, K. U., De Koninck, P. & Schulman, H. Alternative splicing modulates the frequency-dependent response of CaMKII to $Ca(^{2+})$ oscillations. *EMBO J* **21**, 3590-3597, (2002).

33 De Koninck, P. & Schulman, H. Sensitivity of CaM kinase II to the frequency of Ca^{2+} oscillations. *Science* **279**, 227-230, (1998).

34 Jouaville, L. S., Ichas, F., Holmuhamedov, E. L., Camacho, P. & Lechleiter, J. D. Synchronization of calcium waves by mitochondrial substrates in Xenopus laevis oocytes. *Nature* **377**, 438-441, (1995).

35 Kaftan, E. J., Xu, T., Abercrombie, R. F. & Hille, B. Mitochondria shape hormonally induced cytoplasmic calcium oscillations and modulate exocytosis. *J Biol Chem* **275**, 25465-25470, (2000).

36 Denton, R. M. & McCormack, J. G. The role of calcium in the regulation of mitochondrial metabolism. *Biochem Soc Trans* **8**, 266-268, (1980).

37 Bernardi, P. & Rasola, A. Calcium and cell death: the mitochondrial connection. *Subcell Biochem* **45**, 481-506, (2007).

38 Hajnóczky, G. *et al.* Mitochondrial calcium signalling and cell death: approaches for assessing the role of mitochondrial Ca^{2+} uptake in apoptosis. *Cell Calcium* **40**, 553-560, (2006).

39 Balaban, R. S. The role of $Ca(^{2+})$ signaling in the coordination of mitochondrial ATP production with cardiac work. *Biochim Biophys Acta* **1787**, 1334-1341, (2009).

40 Rizzuto, R., Brini, M., Murgia, M. & Pozzan, T. Microdomains with high Ca^{2+} close to IP3-sensitive channels that are sensed by neighboring mitochondria. *Science* **262**, 744-747, (1993).

41 Rizzuto, R. *et al.* Close contacts with the endoplasmic reticulum as determinants of mitochondrial Ca^{2+} responses. *Science* **280**, 1763-1766, (1998).

42 Rizzuto, R., Simpson, A. W., Brini, M. & Pozzan, T. Rapid changes of mitochondrial Ca^{2+} revealed by specifically targeted recombinant aequorin. *Nature* **358**, 325-327, (1992).

43 Pinton, P., Giorgi, C., Siviero, R., Zecchini, E. & Rizzuto, R. Calcium and apoptosis: ER-mitochondria Ca^{2+} transfer in the control of apoptosis. *Oncogene* **27**, 6407-6418, (2008).

44 Mendes, C. C. *et al.* The type III inositol 1,4,5-trisphosphate receptor preferentially transmits apoptotic Ca^{2+} signals into mitochondria. *J Biol Chem* **280**, 40892-40900, (2005).

45 Szabadkai, G. *et al.* Chaperone-mediated coupling of endoplasmic reticulum and mitochondrial Ca^{2+} channels. *J Cell Biol* **175**, 901-911, (2006).

46 Csordas, G., Thomas, A. P. & Hajnoczky, G. Quasi-synaptic calcium signal transmission between endoplasmic reticulum and mitochondria. *EMBO J* **18**, 96-108, (1999).

47 Tsien, R. Y. New calcium indicators and buffers with high selectivity against magnesium and protons: design, synthesis, and properties of prototype structures. *Biochemistry* **19**, 2396-2404, (1980).

48 Grynkiewicz, G., Poenie, M. & Tsien, R. Y. A new generation of Ca^{2+} indicators with greatly improved fluorescence properties. *J Biol Chem* **260**, 3440-3450, (1985).

49 Minta, A., Kao, J. P. & Tsien, R. Y. Fluorescent indicators for cytosolic calcium based on rhodamine and fluorescein chromophores. *J Biol Chem* **264**, 8171-8178, (1989).

50 Hofer, A. M. & Machen, T. E. Direct measurement of free Ca in organelles of gastric epithelial cells. *Am J Physiol* **267**, G442-451, (1994).

51 Diliberto, P. A., Wang, X. F. & Herman, B. Confocal imaging of Ca^{2+} in cells. *Methods Cell Biol* **40**, 243-262, (1994).

52 Floto, R. A., Mahaut-Smith, M. P., Somasundaram, B. & Allen, J. M. IgG-induced Ca^{2+} oscillations in differentiated U937 cells; a study using laser scanning confocal microscopy and co-loaded fluo-3 and fura-red fluorescent probes. *Cell Calcium* **18**, 377-389, (1995).

53 Lipp, P. & Niggli, E. Ratiometric confocal $Ca(^{2+})$-measurements with visible wavelength indicators in isolated cardiac myocytes. *Cell Calcium* **14**, 359-372, (1993).

54 Srivastava, S. K., Wang, L. F., Ansari, N. H. & Bhatnagar, A. Calcium homeostasis of isolated single cortical fibers of rat lens. *Invest Ophthalmol Vis Sci* **38**, 2300-2312, (1997).

55 Chacon, E. *et al.* Mitochondrial free calcium transients during excitation-contraction coupling in rabbit cardiac myocytes. *FEBS Lett* **382**, 31-36, (1996).

56 Simpson, P. B. & Russell, J. T. Mitochondria support inositol 1,4,5-trisphosphate-mediated Ca^{2+} waves in cultured oligodendrocytes. *J Biol Chem* **271**, 33493-33501, (1996).

57 Babcock, D. F., Herrington, J., Goodwin, P. C., Park, Y. B. & Hille, B. Mitochondrial participation in the intracellular Ca^{2+} network. *J Cell Biol* **136**, 833-844, (1997).

58 Hoth, M., Fanger, C. M. & Lewis, R. S. Mitochondrial regulation of store-operated calcium signaling in T lymphocytes. *J Cell Biol* **137**, 633-648, (1997).

59 Trollinger, D. R., Cascio, W. E. & Lemasters, J. J. Selective loading of Rhod 2 into mitochondria shows mitochondrial Ca^{2+} transients during the contractile cycle in adult rabbit cardiac myocytes. *Biochem Biophys Res Commun* **236**, 738-742, (1997).

60 Jou, M. J., Peng, T. I. & Sheu, S. S. Histamine induces oscillations of mitochondrial free Ca^{2+} concentration in single cultured rat brain astrocytes. *J Physiol* **497 (Pt 2)**, 299-308, (1996).

61 Golovina, V. A. & Blaustein, M. P. Spatially and functionally distinct Ca^{2+} stores in sarcoplasmic and endoplasmic reticulum. *Science* **275**, 1643-1648, (1997).

62 Hofer, A. M. & Machen, T. E. Technique for in situ measurement of calcium in intracellular inositol 1,4,5-trisphosphate-sensitive stores using the fluorescent indicator mag-fura-2. *Proc Natl Acad Sci U S A* **90**, 2598-2602, (1993).

63 Roe, M. W., Lemasters, J. J. & Herman, B. Assessment of Fura-2 for measurements of cytosolic free calcium. *Cell Calcium* **11**, 63-73, (1990).

64 Shimomura, O., Johnson, F. H. & Saiga, Y. Microdetermination of Calcium by Aequorin Luminescence. *Science* **140**, 1339-1340, (1963).

65 Shimomura, O., Musicki, B. & Kishi, Y. Semi-synthetic aequorin. An improved tool for the measurement of calcium ion concentration. *Biochem J* **251**, 405-410, (1988).

66 Baird, G. S., Zacharias, D. A. & Tsien, R. Y. Circular permutation and receptor insertion within green fluorescent proteins. *Proc Natl Acad Sci U S A* **96**, 11241-11246, (1999).

67 Griesbeck, O., Baird, G. S., Campbell, R. E., Zacharias, D. A. & Tsien, R. Y. Reducing the environmental sensitivity of yellow fluorescent protein. Mechanism and applications. *J Biol Chem* **276**, 29188-29194, (2001).

68 Nakai, J., Ohkura, M. & Imoto, K. A high signal-to-noise Ca($^{2+}$) probe composed of a single green fluorescent protein. *Nat Biotechnol* **19**, 137-141, (2001).

69 Ohkura, M., Matsuzaki, M., Kasai, H., Imoto, K. & Nakai, J. Genetically encoded bright Ca^{2+} probe applicable for dynamic Ca^{2+} imaging of dendritic spines. *Anal Chem* **77**, 5861-5869, (2005).

70 Nagai, T., Sawano, A., Park, E. S. & Miyawaki, A. Circularly permuted green fluorescent proteins engineered to sense Ca^{2+}. *Proc Natl Acad Sci U S A* **98**, 3197-3202, (2001).

71 Souslova, E. A. *et al.* Single fluorescent protein-based Ca^{2+} sensors with increased dynamic range. *BMC Biotechnol* **7**, 37, (2007).

72 Zou, J. *et al.* Developing sensors for real-time measurement of high Ca^{2+} concentrations. *Biochemistry* **46**, 12275-12288, (2007).

73 Tallini, Y. N. *et al.* Imaging cellular signals in the heart in vivo: Cardiac expression of the high-signal Ca^{2+} indicator GCaMP2. *Proc Natl Acad Sci U S A* **103**, 4753-4758, (2006).

74 Miyawaki, A., Griesbeck, O., Heim, R. & Tsien, R. Y. Dynamic and quantitative Ca^{2+} measurements using improved cameleons. *Proc Natl Acad Sci U S A* **96**, 2135-2140, (1999).

75 Miyawaki, A. *et al.* Fluorescent indicators for Ca^{2+} based on green fluorescent proteins and calmodulin. *Nature* **388**, 882-887, (1997).

76 Truong, K. *et al.* FRET-based in vivo Ca^{2+} imaging by a new calmodulin-GFP fusion molecule. *Nat Struct Biol* **8**, 1069-1073, (2001).

77 Romoser, V. A., Hinkle, P. M. & Persechini, A. Detection in living cells of Ca^{2+}-dependent changes in the fluorescence emission of an indicator composed of two green fluorescent protein variants linked by a calmodulin-binding sequence. A new class of fluorescent indicators. *J Biol Chem* **272**, 13270-13274, (1997).

78 Palmer, A. E. *et al.* Ca^{2+} indicators based on computationally redesigned calmodulin-peptide pairs. *Chem Biol* **13**, 521-530, (2006).

79 Palmer, A. E., Jin, C., Reed, J. C. & Tsien, R. Y. Bcl-2-mediated alterations in endoplasmic reticulum Ca^{2+} analyzed with an improved genetically encoded fluorescent sensor. *Proc Natl Acad Sci USA* **101**, 17404-17409, (2004).

80 Mank, M. *et al.* A FRET-based calcium biosensor with fast signal kinetics and high fluorescence change. *Biophys J* **90**, 1790-1796, (2006).

81 Ishii, K., Hirose, K. & Iino, M. Ca^{2+} shuttling between endoplasmic reticulum and mitochondria underlying Ca^{2+} oscillations. *EMBO Rep* **7**, 390-396, (2006).

82 Heim, N. & Griesbeck, O. Genetically encoded indicators of cellular calcium dynamics based on troponin C and green fluorescent protein. *J Biol Chem* **279**, 14280-14286, (2004).

83 Alonso, M. T. *et al.* Functional measurements of $[Ca^{2+}]$ in the endoplasmic reticulum using a herpes virus to deliver targeted aequorin. *Cell Calcium* **24**, 87-96, (1998).

84 Button, D. & Eidsath, A. Aequorin targeted to the endoplasmic reticulum reveals heterogeneity in luminal Ca++ concentration and reports agonist- or IP3-induced release of Ca++. *Mol Biol Cell* **7**, 419-434, (1996).

85 Kendall, J. M., Dormer, R. L. & Campbell, A. K. Targeting aequorin to the endoplasmic reticulum of living cells. *Biochem Biophys Res Commun* **189**, 1008-1016, (1992).

86 Montero, M. *et al.* Monitoring dynamic changes in free Ca^{2+} concentration in the endoplasmic reticulum of intact cells. *EMBO J* **14**, 5467-5475, (1995).

87 Robert, V., De Giorgi, F., Massimino, M. L., Cantini, M. & Pozzan, T. Direct monitoring of the calcium concentration in the sarcoplasmic and endoplasmic reticulum of skeletal muscle myotubes. *J Biol Chem* **273**, 30372-30378, (1998).

88 Pinton, P., Pozzan, T. & Rizzuto, R. The Golgi apparatus is an inositol 1,4,5-trisphosphate-sensitive Ca^{2+} store, with functional properties distinct from those of the endoplasmic reticulum. *EMBO J* **17**, 5298-5308, (1998).

89 Rizzuto, R., Bastianutto, C., Brini, M., Murgia, M. & Pozzan, T. Mitochondrial Ca^{2+} homeostasis in intact cells. *J Cell Biol* **126**, 1183-1194, (1994).

90 Rutter, G. A. *et al.* Subcellular imaging of intramitochondrial Ca^{2+} with recombinant targeted aequorin: significance for the regulation of pyruvate dehydrogenase activity. *Proc Natl Acad Sci U S A* **93**, 5489-5494, (1996).

91 Nagai, T., Yamada, S., Tominaga, T., Ichikawa, M. & Miyawaki, A. Expanded dynamic range of fluorescent indicators for $Ca(^{2+})$ by circularly permuted yellow fluorescent proteins. *Proc Natl Acad Sci U S A* **101**, 10554-10559, (2004).

92 Mank, M. *et al.* A genetically encoded calcium indicator for chronic in vivo two-photon imaging. *Nat Methods* **5**, 805-811, (2008).

93 Yuste, R., Majewska, A. & Holthoff, K. From form to function: calcium compartmentalization in dendritic spines. *Nat Neurosci* **3**, 653-659, (2000).

94 Burnashev, N. & Rozov, A. Presynaptic Ca^{2+} dynamics, Ca^{2+} buffers and synaptic efficacy. *Cell Calcium* **37**, 489-495, (2005).

95 Hartmann, J. & Konnerth, A. Determinants of postsynaptic Ca^{2+} signaling in Purkinje neurons. *Cell Calcium* **37**, 459-466, (2005).

96 Murray, F. E., Landsberg, J. P., Williams, R. J., Esiri, M. M. & Watt, F. Elemental analysis of neurofibrillary tangles in Alzheimer's disease using proton-induced X-ray analysis. *Ciba Found Symp* **169**, 201-210; discussion 210-206, (1992).

97 Nixon, R. A. The calpains in aging and aging-related diseases. *Ageing Res Rev* **2**, 407-418, (2003).

98 Beal, M. F. Excitotoxicity and nitric oxide in Parkinson's disease pathogenesis. *Ann Neurol* **44**, S110-114, (1998).

99 Yamada, T., McGeer, P. L., Baimbridge, K. G. & McGeer, E. G. Relative sparing in Parkinson's disease of substantia nigra dopamine neurons containing calbindin-D28K. *Brain Res* **526**, 303-307, (1990).

100 Mouatt-Prigent, A., Agid, Y. & Hirsch, E. C. Does the calcium binding protein calretinin protect dopaminergic neurons against degeneration in Parkinson's disease? *Brain Res* **668**, 62-70, (1994).

101 Liang, Z. Q. *et al.* Susceptibility of striatal neurons to excitotoxic injury correlates with basal levels of Bcl-2 and the induction of P53 and c-Myc immunoreactivity. *Neurobiol Dis* **20**, 562-573, (2005).

102 Tang, T. S. *et al.* Disturbed Ca^{2+} signaling and apoptosis of medium spiny neurons in Huntington's disease. *Proc Natl Acad Sci U S A* **102**, 2602-2607, (2005).

103 Stutzmann, G. E., Caccamo, A., LaFerla, F. M. & Parker, I. Dysregulated IP3 signaling in cortical neurons of knock-in mice expressing an Alzheimer's-linked mutation in

presenilin1 results in exaggerated Ca^{2+} signals and altered membrane excitability. *J Neurosci* **24**, 508-513, (2004).

104 Tu, H. *et al.* Presenilins form ER Ca^{2+} leak channels, a function disrupted by familial Alzheimer's disease-linked mutations. *Cell* **126**, 981-993, (2006).

105 Smith, I. F., Hitt, B., Green, K. N., Oddo, S. & LaFerla, F. M. Enhanced caffeine-induced Ca^{2+} release in the 3xTg-AD mouse model of Alzheimer's disease. *J Neurochem* **94**, 1711-1718, (2005).

106 Chan, S. L., Mayne, M., Holden, C. P., Geiger, J. D. & Mattson, M. P. Presenilin-1 mutations increase levels of ryanodine receptors and calcium release in PC12 cells and cortical neurons. *J Biol Chem* **275**, 18195-18200, (2000).

107 Nelson, O. *et al.* Familial Alzheimer disease-linked mutations specifically disrupt Ca^{2+} leak function of presenilin 1. *J Clin Invest* **117**, 1230-1239, (2007).

108 Zatti, G. *et al.* Presenilin mutations linked to familial Alzheimer's disease reduce endoplasmic reticulum and Golgi apparatus calcium levels. *Cell Calcium* **39**, 539-550, (2006).

109 Leissring, M. A. *et al.* Capacitative calcium entry deficits and elevated luminal calcium content in mutant presenilin-1 knockin mice. *J Cell Biol* **149**, 793-798, (2000).

110 Leissring, M. A., Paul, B. A., Parker, I., Cotman, C. W. & LaFerla, F. M. Alzheimer's presenilin-1 mutation potentiates inositol 1,4,5-trisphosphate-mediated calcium signaling in Xenopus oocytes. *J Neurochem* **72**, 1061-1068, (1999).

111 Stutzmann, G. E. *et al.* Enhanced ryanodine receptor recruitment contributes to Ca^{2+} disruptions in young, adult, and aged Alzheimer's disease mice. *J Neurosci* **26**, 5180-5189, (2006).

112 Volles, M. J. & Lansbury, P. T., Jr. Vesicle permeabilization by protofibrillar alpha-synuclein is sensitive to Parkinson's disease-linked mutations and occurs by a pore-like mechanism. *Biochemistry* **41**, 4595-4602, (2002).

113 Furukawa, K. *et al.* Plasma membrane ion permeability induced by mutant alpha-synuclein contributes to the degeneration of neural cells. *J Neurochem* **97**, 1071-1077, (2006).

114 Bezprozvanny, I. & Hayden, M. R. Deranged neuronal calcium signaling and Huntington disease. *Biochem Biophys Res Commun* **322**, 1310-1317, (2004).

115 Field, M., Graf, L. H., Jr., Laird, W. J. & Smith, P. L. Heat-stable enterotoxin of Escherichia coli: in vitro effects on guanylate cyclase activity, cyclic GMP concentration, and ion transport in small intestine. *Proc Natl Acad Sci U S A* **75**, 2800-2804, (1978).

116 Chaudhuri, A. G. & Ganguly, U. Evidence for stimulation of the inositol triphosphate-Ca^{2+} signalling system in rat enterocytes by heat stable enterotoxin of Escherichia coli. *Biochim Biophys Acta* **1267**, 131-133, (1995).

117 Crane, J. K. *et al.* Regulation of intestinal guanylate cyclase by the heat-stable enterotoxin of Escherichia coli (STa) and protein kinase C. *Infect Immun* **60**, 5004-5012, (1992).

118 Ganguly, U., Chaudhury, A. G., Basu, A. & Sen, P. C. STa-induced translocation of protein kinase C from cytosol to membrane in rat enterocytes. *FEMS Microbiol Lett* **204**, 65-69, (2001).

119 Chaudhuri, A. G., Bhattacharya, J., Nair, G. B., Takeda, T. & Chakrabarti, M. K. Rise of cytosolic Ca^{2+} and activation of membrane-bound guanylyl cyclase activity in rat enterocytes by heat-stable enterotoxin of Vibrio cholerae non-01. *FEMS Microbiol Lett* **160**, 125-129, (1998).

120 Kumar, P., Ahuja, N. & Bhatnagar, R. Anthrax edema toxin requires influx of calcium for inducing cyclic AMP toxicity in target cells. *Infect Immun* **70**, 4997-5007, (2002).

121 Tran Van Nhieu, G., Bourdet-Sicard, R., Dumenil, G., Blocker, A. & Sansonetti, P. J. Bacterial signals and cell responses during Shigella entry into epithelial cells. *Cell Microbiol* **2**, 187-193, (2000).

122 Zhou, D., Chen, L. M., Hernandez, L., Shears, S. B. & Galan, J. E. A Salmonella inositol polyphosphatase acts in conjunction with other bacterial effectors to promote host cell actin cytoskeleton rearrangements and bacterial internalization. *Mol Microbiol* **39**, 248-259, (2001).

123 Pace, J., Hayman, M. J. & Galan, J. E. Signal transduction and invasion of epithelial cells by S. typhimurium. *Cell* **72**, 505-514, (1993).

124 Pace, J. L. & Galan, J. E. Measurement of free intracellular calcium levels in epithelial cells as consequence of bacterial invasion. *Methods Enzymol* **236**, 482-490, (1994).

125 Ruschkowski, S., Rosenshine, I. & Finlay, B. B. Salmonella typhimurium induces an inositol phosphate flux in infected epithelial cells. *FEMS Microbiol Lett* **74**, 121-126, (1992).

126 Tran Van Nhieu, G. *et al.* Connexin-dependent inter-cellular communication increases invasion and dissemination of Shigella in epithelial cells. *Nat Cell Biol* **5**, 720-726, (2003).

127 Foubister, V., Rosenshine, I. & Finlay, B. B. A diarrheal pathogen, enteropathogenic Escherichia coli (EPEC), triggers a flux of inositol phosphates in infected epithelial cells. *J Exp Med* **179**, 993-998, (1994).

128 Dytoc, M., Fedorko, L. & Sherman, P. M. Signal transduction in human epithelial cells infected with attaching and effacing Escherichia coli in vitro. *Gastroenterology* **106**, 1150-1161, (1994).

129 Brown, M. D., Bry, L., Li, Z. & Sacks, D. B. Actin pedestal formation by enteropathogenic Escherichia coli is regulated by IQGAP1, calcium, and calmodulin. *J Biol Chem* **283**, 35212-35222, (2008).

Chapter 2

Using a genetically targeted sensor to investigate the role of presenilin-1 in ER Ca^{2+} levels and dynamics

Janet E. McCombs, Emily A. Gibson, Amy E. Palmer
Mol. BioSyst. **6:**1640-1649 (2010)

2.1 Abstract

The ER plays a fundamental role in storing cellular Ca^{2+}, generating Ca^{2+} signals, and modulating Ca^{2+} in both the cytosol and mitochondria. Genetically encoded Ca^{2+} sensors can be explicitly targeted to the ER to directly define Ca^{2+} levels and monitor fluxes of Ca^{2+} within this organelle. In this study we use an ER-targeted Ca^{2+} sensor to define both the level and dynamics of ER Ca^{2+} in cells expressing mutant presenilin proteins. Growing evidence suggests the enigmatic presenilin-1 plays a role in regulating ER Ca^{2+}. Presenilin-1 was initially identified in a screen for genetic causes of inherited familial Alzheimer's disease (fAD). The connection between presenilin-1, calcium regulation, and Alzheimer's disease may provide the key to understanding the long-observed, but poorly understood, link between Alzheimer's disease and Ca^{2+} dysregulation. In this study we examined seven fAD-causing mutations in presenilin-1 to define how they influence ER Ca^{2+} levels and dynamics. We observed that some, but not all, mutations in PS1 decrease the level of Ca^{2+} within the ER and this difference depends on the enzymatic activity of PS1. Two mutations tested altered the kinetics of Ca^{2+} release from the ER upon ATP stimulation, resulting in faster spiking. Combined, these results indicate that mutations in PS1 can alter the balance of Ca^{2+} in cells and have the potential to influence the nature of Ca^{2+} signals.

2.2 Introduction

Ca^{2+} is an essential and tightly regulated cellular second messenger, important for the maintenance of many cellular processes and functions. Ca^{2+} signals can be generated by influx across the plasma membrane or release of Ca^{2+} from the endoplasmic reticulum (ER), which serves as the storehouse and signaling hub of Ca^{2+}. Recently, presenilin-1 (PS1) has emerged as

a central player in the regulation of ER Ca^{2+} [1-3]. An integral membrane protein predominantly localized to the ER, PS1 has been proposed to: form a Ca^{2+} leak channel in the ER [1]; interact with and regulate the Sarco/endoplasmic reticulum Ca^{2+} ATPase (SERCA) [2]; modulate release of Ca^{2+} through the IP_3 receptor (IP_3R) [3]; and interact with, change the expression levels of, and modify Ca^{2+} release through the Ryanodine Receptor (RyR) [4, 5].

PS1 was originally identified in a genetic screen for causative agents of familial Alzheimer's disease (fAD) [6]. Since then, over 150 mutations in PS1 have been identified that give rise to fAD. The involvement of PS1 in Alzheimer's disease pathology has been primarily ascribed to altered processing of the amyloid precursor protein (APP) by gamma-secretase, a multi-protein complex containing PS1 [7]. Both sporadic and inherited cases of Alzheimer's disease are characterized by Ca^{2+} imbalance, and growing evidence indicates that Ca^{2+} dysregulation is correlated with disease pathogenesis [8-10]. To assess whether the Ca^{2+}-regulatory function of PS1 is relevant to fAD, it is important to define how mutations in PS1 alter these functions. Though its exact role is unclear, mutations in PS1 have been suggested to cause both overloading and under-filling of ER Ca^{2+} stores, and to both increase and decrease Ca^{2+} release from the ER [1, 3, 11-15].

Due to the complexity of cellular Ca^{2+} regulation, live cell imaging of Ca^{2+} signaling events are greatly benefited by sensors targeted to specific subcellular compartments. However, many studies investigating the role of PS1 mutations on Ca^{2+} dyshomeostasis have inferred the impact on ER Ca^{2+} by measuring changes in cytosolic Ca^{2+}. Such studies may be confounded by changes in cytosolic clearance mechanisms and discrepancies between ER Ca^{2+} load and Ca^{2+} release. Genetically encoded Ca^{2+} sensors, such as cameleons, can be specifically targeted to the ER, permitting investigators to monitor Ca^{2+} within the ER (i.e. ER Ca^{2+} load), directly observe

the leak or release of Ca^{2+} from this organelle, and examine SERCA activity by measuring Ca^{2+} uptake. Despite these advantages, these sensors have remained underutilized tools in studies examining effects of disease on cellular Ca^{2+} homeostasis. In the present study, we apply one such sensor, D1ER [16], and examine a panel of fAD-associated mutations in PS1 to determine their effects on ER Ca^{2+} levels and dynamics. We found that mutations in PS1 indeed alter ER Ca^{2+}, but not all mutations have the same effect. Alteration of ER Ca^{2+} levels by mutant PS1 could be reversed by addition of a gamma-secretase inhibitor, suggesting that PS1 enzymatic activity impacts ER Ca^{2+} levels. In addition, because ER Ca^{2+} release can impact downstream signaling processes, we examined whether mutations in PS1 affected Ca^{2+} release from the ER upon stimulation with ATP. Two mutants tested led to an increase in the frequency of Ca^{2+} spikes, suggesting that mutations in PS1 affect the nature of ER Ca^{2+} release.

2.3 Results

To examine whether mutations in PS1 affect Ca^{2+} in a universal manner we chose a range of mutations localized throughout PS1 that vary in their average age of Alzheimer's disease onset (**Figure 2.1A**). Mouse embryonic fibroblast (MEF) cells deficient in PS1 and PS2 (double knock out, DKO) were used as a model to eliminate potential effects of endogenous PS on the Ca^{2+} phenotype [17, 18]. DKO MEF cells were reconstituted with WT or mutant PS1 by transient transfection and the presence of PS1 in cells was confirmed by GFP or mCherry fluorescence. Reconstitution of PS1 was corroborated by Western blot (**Figure 2.1B**).

2.3.1 Mutations in PS1 have differential effects on ER Ca^{2+} store levels

The amount of Ca^{2+} within the ER is a balance of the ER buffering capacity, activity of the SERCA pump, release through channels and a passive "leak" of Ca^{2+} out of the ER. For this

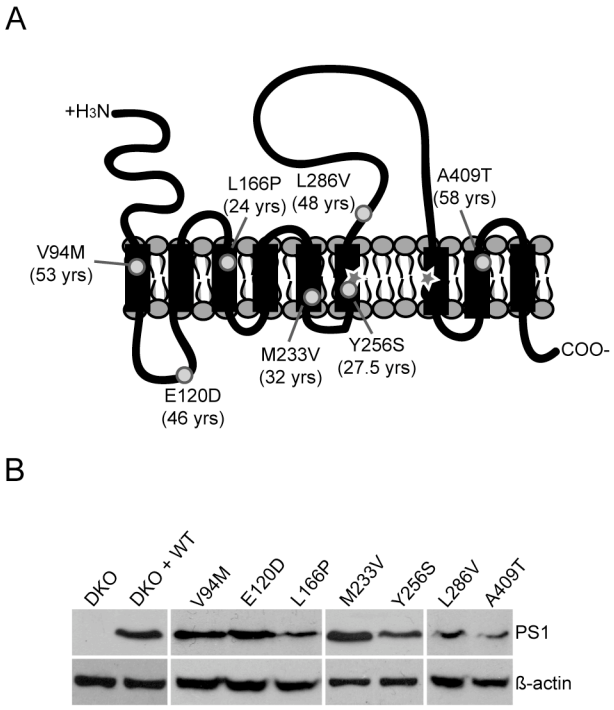

Figure 2.1 Verification of PS1 in cells. (A) Schematic of PS1 showing proposed membrane topology and relative locations of the mutations (circles) chosen for this study. Critical aspartates are denoted by a star. Average age at onset is indicated in parentheses. (B) Western blot showing relative expression levels of the PS1 variants upon transient transfection into DKO cells.

study, steady state levels of ER Ca^{2+} were determined by measuring the resting FRET ratio (R) using the D1ER cameleon sensor. Subsequent inhibition of SERCA with thapsigargin led to a decrease in R as Ca^{2+} slowly leaks out of the ER (**Figure 2.2A**), enabling us to determine relative ER Ca^{2+} levels. Under resting conditions, DKO cells exhibited a higher normalized ratio (ΔR), indicative of higher $[Ca^{2+}]_{ER}$ when compared to WT and DKO cells reconstituted with WT PS1 (referred to as DKO + WT, **Figure 2.2B**). This is consistent with previous studies using these MEF cells in which the low affinity Ca^{2+} sensor MagFura-2 was used to measure $[Ca^{2+}]_{ER}$ [1, 12].

Figure 2.2B also presents results for the PS1 variants examined in this study, illustrating that different mutants have differential effects on ER Ca^{2+} stores. WT cells consistently yielded a Ca^{2+} phenotype that was the same as DKO + WT. For statistical analysis, all mutant PS1 were compared to DKO + WT, allowing direct comparison of the impact of a specific mutation on Ca^{2+} within the same genetic background. Compared to DKO + WT, only M233V and A409T showed a statistically significant decrease in $[Ca^{2+}]_{ER}$ ($P < 0.05$, ANOVA). V94M appeared to have a slightly increased Ca^{2+} level compared to reconstituted cells; however, this difference was not statistically significant. Our data support a role for PS1 in regulation of ER Ca^{2+} levels, though it is clear that not all mutations in PS1 affect the Ca^{2+} level within the ER.

Green, *et al.*, recently proposed that PS1 regulates SERCA pump activity [2]. Since SERCA is responsible for pumping Ca^{2+} into the ER, an over- or under-active SERCA could result in over- or under-filling of the ER store. To examine SERCA pump activity, cells were treated with the reversible SERCA inhibitor tBHQ leading to depletion of ER Ca^{2+}. Once ER Ca^{2+} levels stabilized, tBHQ was washed out and Ca^{2+} added back, causing an influx of Ca^{2+} into internal stores through the SERCA pump. D1ER enabled us to directly monitor changes in $[Ca^{2+}]_{ER}$ as shown in **Figure 2.2C**. The rate constant for re-filling was found by fitting the Ca^{2+}

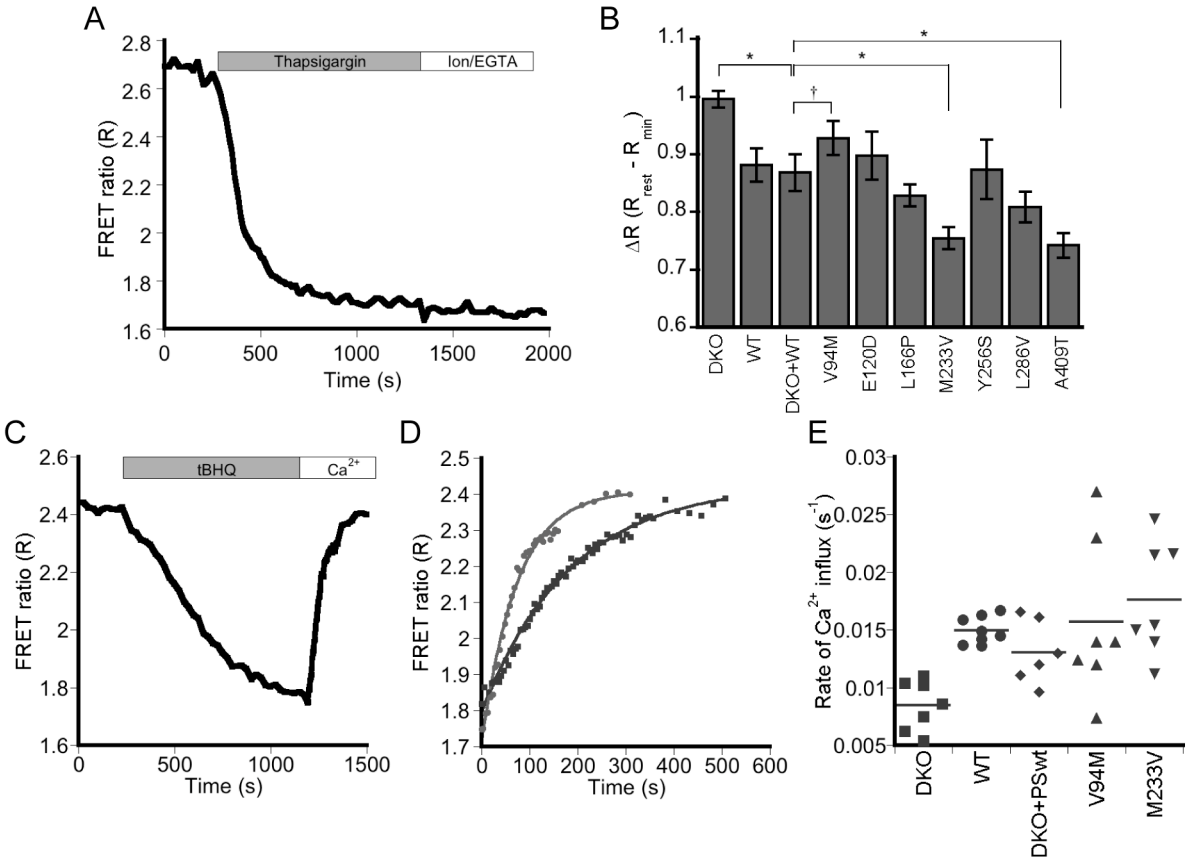

Figure 2.2 Impact of PS1 on Ca^{2+} within the ER. (A) Representative experiment measuring ER Ca^{2+} load using the D1ER Ca^{2+} sensor. MEF cells transfected with the PS1 mutants were treated with thapsigargin in the absence of extracellular Ca^{2+} before calibrating the sensor with EGTA and ionomycin to obtain R_{min}. (B) Bar graph showing ΔR at rest in the ER. Error bars indicate SEM. Asterisk: $P < 0.05$, ANOVA with Student-Newman-Keuls post-hoc test. Dagger: V94M appears to have more Ca^{2+} in the ER compared to control, though the difference is not statistically significant.WT: n = 17 (5 exps); DKO: n = 24 (9 exps); DKO + WT: n = 8 (6 exps), E120D: n = 8 (6 exps); V94M: n = 11 (7 exps); L166Pn = 13 (6 exps); M233V: n = 9 (4 exps); Y256S: n = 7 (3 exps); L286V: n = 13 (5 exps); A409T: n = 9 (5 exps). (C) Representative experiment examining the refilling of ER Ca^{2+} stores using D1ER. Cells were treated with tBHQ before adding excess Ca^{2+} to reload the ER. (D) Rates of ER refilling in WT (gray circles) and DKO (black squares). Data are fit to an exponential rise, $A(t) = A_0(1 - e^{-kt})$. (E) Plot of Ca^{2+} influx rate constants (k). Only DKO shows significant difference from WT ($P < 0.015$, ANOVA with Student-Newman-Keuls post-hoc test). Each point represents the k from an individual experiment and the horizontal line marks the mean k value for each data set. WT: n = 8 from 3 exps; DKO: n = 7 from 5 exps; DKO + WT: n = 6 from 4 exps; V94M: n = 7 from 4 exps; M233V: n = 7 from 3 exps.

influx curve to a single exponential rise (**Figure 2.2D**), and was significantly higher in WT as compared to DKO cells (k_{WT} = 15.0 x 10^{-3} ± 1.2 x 10^{-3} s^{-1}, k_{DKO} = 8.1 x 10^{-3} ± 2.2 x 10^{-3} s^{-1}, $P <$ 0.015, ANOVA), consistent with previous findings suggesting PS1 increases SERCA pump activity [2]. To examine whether mutations in PS1 affect this regulatory function, we focused on PS1 variants that led to a detectable change in ER Ca^{2+} levels. However, we found that none of the mutants tested had an effect on Ca^{2+} influx through SERCA (**Figure 2.2E**), indicating that although PS1 impacts SERCA pump activity, the mutations in PS1examined here do not appear to affect this function. Interestingly, the differences in the ER Ca^{2+} load can not be explained by SERCA activity alone, as cells containing WT PS1 had greater SERCA activity, but overall lower Ca^{2+} when compared to DKO.

In addition to regulating ER Ca^{2+} stores, previous studies have suggested PS1 forms a leak channel in the ER [1] or contributes to the rate at which Ca^{2+} leaks out of the ER [3]. To examine the leak rate, the change in R within the ER was monitored upon inhibition of SERCA with thapsigargin. **Figure 2.3** presents the initial rate of decay (linear fit to the first 150 s of the R curve upon thapsigargin treatment) and the rate of change as a function of the Ca^{2+} level ($d\Delta R/dt$). Because PS mutations differentially affect the level of Ca^{2+} in the ER (**Figure 2.2B**), we felt it was important to compare the leak rate as a function of Ca^{2+} to ensure that any potential differences in leak rate were not simply reflections of the different amount of Ca^{2+} at a given point in time. No difference in Ca^{2+} leak rate was observed between DKO and WT cells (**Figure 2.3A** and **2.3B**); however, three of the mutants tested exhibited an altered leak rate compared to WT cells. V94M exhibited a greater leak for both the initial rate and the leak rate as a function of ER Ca^{2+} level, while M233V and A409T both exhibited a lower leak (**Figure 2.3**).These results indicate that mutations in PS1 can affect the rate at which Ca^{2+} leaks out of the ER, with

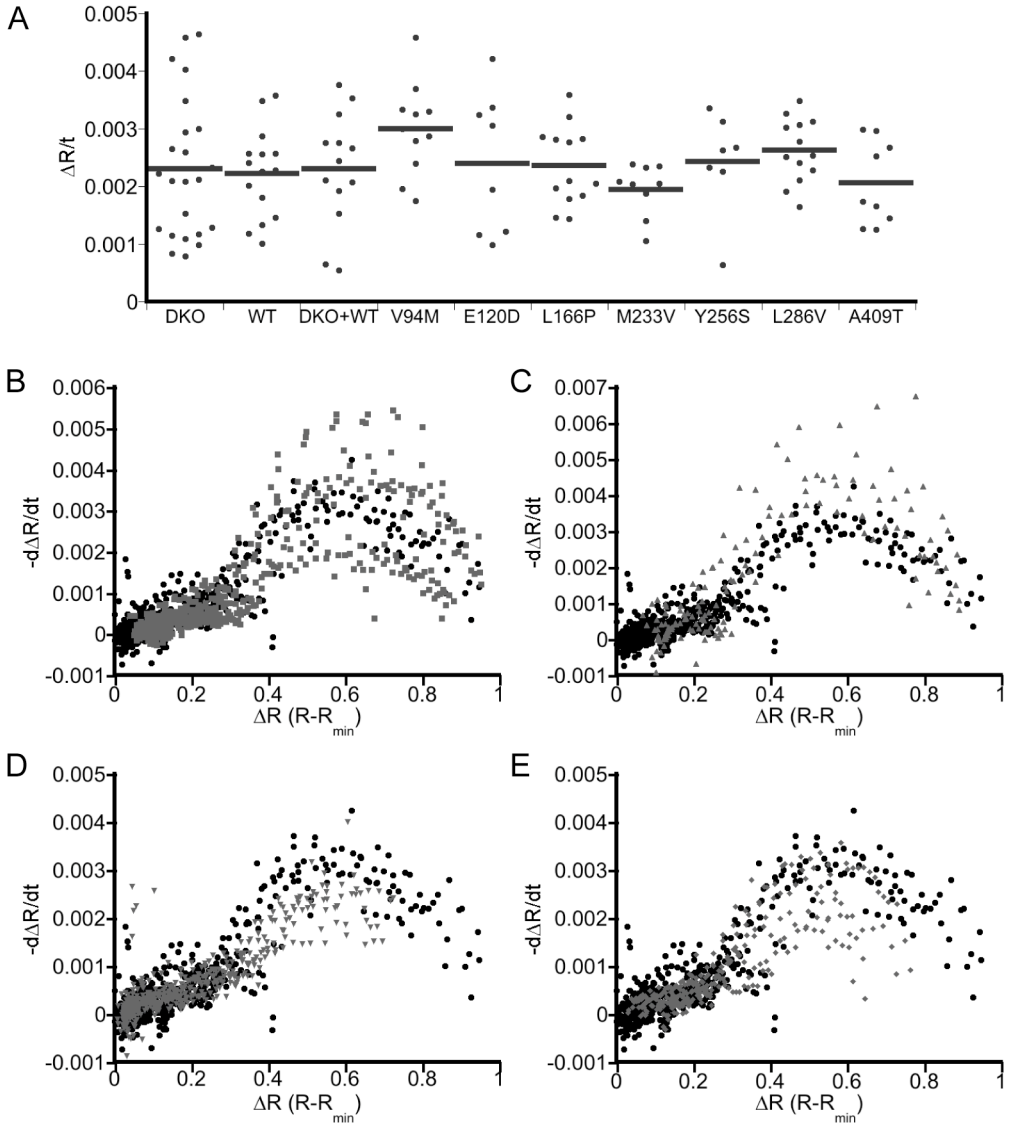

Figure 2.3 Effect of PS1 on ER Ca^{2+} leak rates. (A) Initial Ca^{2+} leak rate, defined as the change in ratio per unit time (ΔR/t). Rates were determined from the first 150 s after treatment of cells with 4 μM thapsigargin using a linear fit. (B – E) Comparison of Ca^{2+} leak rate as a function of Ca^{2+} concentration, reported as the rate of change of the ratio (dΔR/dt) as a function of the ΔR for WT (black) versus DKO (B), V94M (C), M233V (D) and A409T (E) in gray.

some mutations causing an increase in the leak and some causing a decrease. However, it is clear that the ER Ca^{2+} load is not defined by the leak rate, but rather the altered leak rate may be a consequence of altered Ca^{2+} load as mutations that cause a decrease in the ER Ca^{2+} load yield a lower leak rate, and vice versa.

2.3.2 ER levels are regulated by PS1 activity

In addition to its Ca^{2+} regulatory functions, PS1 serves as the catalytic subunit of the multi-protein gamma-secretase complex, which cleaves a number of substrates in the cell, including APP. APP is a single pass transmembrane protein that is cleaved by gamma-secretase into two fragments: an intracellular domain and an extracellular peptide called amyloid beta (Aβ). The activity of our PS1 mutants within the gamma-secretase complex was verified using an APP-C99-mCherry probe to show cleavage of APP in cells (**Figure 2.4**). As altered ER Ca^{2+} levels could not be explained by SERCA activity or the leak rate of Ca^{2+} out of the ER, we next examined whether the activity of PS1 as part of the gamma-secretase complex affected ER Ca^{2+} homeostasis by using the small molecule gamma-secretase inhibitor N-[N-(3,5-Difluorophenacetyl-L-alanyl)]-S-phenylglycine *t*-Butyl Ester (DAPT). Treatment with DAPT had no effect on $[Ca^{2+}]_{ER}$ in DKO + WT, V94M, and L166P cells. However, inhibition of gamma-secretase activity resulted in an enhancement of ER Ca^{2+} levels for both M233V and A409T, raising them to DKO + WT levels (**Figure 2.5A**). Moreover the leak rates for all mutants examined were comparable to WT, consistent with leak rate being a consequence of the ER Ca^{2+} load (**Figure 2.5B – D**). To assess whether changes in Ca^{2+} could be attributed to the gamma-secretase mediated cleavage products of APP, the relative amounts of two cleavage products (Aβ40 and Aβ42) were determined by ELISA (**Figure 2.6**). While the observed changes in Aβ cleavage products are intriguing and may have implications for Alzheimer's

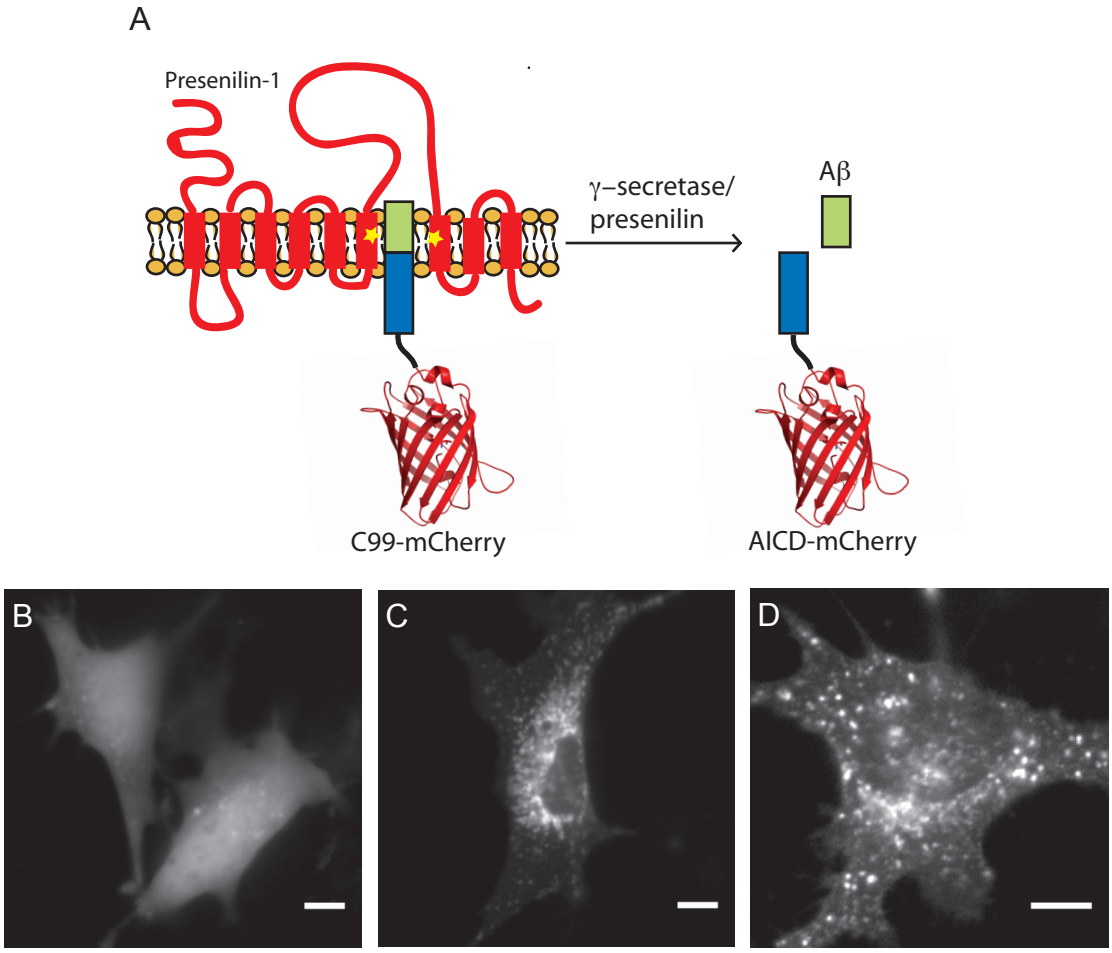

Figure 2.4 Demonstration of gamma-secretase activity in MEF cells. (A) Schematic representation of the C99-mCherry probe consisting of post-β-secretase cleaved APP with the mCherry fluorophore on its C-terminus. Upon recognition by the gamma-secretase complex, PS cleaves the probe into its intracellular domain (AICD) and Aβ fragments. (B) The C99-mCherry probe in WT MEF cells displaying diffuse cytosolic fluorescence. (C) WT MEF cells treated with the gamma-secretase inhibitor DAPT and expressing the C99-mCherry probe displaying punctate fluorescence. (D) DKO MEF cells expressing the C99-mCherry probe. Fluorescence is comparable to WT + DAPT cells, as there is no PS and thus no cleavage of the probe in cells. Scale bar is 10μm.

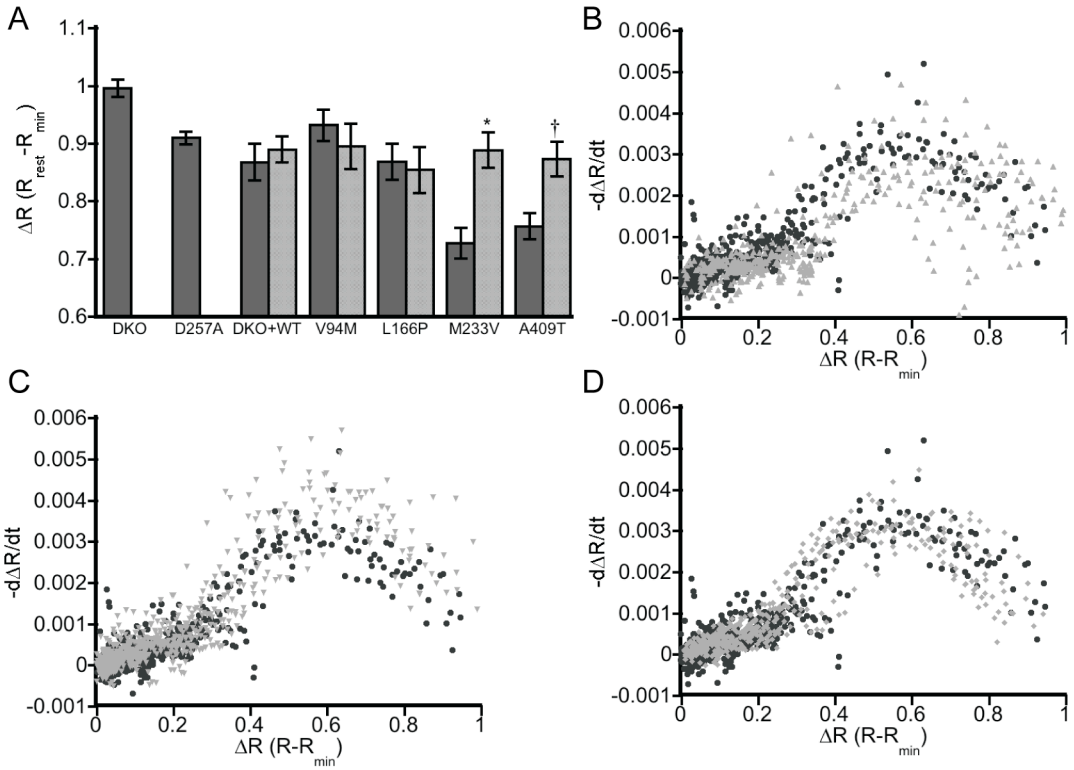

Figure 2.5 Gamma-secretase activity affects ER Ca^{2+} levels. (A) Bar graph depicting ΔR at rest in the ER for cells with (light gray) and without (dark gray) 24 h treatment with the gamma-secretase inhibitor DAPT. Error bars indicate SEM. Asterisk: $P < 0.0005$, unpaired t-test; Dagger: $P < 0.005$, unpaired t-test. DKO + WT: n = 6 (3 exps); V94M: n = 14 (2 exps); L166P: n = 13 (4 exps); M233V: n = 23 (4 exps); A409T: n = 16 (4 exps). (B – D) Comparison of the ER Ca^{2+} leak rate as a function of relative Ca^{2+} concentration. Leak rates are reported as a rate of change in the normalized ratio (ΔR) versus ΔR for V94M (B), M233V (C) and A409T (D). Graphs depict mutant leak rates (gray) compared to leaks rates in WT not treated with DAPT (black)

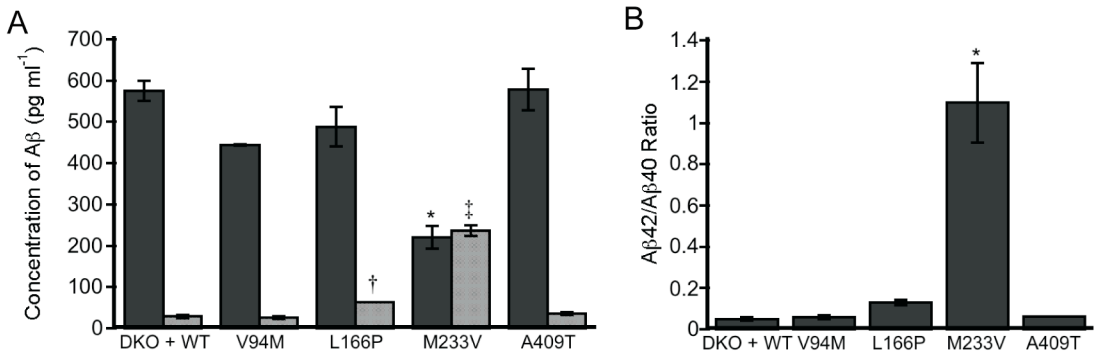

Figure 2.6 Examination of gamma-secretase mediated cleavage of APP. (A) Relative amounts of Aβ40 (dark gray) and Aβ42 (light gray) in cells expressing a subset of the PS1 mutants. Both L166P and M233V led to an increase in Aβ42 levels. M233V also led to a significant decrease in Aβ40 levels. Asterisk: $P < 0.005$; Dagger: $P < 0.05$; Double dagger: $P < 0.0001$. (B) Relative ratios of Aβ42/40 for a subset of the PS1 mutants. Asterisk: $P < 0.002$. All statistics were calculated using an ANOVA with Student-Newman-Keuls post-hoc test. Error bars indicate SEM.

disease progression (L166P and M233V have the highest Aβ42/40 ratios and the earliest ages of onset in 24 and 32 yrs, respectively), these changes do not correlate with changes in ER Ca^{2+}. For example, M233V and A409T are the two mutants with reduced ER Ca^{2+} and inhibition of gamma-secretase increases Ca^{2+} to WT levels. However these two mutants have very different Aβ profiles. Therefore, while gamma-secretase activity plays a role in influencing ER Ca^{2+} levels, this can not be easily ascribed to Aβ cleavage products. Overall our data reveal that there may be multiple mechanisms by which PS1 affects ER Ca^{2+} levels, one dependent on and another independent of gamma-secretase activity. Comparison of DKO and DKO + WT reveals that PS1 lowers ER Ca^{2+} levels regardless of its enzymatic activity. This is confirmed by measurement of the ER Ca^{2+} load in DKO cells expressing a catalytically inactive PS1 mutant (D257A) which phenocopies the DAPT-inhibited DKO + WT cells. However AD-causing mutations in PS1 can lead to additional alterations in ER Ca^{2+} (i.e. a further decrease for M233V and A409T compared to WT PS1), and this additional perturbation is clearly dependent on gamma-secretase activity as the difference could be reversed by DAPT inhibition.

2.3.3 Mutations in PS1 affect the kinetics of ER Ca^{2+} release

As the central storehouse of Ca^{2+} the ER plays a central role in generation of Ca^{2+} signals. For example, activation of P2Y G-protein coupled receptors by ATP leads to the production of IP_3 and release of Ca^{2+} from the ER. Repetitive release leads to the generation of Ca^{2+} oscillations in the cytosol, the duration, amplitude and frequency of which affect downstream processes such as cell cycle regulation, gene transcription, and differentiation [19]. A recent report indicates that PS1 interacts with the IP_3R to modulate the open probability and hence release of Ca^{2+} from the ER [3]. Moreover, an fAD-associated mutation (M146L) was shown to alter release of Ca^{2+} through the IP_3R independent of Ca^{2+} load. For this study, we chose to examine the

L166P, M233V, and A409T mutants as they showed a change in Aβ production and/or lowered $[Ca^{2+}]_{ER}$ levels. Cells stimulated with 5 μM ATP exhibited two categories of response: immediate response with rapid Ca^{2+} spiking followed by slower irregular transients or a delayed response with no repetitive Ca^{2+} fluctuations. Investigation into the nature of ATP-induced Ca^{2+} release resulted in no observable difference in ATP sensitivity for L166P and A409T, but a decrease in sensitivity (as defined by decreased responsiveness to ATP) for M233V (**Figure 2.7A and B**). A general decrease in the amplitude of Ca^{2+} release was observed for L166P and M233V, but not A409T, even though it contains less Ca^{2+} in the ER than WT (**Figure 2.7C – H**).

Given the versatility of Ca^{2+} signaling, cells can interpret changes in frequency of Ca^{2+} oscillations in order to differentially control multiple cellular processes [19]. Because of this, changes in the kinetics of Ca^{2+} release through the IP_3R could alter the fate of a cell, contributing to a diseased state. We therefore examined how the mutations studied here affected the frequency of the ATP-induced Ca^{2+} signals. Treatment of cells with 5 μM ATP lead to a rapid burst of Ca^{2+} spikes superimposed on a broad Ca^{2+} decay curve (**Figure 2.8A** left side). Longer imaging revealed irregular slower Ca^{2+} transients in a small subset of cells (**Figure 2.8A** right side). Attempts to elicit more regular extended oscillations in a larger fraction of cells using different stimuli (ATP, UTP, histamine, and carbachol) and lower doses of stimuli (i.e. 1 μM ATP vs. 5 μM ATP) were unsuccessful. Therefore we focused our analysis on the rapid initial bursting of Ca^{2+}, as this bursting is still dependent on release from the IP_3R and allows comparison of the kinetics of release between the different mutants. **Figure 2.8B – F** shows representative traces which reveal that cells expressing M233V and A409T, but not L166P, exhibited faster spiking than either WT or DKO cells. In an attempt to quantify the differences between cells expressing mutant PS1, we calculated the spike period (i.e. time between spikes

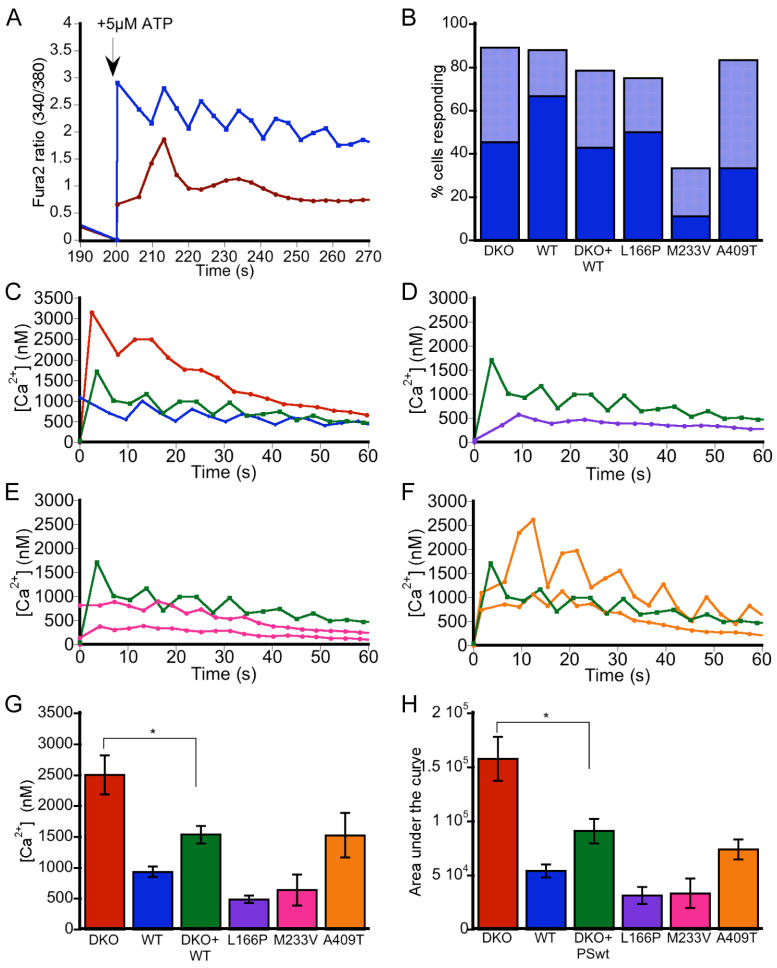

Figure 2.7 The effect of PS1 on ATP-induced ER Ca^{2+} release. (A) Upon treatment with ATP, Ca^{2+} release from cells either occurred immediately (blue) or displayed a noticeable delay (red), with a comparatively smaller Ca^{2+} response. (B) Percent of responding cells that showed immediate (dark blue) or delayed (light blue) Ca^{2+} release. Cells showed similar responsiveness (~ 80%) except for DKO + M233V, which had decreased ATP sensitivity. WT: n = 42; DKO: n = 56; DKO + WT: 14; L166P: n = 8; M233V: n = 18; A409T: n = 12. (C – F) Representative oscillation curves for the amount of Ca^{2+} released in immediately responding cells for DKO (red), WT (blue) and DKO + WT (green); (D – F) Comparison of the amount of Ca^{2+} released upon stimulation with ATP for DKO + WT (green) versus L166P (purple; D), M233V (pink; E), and A409T (orange; F). (G) Maximum [Ca^{2+}] peak heights upon addition of 5μM ATP. Asterisk: $P < 0.05$, ANOVA with Student-Newman-Keuls post-hoc test. WT: n = 27; DKO: n = 25; DKO + WT: n = 6; L166P: n = 3; M233V: n = 2; A409T: n = 4. (H) Amount of Ca^{2+} released from the ER upon ATP treatment. Data represent area under the oscillation curve. DKO cells released more Ca^{2+} upon stimulation with ATP than DKO + WT, consistent with levels of ER Ca^{2+}. However, though not significant, L166P appeared to release less Ca^{2+} upon treatment with ATP though the ER concentration of Ca^{2+} was similar to WT. M233V also appeared to release less Ca^{2+} than WT, consistent with the lower level of ER Ca^{2+}, though differences were not significant. Interestingly, the Ca^{2+} response for the A409T mutant was similar to WT despite this mutant having a lower ER Ca^{2+} load. Asterisk: $P < 0.05$, ANOVA with Student-Newman-Keuls post-hoc test. Error bars indicate SEM.

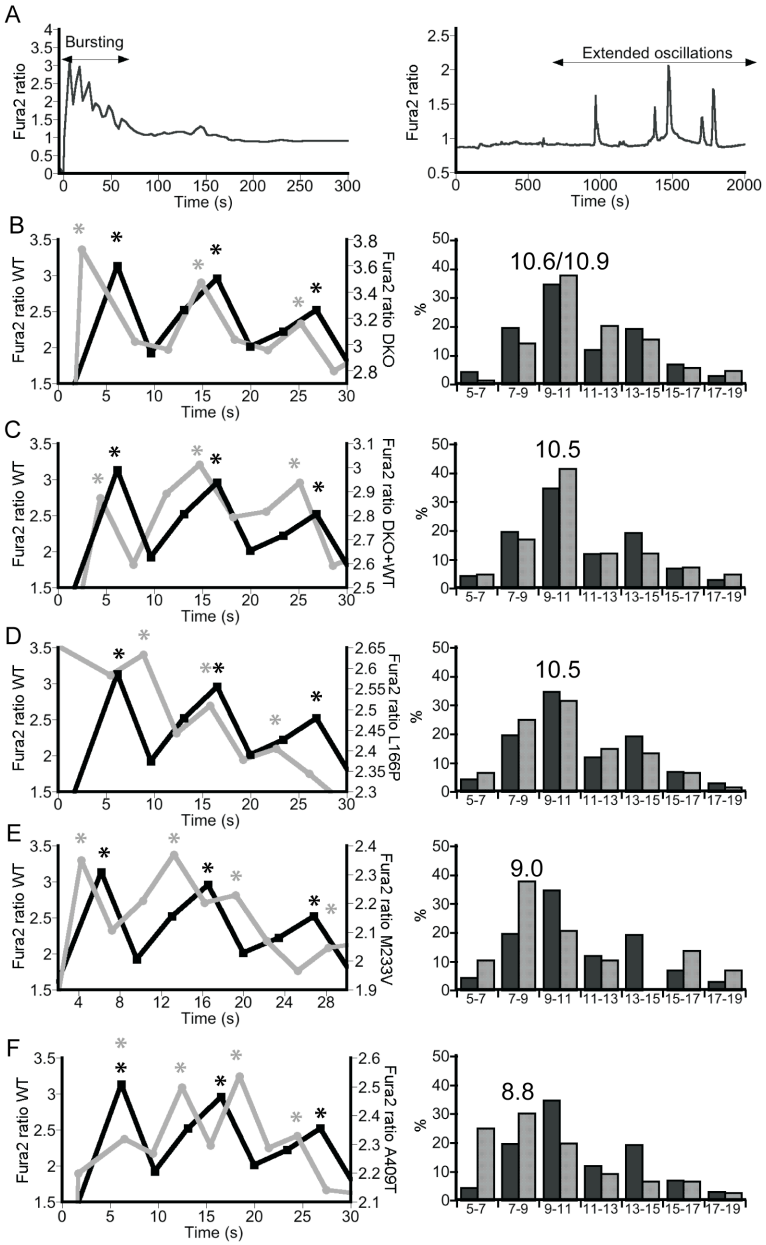

Figure 2.8 Effect of mutations in PS1 on kinetics of ER Ca^{2+} release. (A) Cells exhibited either a burst in Ca^{2+} from the ER (left) or, less frequently, irregular extended Ca^{2+} oscillations (right) in response to ATP. Bursting activity was examined to compare mutations in these studies. (B – F) Representative traces of Ca^{2+} bursts (left) compare differences between WT (black) and transfected DKO (gray) in initial release of Ca^{2+} from the ER. Peaks of each spike are indicated by an asterisk. Histograms (right) show the distribution of Ca^{2+} spike periods compared to WT (black; n = 274, 34 cells, 3 exps) for (B) DKO (n = 211, 25 cells, 3 exps), (C) DKO + WT (n = 41, 5 cells, 3 exps), (D) DKO + L166P (n = 60, 5 cells, 4 exps), (E) DKO + M233V (n = 29, 4cells, 2 exps) and (F) DKO + A409T (n = 76, 6 cells, 2 exps) after treatment with 5 μM ATP. The median period for spiking is given above the histogram.

from peak to peak) for every cell that exhibited repetitive spiking (see experimental section). These data are presented in the histograms (**Figure 2.8**, right side) which show that cells expressing M233V or A409T exhibit a greater percentage of faster spike periods (histogram shifted to lower time intervals). Given that many downstream effectors of Ca^{2+} signaling "read-out" both the amplitude and frequency of the Ca^{2+} signal, the fact that mutations in PS1 can alter the kinetics of ER Ca^{2+} release may play a significant role in eliciting Ca^{2+} dyshomeostasis.

2.4 Discussion

Calcium homeostasis is tightly regulated by dynamic interplay between channels, pumps, and transporters that control Ca^{2+} levels in the ER, mitochondria, and cytosol. Genetically targeted sensors provide a powerful way of monitoring Ca^{2+} directly within each of these locales. This feature may be especially important because cells appear to be adept at compensating for perturbations to Ca^{2+} homeostatic mechanisms. If a perturbation, such as expression of mutant PS1, alters Ca^{2+} homeostasis the cell may compensate to minimize the perturbation, such as upregulating or downregulating channels or pumps. Indeed, in this study we found that the ER Ca^{2+} leak is altered by changes in ER Ca^{2+} levels such that lower ER Ca^{2+} levels lead to a decreased leak rate. This compensation is dynamic and could be reversed by elevating ER Ca^{2+} levels using DAPT. These results reinforce the importance of directly measuring $[Ca^{2+}]_{ER}$ to investigate ER Ca^{2+} homeostasis, as measurement of cytosolic Ca^{2+} to interpret ER load may be confounded by compensatory changes in channels and pumps that exist to maintain cytosolic Ca^{2+}.

Deletion of PS1 caused a significant increase in ER Ca^{2+}, consistent with some, but not all studies which have measured Ca^{2+} directly within the ER. There are three methods for

measuring Ca^{2+} within the ER: the D1ER sensor employed in this study, the low affinity Ca^{2+} indicator MagFura-2, and an ER-targeted aequorin-based sensor. It should be noted that a fourth method has been used to indirectly infer the ER Ca^{2+} load by measuring how much Ca^{2+} is released into the cytosol upon treatment with the ionophore ionomycin [1, 12]. This approach suffers from two drawbacks: it measures release from all internal compartments, not just the ER, and it cannot account for potential differences in cytosolic clearance mechanisms that may arise if Ca^{2+} homeostasis is perturbed. Given that PS1 alters many aspects of Ca^{2+} homeostasis, we suspect direct measurement of ER Ca^{2+} is likely to be a more accurate measure of the ER Ca^{2+} load and for this, D1ER possesses some advantages. First, both MagFura-2 and aequorin require additional cellular manipulation for loading the sensors into internal compartments. MagFura-2 relies on permeabilization, ER store depletion, and addition of MgATP to activate store re-filling, while aequorin requires ER store depletion, reconstitution of cells with coelenterazine, and store re-filling upon addition of extracellular Ca^{2+}. Second, both of these approaches infer resting Ca^{2+} levels by monitoring store re-filling after depletion, which may be complicated by differences in SERCA pump activity. For example, in a study using MagFura-2, Cheung et al. found that untransfected DT40 cells filled to a higher level than cells transfected with PS1, consistent with our findings for DKO vs. WT cells [3]. However, two studies using ER-targeted aequorin found that PS1 deficient cells filled to a lower level than cells containing PS1 [13, 20]. These experiments inadvertently rely on SERCA activity for measuring ER load, and one interpretation of the reported discrepancies is that different conditions for re-loading intracellular stores may promote differential re-filling of the ER.

By using the genetically encoded Ca^{2+} sensor D1ER, we were able to directly monitor ER Ca^{2+} levels and dynamics, including leak rates of Ca^{2+} out of the ER and uptake into the ER. We

discovered that fAD-associated mutations in PS1 differentially affect levels of Ca^{2+} in the ER and leak from the ER. This helps put into context the numerous, but often conflicting studies that have examined individual mutations in PS1. Here we found one mutation that appeared to increase both ER Ca^{2+} and the leak rate (V94) and two that decreased ER Ca^{2+} and the leak rate (M233V and A409T). However, a number of mutations had no effect on ER Ca^{2+} levels, further suggesting that there is not a universal phenotype for perturbation of ER Ca^{2+} by mutant PS1. Unfortunately, the mechanism(s) by which PS1 mutations alter ER Ca^{2+} levels remain enigmatic. In particular, changes in the leak rate appeared to be a consequence rather than a cause of altered ER Ca^{2+}. Likewise, PS1 increases SERCA activity, but leads to a decrease in ER Ca^{2+} load. Intriguingly, inhibition of the proteolytic activity of PS1 (as part of the gamma-secretase complex) affected cells expressing mutant PS1 but not WT PS1 strongly suggesting there are multiple mechanisms by which PS1 can influence ER Ca^{2+}. Combined, these factors (compensatory changes and the possibility of multiple mechanisms) make it difficult for us to define the molecular mechanism by which fAD causing mutations in PS1 alter ER Ca^{2+}, and thus these mechanism(s) remain elusive. On the other hand, our results do help provide a framework for understanding the sometimes conflicting studies on PS1 and fAD-causing mutations. In particular, they highlight that different mutations in PS1 give rise to different Ca^{2+} phenotypes and that many aspects of Ca^{2+} regulation may be altered in mutant PS1 cells, some of which are compensatory changes that result from PS1 expression.

The two mutations that lead to a significant decrease in ER Ca^{2+} (M233V and A409T) also gave rise to altered kinetics of Ca^{2+} release from the ER upon ATP stimulation, exhibiting an increase in the frequency of Ca^{2+} bursting. To our knowledge, M146L is the only other PS1 mutation examined for its ability to influence release kinetics. Cheung, *et al*.[3] found that M146L

lead to enhanced Ca^{2+} oscillation frequency and this was due to altered gating of the IP_3R. Interestingly, this mutant also gave rise to a lower ER Ca^{2+} load. Our results are consistent with this finding, further supporting the notion that PS1 interacts with and modulates the IP_3R. Given that release of Ca^{2+} from the ER results in signals that are decoded by the cell to control cellular function, an important next step will be to identify the consequences of these altered signals and what role, if any, these changes play in Alzheimer's disease. A growing body of evidence including the results presented here, indicate that in addition to modulating ER Ca^{2+} levels, fAD-causing mutations in PS1 contribute to an overall dysregulation of Ca^{2+}, including alteration of fundamental Ca^{2+} signals.

In summary, our study demonstrates the power of an ER-targeted Ca^{2+} sensor by illustrating that the sensor can be used to directly monitor Ca^{2+} levels, Ca^{2+} leak from the ER, and uptake into the ER. Overall, we show that mutations in PS1 give rise to numerous and varied changes in Ca^{2+} which we hope will provide a framework for interpreting reports on ER Ca^{2+} in AD as well as other diseases.

2.5 Acknowledgements

We would like to thank the following sources for financial support: University of Colorado Signaling and Cell Cycle Regulation Training Grant (NIH T32 GM08759), NIH GM084027 to A. E. P., and the University of Colorado.

2.6 Experimental Procedures

Cell culture and transfections. Wild type (WT) and presenilin-1/2- double knock out (DKO) mouse embryonic fibroblasts (MEFs) were obtained from Dr. Bart de Strooper,

Katholieke Universiteit Leuven, Leuven, Netherlands [17, 18] and were cultured in DMEM supplemented with 10% (v/v) FBS and 1% (v/v) penicillin and streptomycin. Due to the propensity for MEFs to accumulate mutations over time, cells were only used through passage number 20. DKO cells were reconstituted with either mutant or WT PS1 by transient transfection using TransIT (Mirus), and the resulting Ca^{2+}-phenotype was compared to WT MEF cells. Cells were imaged 24-48 h post-transfection.

Cloning and constructs. For PS1 constructs, the I-467 isomer of human PS1 (NM_000021) was purchased from OriGene Technologies, Inc. AD-causing mutations were generated using QuikChange® Site-Directed Mutagenesis (Stratagene). PS1 variants were cloned into pRex-IRES-GFP and pRex-IRES-mCherry vectors (Dr. Xuedong Liu, University of Colorado-Boulder) between BamHI and NotI sites. These vectors encode an internal ribosomal entry site between the PS1 and fluorescent protein gene, enabling the selection of PS1-expressing cells on the basis of fluorescence.

Western blotting. Cells transfected with mutant PS1 in the pRex-IRES-GFP vector were washed in ice-cold Phosphate Buffered Saline (PBS) before being scraped into 1 mL PBS and spun down at 3000 *g* for 5 minutes. To lyse cells, pellets were re-suspended in STEN buffer (50mM Tris-HCl, pH 7.6, 150mM NaCl, 2mM EDTA, 1% TritonX-100 and 0.2% NP-40, plus protease inhibitor cocktail) and incubated on ice for 30 minutes. Lysis suspensions were spun down at 21000 *g* for 20 minutes to remove cell debris. Total protein concentration was determined using the BCA Protein Assay kit (Pierce) prior to separation on a 4 - 20% Tris-HEPES-SDS polyacrylimide gel and transfer to a PVDF membrane. Membranes were blocked in Tris-buffered saline supplemented with 0.1% (v/v) Tween-20 (TBS-T) and 5% (w/v) milk for 1 h at room temperature. To probe membranes, we used the anti-PS1 antibody APS18 (3µg/mL;

Novus Biologicals) and anti-β-actin antibody (1:5000; Sigma). Proteins were detected by incubating in a Rabbit anti-mouse HRP conjugated secondary antibody (Zymed). Although we attempted numerous times, we could not get the APS18 antibody to detect the endogenous mouse PS1 in MEF cells. Therefore we cannot directly compare the level of human PS1 in reconstituted cells, to endogenous levels of mouse PS1.

Instrumentation for fluorescence microscopy. For imaging experiments, cells were washed and placed in Hank's Balanced Salt Solution with HEPES (20mM HEPES, 1X HBSS (Gibco), and 2g/L D-glucose, pH 7.2) or Ca^{2+}-free HHBSS (20mM HEPES, 1X HBSS without Ca^{2+}, Mg^{2+}, or sodium bicarbonate, 2g/L D-glucose, 490μM $MgCl_2$, 450μM $MgSO_4$, pH 7.2). Imaging experiments were conducted at room temperature (25 ºC). Fluorescence imaging was performed on an Axiovert 200M wide-field microscope (Zeiss) equipped with a Lambda 10-3 filter changer (Sutter Instruments) and Cascade 512B camera (Photometrics) for rapid acquisition of ratio images. Images were acquired using METAFLUOR software (Universal Imaging). All experiments were performed using a 1.3 NA 40X objective (Zeiss). The filter combinations used were as follows: Fura-2: 340/26 (excitation), 380/10 (excitation), 535/40 (emission), 455 (dichroic); YFP FRET: 430/24 (excitation), 535/25 (emission), 455 (dichroic); CFP: 430/24 (excitation), 470/24 (emission), 455 (dichroic); YFP: 495/10 (excitation), 535/25 (emission), 515 (dichroic); GFP: 480/20 (excitation), 510/20 (emission), 495 (dichroic); mCherry: 577/20 (excitation), 630/60 (emission), 595 (dichroic).

Calcium imaging. MEF DKO cells reconstituted with PS1 (WT or mutant) were identified by mCherry or GFP fluorescence. In general we selected cells expressing a similar amount of mCherry (or GFP) fluorescence as this would indicate a similar amount of PS1

expression. Over the range of intensities, we did not see a correlation between expression level (as assessed by mCherry or GFP) and calcium phenotypes.

For Fura-2 studies, cells were incubated at room temperature with 5μM Fura-2-AM and 3μM Pluronic® F-127 (Invitrogen) for 45 minutes followed by a 15 minute incubation in 1 mL HHBSS to allow for cleavage of the AM-ester. Cells were placed in fresh HHBSS (1 mL) before imaging. Calcium release from the ER was induced by 5 μM ATP (Sigma). At the end of each experiment, Fura-2 was calibrated by adding 5 mM EGTA and 5 μM ionomycin to obtain an R_{min} before adding 5 μM ionomycin and 10 mM Ca^{2+} to obtain an R_{max}. Concentrations of Ca^{2+} were determined using the formula $[Ca^{2+}] = K_d[(R_{max}-R)/(R-R_{min})]*S_f/S_b$, where K_d is 220nM, R is the ratio of emission intensity at 535 nm upon excitation at 340 nm divided by the emission intensity at 535 nm upon excitation at 380 nm at each time point, S_f is the emission intensity upon excitation at 380nm in the Ca^{2+}-depleted state, and S_b is the emission intensity upon excitation at 380nm in the maximum Ca^{2+} state [21]. R_{max}, R_{min}, S_f, and S_b were determined individually for each cell. All images were background corrected prior to determining the ratio (R).

For studies using D1ER, cells were transfected 48 h prior to imaging. Cells were either treated with 4 μM thapsigargin or 3 μM 2,5-Di-(*t*-butyl)-1,4-hydroquinone (tBHQ) (Calbiochem) in Ca^{2+}-free HHBSS. These concentrations were chosen to obtain robust release of Ca^{2+} from the ER. For SERCA activity experiments, cells were washed in Ca^{2+}-free HHBSS to remove tBHQ before adding Ca^{2+}. The D1ER sensor was calibrated in cells at the end of each experiment using 5 μM ionomycin and 5 mM EGTA to obtain an R_{min}. The FRET ratio (R) is proportional to the amount of Ca^{2+} and is defined as the emission intensity in the FRET channel (CFP excitation, YFP emission) divided by the emission intensity in the CFP channel (CFP

excitation, CFP emission). We attempted to find the maximum ratio of the sensor (R_{max}) when saturated with Ca^{2+} using established methods [22]; however, the cells did not survive the calibration procedure. Because R_{max} is necessary to convert the FRET ratio into a $[Ca^{2+}]$, we instead report the ΔR ($R- R_{min}$), which is proportional to $[Ca^{2+}]$ and allows comparison of the relative amount of Ca^{2+} in cells expressing the various PS1 mutants. We find this is more accurate than simply comparing R because it incorporates the calibration for R_{min} in each individual cell. All intensities were background corrected before ratioing.

Analysis of calcium spiking. To quantify the period between individual Ca^{2+} spikes, the broad Ca^{2+} decay curves were fit to a single exponential, which was then subtracted from the response curve. The obtained residuals correspond to the oscillatory component of the signal (**Figure 2.9**). The spiking period was then calculated using the peak finding routine in IGOR Pro (Wavemetrics Inc.). The number of spikes in each time period was normalized to the total number of spikes to obtain the percent of spikes that fell in each time period. The total number of spikes for each cell condition was as follows: DKO 211 spikes (25 cells from 3 exps); WT 274 spikes (34 cells from 3 exps); DKO + WT 41 spikes (5 cells from 3 exps); DKO + L166P 60 spikes (5 cells from 4 exps); DKO + M233V 29 spikes (4 cells from 2 exps); DKO + A409T 76 spikes (6 cells from 2 exps). Because images were acquired every 3 sec oscillations with a period faster than 6 sec could not be measured due to the Nyquist criterion.

Statistical Analysis. Statistical analysis on data was performed using Kaleidagraph 4.0 (Synergy Software). Data are represented as the mean ± SEM. Differences between the means were compared using an ANOVA with Student-Newman-Keuls post-hoc test to determine statistical significance ($P < 0.05$).

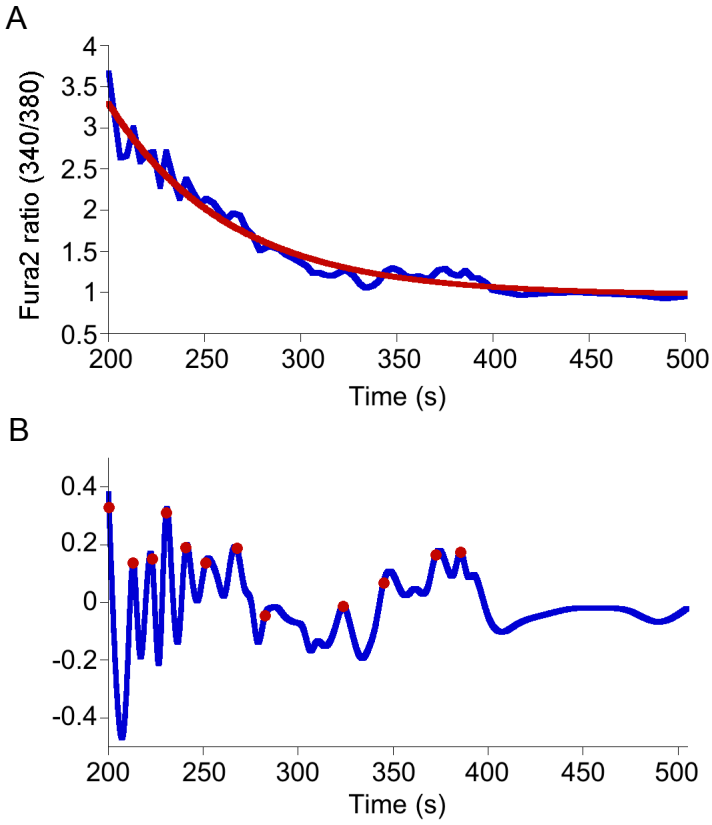

Figure 2.9 Analysis of calcium spiking data using IGOR Pro. (A) Representative curve (blue) fit to an exponential decay (red), $A(t) = A_0 e^{-(t - t_0)k}$. (B) The exponential decay fit from *A* is subtracted from the data curve to enhance the peaks. Peak values (depicted by red dots) are determined using the Peak AutoFind macro in IGOR Pro.

Cloning and constructs. To confirm gamma-secretase activity in individual cells, a fluorescently-tagged APP substrate (termed C99-mCherry) was designed. C99-mCherry was generated by PCR amplification of the APP signal sequence (residues 1 – 21) and its post β-secretase cleaved C-terminus (residues 653 – 751) from Gene Pool™ cDNA Human Normal Adult Brain library (Invitrogen). The signal sequence was ligated between HindIII and KpnI into the multiple cloning site of pcDNA3 (Invitrogen). The C99-APP fragment was subsequently ligated into the same vector between KpnI and NotI. The mCherry fluorescent protein was ligated into the APP-pcDNA3 vector between NotI and XbaI in order to tag the C-terminus of C99-APP.

Aβ ELISA. MEF cells were doubly transfected with full-length APP and PS1 mutants 72 hours prior to carrying out the assay and media was changed 18 hours post-transfection. Analysis was performed using the BetaMark x-40 and BetaMark x-42 ELISA Kits (Covance). Secreted Aβ protein in the media was concentrated using Amicon Ultra 3K centrifugal filter devices (Millipore). Samples diluted 1:2 in working incubation buffer were run in duplicate according to manufacturer recommended protocol.

2.7 References

1 Tu, H. *et al.* Presenilins form ER Ca^{2+} leak channels, a function disrupted by familial Alzheimer's disease-linked mutations. *Cell* **126**, 981-993 (2006).

2 Green, K. N. *et al.* SERCA pump activity is physiologically regulated by presenilin and regulates amyloid beta production. *The Journal of cell biology* **181**, 1107-1116 (2008).

3 Cheung, K. H. *et al.* Mechanism of Ca^{2+} disruption in Alzheimer's disease by presenilin regulation of InsP3 receptor channel gating. *Neuron* **58**, 871-883 (2008).

4 Smith, I. F., Hitt, B., Green, K. N., Oddo, S. & LaFerla, F. M. Enhanced caffeine-induced Ca^{2+} release in the 3xTg-AD mouse model of Alzheimer's disease. *Journal of neurochemistry* **94**, 1711-1718 (2005).

5 Chan, S. L., Mayne, M., Holden, C. P., Geiger, J. D. & Mattson, M. P. Presenilin-1 mutations increase levels of ryanodine receptors and calcium release in PC12 cells and cortical neurons. *The Journal of biological chemistry* **275**, 18195-18200 (2000).

6 Sherrington, R. *et al.* Cloning of a gene bearing missense mutations in early-onset familial Alzheimer's disease. *Nature* **375**, 754-760 (1995).

7 Duff, K. *et al.* Increased amyloid-beta42(43) in brains of mice expressing mutant presenilin 1. *Nature* **383**, 710-713 (1996).

8 Marx, J. Alzheimer's disease. Fresh evidence points to an old suspect: calcium. *Science (New York, N.Y* **318**, 384-385 (2007).

9 LaFerla, F. M. Calcium dyshomeostasis and intracellular signalling in Alzheimer's disease. *Nat Rev Neurosci* **3**, 862-872 (2002).

10 Bezprozvanny, I. & Mattson, M. P. Neuronal calcium mishandling and the pathogenesis of Alzheimer's disease. *Trends in neurosciences* **31**, 454-463 (2008).

11 Stutzmann, G. E., Caccamo, A., LaFerla, F. M. & Parker, I. Dysregulated IP3 signaling in cortical neurons of knock-in mice expressing an Alzheimer's-linked mutation in presenilin1 results in exaggerated Ca^{2+} signals and altered membrane excitability. *J Neurosci* **24**, 508-513 (2004).

12 Nelson, O. *et al.* Familial Alzheimer disease-linked mutations specifically disrupt Ca^{2+} leak function of presenilin 1. *The Journal of clinical investigation* **117**, 1230-1239 (2007).

13 Zatti, G. *et al.* Presenilin mutations linked to familial Alzheimer's disease reduce endoplasmic reticulum and Golgi apparatus calcium levels. *Cell calcium* **39**, 539-550 (2006).

14 Leissring, M. A. *et al.* Capacitative calcium entry deficits and elevated luminal calcium content in mutant presenilin-1 knockin mice. *The Journal of cell biology* **149**, 793-798 (2000).

15 Leissring, M. A., Paul, B. A., Parker, I., Cotman, C. W. & LaFerla, F. M. Alzheimer's presenilin-1 mutation potentiates inositol 1,4,5-trisphosphate-mediated calcium signaling in Xenopus oocytes. *Journal of neurochemistry* **72**, 1061-1068 (1999).

16 Palmer, A. E., Jin, C., Reed, J. C. & Tsien, R. Y. Bcl-2-mediated alterations in endoplasmic reticulum Ca^{2+} analyzed with an improved genetically encoded fluorescent sensor. *Proceedings of the National Academy of Sciences of the United States of America* **101**, 17404-17409 (2004).

17 Herreman, A. *et al.* Presenilin 2 deficiency causes a mild pulmonary phenotype and no changes in amyloid precursor protein processing but enhances the embryonic lethal phenotype of presenilin 1 deficiency. *Proceedings of the National Academy of Sciences of the United States of America* **96**, 11872-11877 (1999).

18 Herreman, A. *et al.* gamma-Secretase activity requires the presenilin-dependent trafficking of nicastrin through the Golgi apparatus but not its complex glycosylation. *Journal of cell science* **116**, 1127-1136 (2003).

19 Berridge, M. J., Bootman, M. D. & Roderick, H. L. Calcium signalling: dynamics, homeostasis and remodelling. *Nat Rev Mol Cell Biol* **4**, 517-529 (2003).

20 Kasri, N. N. *et al.* Up-regulation of inositol 1,4,5-trisphosphate receptor type 1 is responsible for a decreased endoplasmic-reticulum Ca^{2+} content in presenilin double knock-out cells. *Cell calcium* **40**, 41-51 (2006).

21 Grynkiewicz, G., Poenie, M. & Tsien, R. Y. A new generation of Ca^{2+} indicators with greatly improved fluorescence properties. *The Journal of biological chemistry* **260**, 3440-3450 (1985).

22 Palmer, A. E. & Tsien, R. Y. Measuring calcium signaling using genetically targetable fluorescent indicators. *Nature protocols* **1**, 1057-1065 (2006).

Chapter 3

Salmonella invasion induces a Ca^{2+} influx through TRPM7 channels dependent on SopB phosphatase activity

Janet E. McCombs, Schuyler B. VanEngelenburg, Weston W. Blakeslee, Amy E. Palmer.

3.1 Introduction

Salmonella enterica serovar Typhimurium is an invasive bacterial pathogen causing food-born illness and gastroenteritis. It is able to infect phagocytic as well as non-phagocytic cells through the use of a highly sophisticated type III secretion system (TTSS). The so-called TTSS1 is encoded by *Salmonella* pathogenicity island-1 (SPI-1) on the chromosome and initiates invasion by secreting *Salmonella* effector proteins through a needle-like translocon inserted into host cell membranes [1]. Once inside the host cell, effectors hijack intracellular signaling pathways to initiate actin polymerization, leading to a dramatic rearrangement of the membrane architecture and engulfment of *Salmonella* [2-4]. This macropinocytosis forms the *Salmonella* containing vacuole (SCV), the intracellular niche of *Salmonella*. A second TTSS, encoded by SPI-2 [1], is activated within the SCV, and the resulting TTSS2 effector proteins are responsible for maturation of the SCV, recruiting a number of late endosomal and early lysosomal proteins to the SCV membrane in order to protect against host cell mediated degradation [5,6]. This process is essential for *Salmonella* survival and replication within the host cell.

The course of *Salmonella* invasion has been linked to changes in intracellular concentrations of Ca^{2+}, an important and vital signaling ion in cells. Ca^{2+} signals impact a number of cellular pathways; therefore, it is essential to determine the mechanisms by which *Salmonella* invasion may induce these signals, influence their nature, and what consequences they may have for infection. To date, invasion has been demonstrated to cause a rapid increase in inositol phosphate pools, which are able to mobilize Ca^{2+} from intracellular stores [7], as well as intracellular Ca^{2+} when measured by bulk assays [8,9]. In addition, influx of Ca^{2+} from *Salmonella*-induced membrane injury was shown to facilitate membrane repair [10], while depletion of intracellular Ca^{2+} impaired bacterial uptake [7]. Despite almost two decades since these

discoveries, the origin and mechanism of intracellular Ca^{2+} increases upon *Salmonella* invasion has not been well characterized.

Cellular Ca^{2+} homeostasis is a tightly regulated and highly coordinated process. Steady-state levels of Ca^{2+} are maintained through the action of a number of channels and pumps in the plasma and organelle membranes [11]. During a signaling event, these pumps shape Ca^{2+} release from intracellular stores to activate downstream processes including gene transcription, actin polymerization, and endocytosis. Given the importance of Ca^{2+} in multiple pathways, it is possible that *Salmonella* could manipulate and utilize host cell Ca^{2+} signaling during invasion. In fact, *Salmonella* effectors are able to modulate levels and distribution of cell phosphoinositides [3,12-14], the precursors to second messengers such as diacylglycerol (DAG) and inositol-1,4,5-trisphosphate (IP_3), which in turn impact host cell Ca^{2+}. Effector modulation of phosphoinositides is essential for the actin rearrangement that causes ruffles as well as SCV biogenesis [3,14,15]. Thus, modulation of Ca^{2+} signaling has the ability to affect both invasion and replication of *Salmonella*.

To define the origin and nature of the Ca^{2+} elevation, we examined *Salmonella* invasion of HeLa cells at the single cell level. We found cells displayed a localized increase in Ca^{2+} at the site of invasion followed by a more general "global" release. Characterization of this initial increase found that the *Salmonella* effector SopB was able to initiate a Ca^{2+} influx through the transient receptor potential melastatin related 7 (TRPM7) Ca^{2+} channel in a manner dependent on its phosphatase activity. This Ca^{2+} rise increased *Salmonella* invasion efficiency, while replication and SCV maturation were unaffected by the Ca^{2+} flux, though were found to depend on the presence of TRPM7 channels in cells. Overall, we suggest a mechanism whereby

Salmonella is able to modulate host cell Ca^{2+} signaling pathways in order to maximize its survival in cells.

3.2 Results

3.2.1 Invasion of host cells by *Salmonella* causes an increase in intracellular Ca^{2+}

While previous studies have shown a dependence of *Salmonella* invasion on intracellular Ca^{2+} [7-9], the nature and mechanism of this relationship remains uncharacterized. We therefore set out to define changes in Ca^{2+} homeostasis induced by invasion of individual cells with *Salmonella*. To do this, we utilized the small molecule Ca^{2+} indicator Fura-2. HeLa cells were stained with Fura-2 and treated with *Salmonella* strain SL1344 grown under SPI-1 inducing conditions (see Experimental Procedures). Invasion of the host cell by *Salmonella* triggered a rearrangement in the membrane architecture indicative of ruffling, followed by bacterial engulfment and membrane restoration. The majority of invasions (83 %) displayed an increase in Ca^{2+} at the site of ruffling in membrane-localized regions, followed by a global rise in Ca^{2+} (**Figure 3.1A** and **B**), which was likely a result of Ca^{2+}-induced Ca^{2+} release from intracellular stores. To verify that the Ca^{2+} rise was TTSS dependent, HeLa cells were treated with *Salmonella* lacking the effector InvA (Δ*InvA*), which is a prominent component of the TTSS translocon and regulates effector protein export [16], as well as with *E. coli*, which does not utilize a TTSS to invade HeLa cells. Neither treatment resulted in Ca^{2+} transients, and instead showed a minor gradual increase in baseline $[Ca^{2+}]_{cyt}$ over time (**Figure 3.2**). We suspect this baseline elevation could be due to lipopolysaccharide (LPS)-mediated activation of Toll-like receptors on the cell surface, as bacterial LPS has been shown to increase cytosolic free Ca^{2+}.

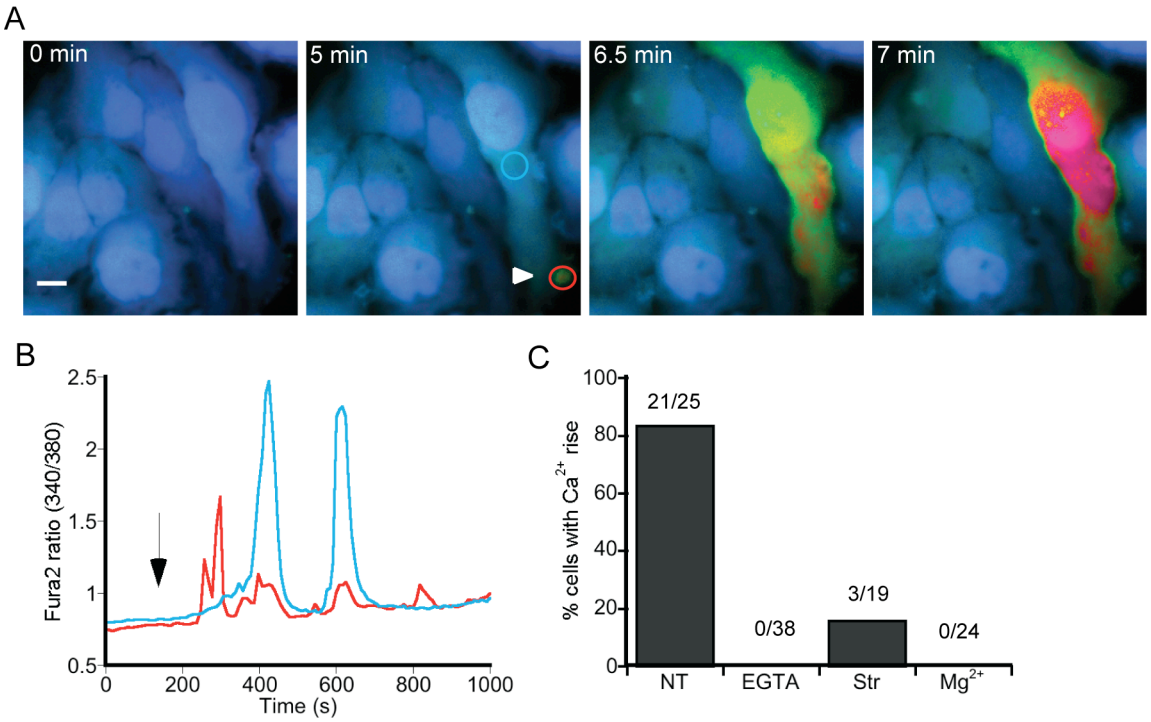

Figure 3.1 Ca^{2+} response in HeLa cells upon *Salmonella* invasion. (A) Pseudo-color ratiometric images of a cell at rest (left panel) before *Salmonella* invasion causes an initial rise in Ca^{2+} at the membrane (arrowhead, middle left panel) and subsequent rise throughout the cell (right two panels). Scale bar is 10 μm. Regions from *B* are encircled. (B) Time course of the invasion depicted in *A*. The Fura-2 ratio is shown as a function of time. The red trace follows changes in Ca^{2+} at the site of invasion, and the blue trace shows changes within the cytosol. (C) Percent of cells displaying an increase in cellular calcium upon invasion for the indicated pharmacological treatments. Number of cells responding is given above each bar. NT, no treatment. Str, streptomycin.

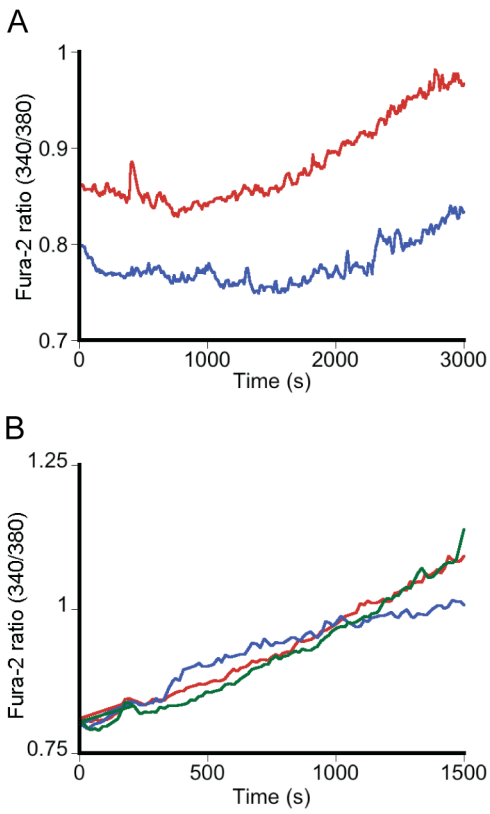

Figure 3.2 Ca^{2+} rise over time independent of TTSS. Time courses of invasions performed with (A) Δ*InvA Salmonella*, and (B) *E. coli*. Each color represents an individual cell.

To characterize whether the *Salmonella*-induced rise in Ca^{2+} originated from an influx of extracellular Ca^{2+} or release of intracellular stores, invasions were carried out in Ca^{2+}-free media supplemented with 2 mM Ethylene glycol-bis-(2-aminoethyl)-N,N,N',N'-tetraacetic acid (EGTA) to deplete extracellular Ca^{2+}. Treatment with EGTA completely abrogated the *Salmonella*-induced Ca^{2+} transients (**Figure 3.1C**), indicating the Ca^{2+} signals originated from extracellular sources. Ca^{2+} entry upon invasion could occur via activation of a plasma membrane Ca^{2+} channel or through a *Salmonella*-induced defect or pore in the plasma membrane. To distinguish these possibilities, we sought to inhibit Ca^{2+} entry through membrane channels. Treatment of cells with 1 mM $LaCl_3$ to inhibit Ca^{2+} influx through membrane channels resulted in no increase of Ca^{2+} upon invasion, implicating Ca^{2+} channels in the Ca^{2+} rise (data not shown). Recently, Wei, et al. found the membrane Ca^{2+} channel TRPM7 to be activated by membrane stretch in cell migration [17]. Given membrane ruffling upon invasion of cells by *Salmonella*, we hypothesized this movement could be akin to membrane movement in cell migration and thus able to activate TRPM7. TRPM7 is characterized by its sensitivity to streptomycin, a stretch-activated Ca^{2+} channel (SACC) inhibitor, and high extracellular Mg^{2+} [18-20]. When treated with *Salmonella* in the presence of 200 μM streptomycin, only 3 out of 19 cells (~16 %) exhibited a rise in Ca^{2+} upon invasion, a five-fold decrease from untreated cells (**Figure 3.1C**), suggesting inhibition of the mechanism for Ca^{2+} influx. Similarly, none of the 24 cells treated with 10 mM Mg^{2+} in HHBSS gave an observable Ca^{2+} response at the site of invasion (**Figure 3.1C**). Ca^{2+} influx upon *Salmonella* invasion likely occurs through a plasma membrane channel and pharmacological inhibition implicates TRPM7 as a potential candidate for the source of this influx at the site of invasion.

3.2.2 Knockdown of TRPM7 Ca^{2+} channels abrogates the Ca^{2+} response

To further investigate the roll of TRPM7 in *Salmonella*-induced Ca^{2+} influx, two shRNAs, designated shRNA1 and shRNA2, were designed to knock down the channel in HeLa cells. The shRNAs were transiently transfected into HeLa cells and confirmed by GFP fluorescence. Analysis by Western blot and RT-PCR revealed both shRNAs knocked down the channel with ~55 – 60 % efficiency (**Figure 3.3A**). An additional shRNA designed to be a control by scrambling 9 bp (designated scrambled control, SC) also partially knocked down channel expression (~37 % knockdown vs. 59 % and 55 % for shRNA1 and shRNA2, respectively). Upon *Salmonella* invasion and membrane ruffling, cells transiently expressing shRNA1 or shRNA2 exhibited a marked decrease in number of cells displaying a Ca^{2+} influx (30 % and 25 % responding, respectively). The scrambled control exhibited a small decrease in the number of invasions with Ca^{2+} influx (62 % responding compared to 83 % for standard invasion) (**Figure 3.3B**). This gradient in the percentage of cells that exhibited Ca^{2+} influx could be due to the relative levels of TRPM7, with untreated exhibiting a higher response and protein expression than scrambled control which was higher than shRNA treated cells. These data indicate the molecular basis for the Ca^{2+} influx observed upon invasion is likely due to influx of Ca^{2+} through TRPM7 channels.

3.2.3 Ca^{2+} influx through TRPM7 is necessary to maintain invasion efficiency.

Ca^{2+} signaling is essential for numerous cellular processes and functions. Notably, actin polymerization and vesicle trafficking are both regulated by Ca^{2+} and are essential for *Salmonella* invasion of cells [3,6]. Given the ability of *Salmonella* to hijack host cell signaling pathways, it seems probable bacteria could manipulate Ca^{2+} signaling once inside the cell or utilize Ca^{2+} dynamics to facilitate survival. To determine whether elevation of host cell Ca^{2+}

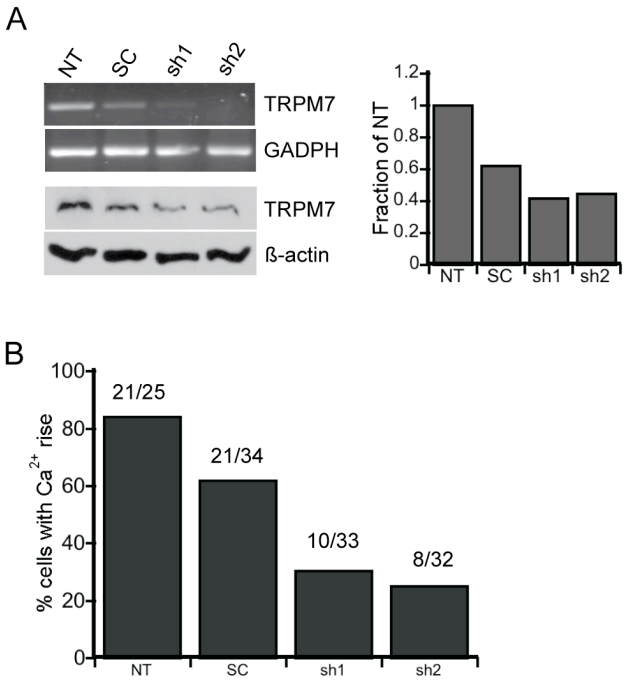

Figure 3.3 Influx of Ca^{2+} occurs through TRPM7 channels. (A) shRNA mediated knock-down of TRPM7 assayed by Western blot (top) and RT-PCR (bottom). Graph shows fraction of TRPM7 protein compared to NT. (B) Percent of cells displaying an increase in Ca^{2+} upon *Salmonella* invasion after transfection with the various shRNA constructs. Number of cells responding is given above each bar. NT, no treatment. SC, scrambled control. sh1, shRNA1. sh2, shRNA2.

impacts *Salmonella* invasiveness, we quantified the number of HeLa cells invaded, the number of bacteria internalized per cell, and the number of cells with multiple invasion sites. Briefly, cells were treated with EGTA or transfected with shRNA and invaded with mCherry labeled *Salmonella* to visualize intracellular bacteria. There was no difference in the number of HeLa cells invaded in the presence (no treatment, NT, and SC) or absence (EGTA treatment and sh2) of Ca^{2+} influx (**Figure 3.4A**). This was not surprising given that the Ca^{2+} elevation occurs upon membrane ruffling, after initiation of invasion. However, efficiency of invasion decreased for cells invaded in the absence of Ca^{2+} influx, with fewer bacteria per cell and fewer cells having multiple invasions (**Figure 3.4B** and **C**), indicating less bacteria were internalized in the absence of Ca^{2+}. Therefore, Ca^{2+} influx through TRPM7 channels appears to enhance invasion efficiency. Cells transfected with the scrambled shRNA had similar invasion efficiency as untreated cells. Since Ca^{2+} plays a role in membrane fusion [10,21,22], we hypothesized that the decrease in the number of internalized bacteria and in the number of invasions/cell could be due to deficiency in macropinocytosis of *Salmonella*. To test this, we developed an assay based on internalization of an extracellular dextran dye to quantify uptake of extracellular fluid upon invasion (**Figure 3.4D**). Conditions were optimized to minimize dextran internalization by endocytosis (**Figure 3.5A**). At sites of invasion, mCherry labeled *Salmonella* co-localized with the Cascade Blue dextran (**Figure 3.4D**). Abrogation of Ca^{2+} influx, by treatment with EGTA or knock down of TRPM7, caused a significant increase in the average fluorescence intensity, indicating a greater amount of internalized dye (**Figure 3.4E**). These results suggest a role for Ca^{2+} in macropinocytosis of *Salmonella*, as in the absence of Ca^{2+} influx, the macropinosome was able to hold more dye. We also observed that, when invasions were carried out in the absence of Ca^{2+}, membrane ruffles were not as compact as invasions in the presence of Ca^{2+}, and we suspect they

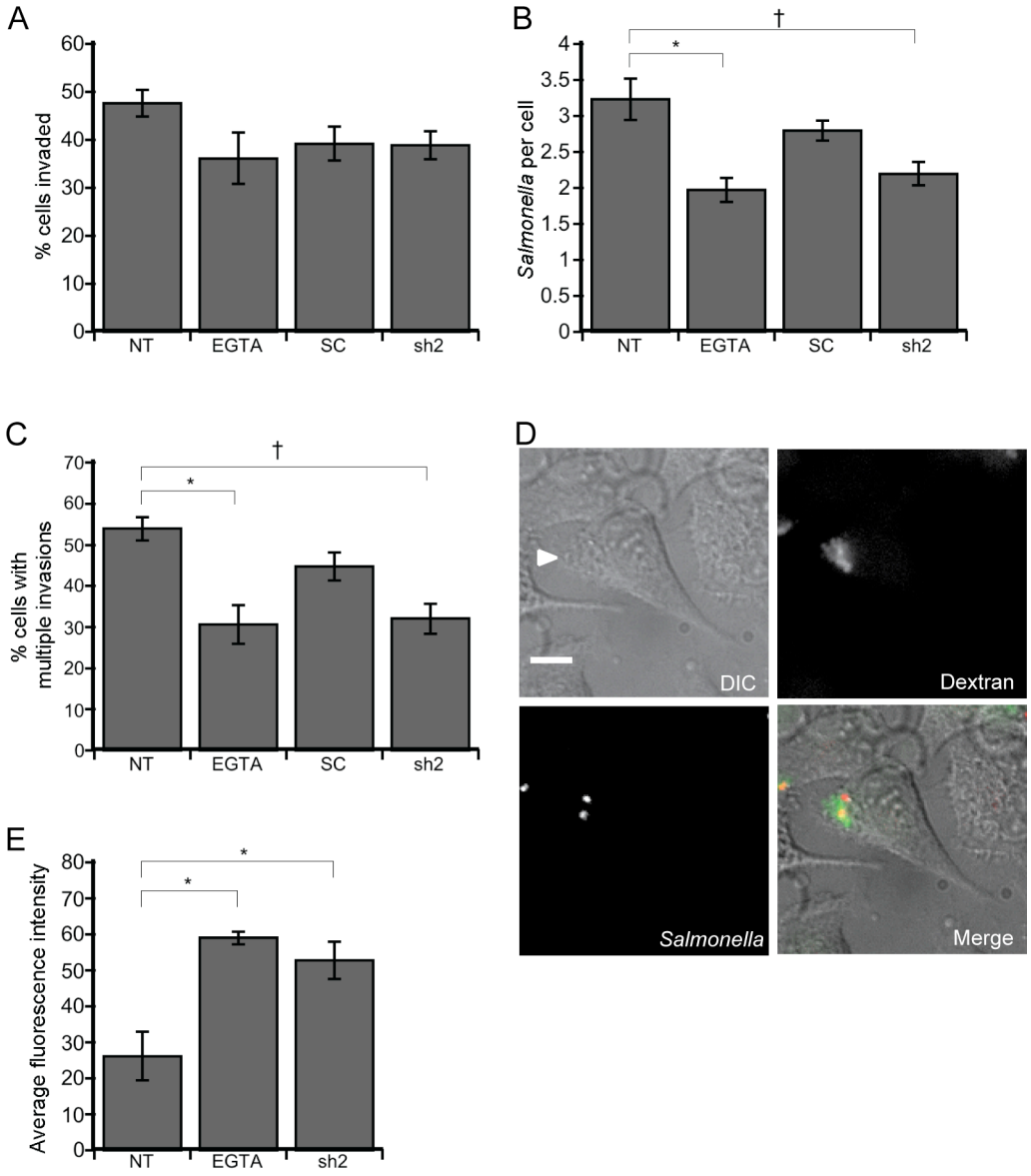

Figure 3.4 Ca^{2+} is necessary for efficient *Salmonella* invasion. (A) Percent of cells invaded by *Salmonella* after 1 hour for the indicated treatment. (B) The average number of *Salmonella* per invaded cell. Asterisk indicates $P < 0.009$. Cross indicates $P < 0.02$. (C) Percent of invaded cells with multiple invasions. Asterisk indicates $P < 0.01$. Cross indicates $P < 0.008$. For the invasion assay, > 100 cells were examined per triplicate. (D) Illustration of the membrane assay. The site of invasion (left), *Salmonella* (middle left) and dextran (middle right) localize to the same part of the cell, as shown in the overlay (right). Scale bar is 10 μm. (E) Average fluorescence intensity of Cascade Blue dextran at sites of invasion. Asterisk indicates $P < 0.02$. Uptake was measured in > 50 cells per triplicate. Error bars represent SEM. NT, no treatment. SC, scrambled control. sh2, shRNA2. M.O.I. = 50 for all experiments.

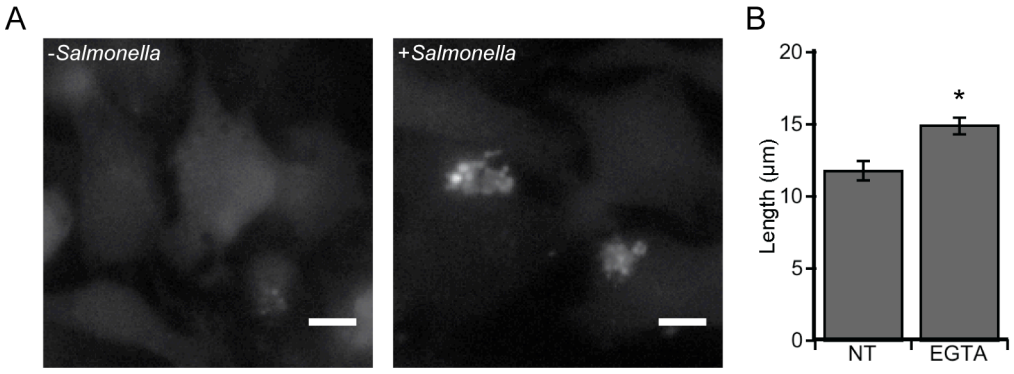

Figure 3.5 Membrane assay. (A) Representative images of cells in the absence (left) and presence (right) of *Salmonella* invasion when treated with Cascade Blue dextran dye. (B) Average length of membrane ruffles as measured using FM4-64 (see Experimental Procedures). Asterisk indicates $P < 0.002$. NT, no treatment. Scale bar is 10 μm.

could be less production as well (**Figure 3.5B**). The process of macropinocytosis is essential for setting up the SCV and establishing an intracellular niche in which *Salmonella* are able to replicate. Therefore, it is possible that Ca^{2+} influx through TRPM7 may affect *Salmonella* uptake, such that in the absence of Ca^{2+} influx, membranes are unable to cease ruffling causing ruffles to extend further along the membrane allowing for a greater uptake of extracellular fluid.

3.2.4 Replication of bacteria in the host cell is dependent on TRPM7.

Once *Salmonella* has invaded a host cell, establishment of a replicative niche is critical for productive infections [5,6]. This niche is facilitated by the development of the SCV, and perturbations in early SCV biogenesis can have a significant impact on downstream bacterial replication [12,13,15]. The SCV acquires a number of late endosomal and lysosomal proteins during maturation and this process is highly dependent on induction of SPI-2 effector proteins. These SPI-2 effectors establish the SCV, regulating its trafficking and formation of the extended network of *Salmonella* induced tubules (SITs) as well as ensuring the proper balance ions and pH within the vacuole [23-28]. Therefore, in order to establish downstream effects on *Salmonella* infection, we assayed for *Salmonella* replication, SPI-2 induction, Lamp1 recruitment and SIT formation 6 hours post-infection. Over 200 cells per phenotype were analyzed for each assay. Replication of bacteria, which begins 3 – 4 hours post-invasion [5], was determined by the presence of *Salmonella* clusters, defined as 5 or more bacteria in close proximity. In the absence of extracellular Ca^{2+}, the number of cells containing *Salmonella* clusters was similar to untreated and scramble control transfected cells (**Figure 3.6A**). In contrast, cells transfected with shRNA2 had fewer clusters of *Salmonella*, suggesting TRPM7 itself may facilitate bacterial replication independently of invasion-induced Ca^{2+} influx. A SPI-2 reporter system consisting of the mKate fluorescent protein driven by the promoter of the SPI-2 regulated *sseA* gene was developed to

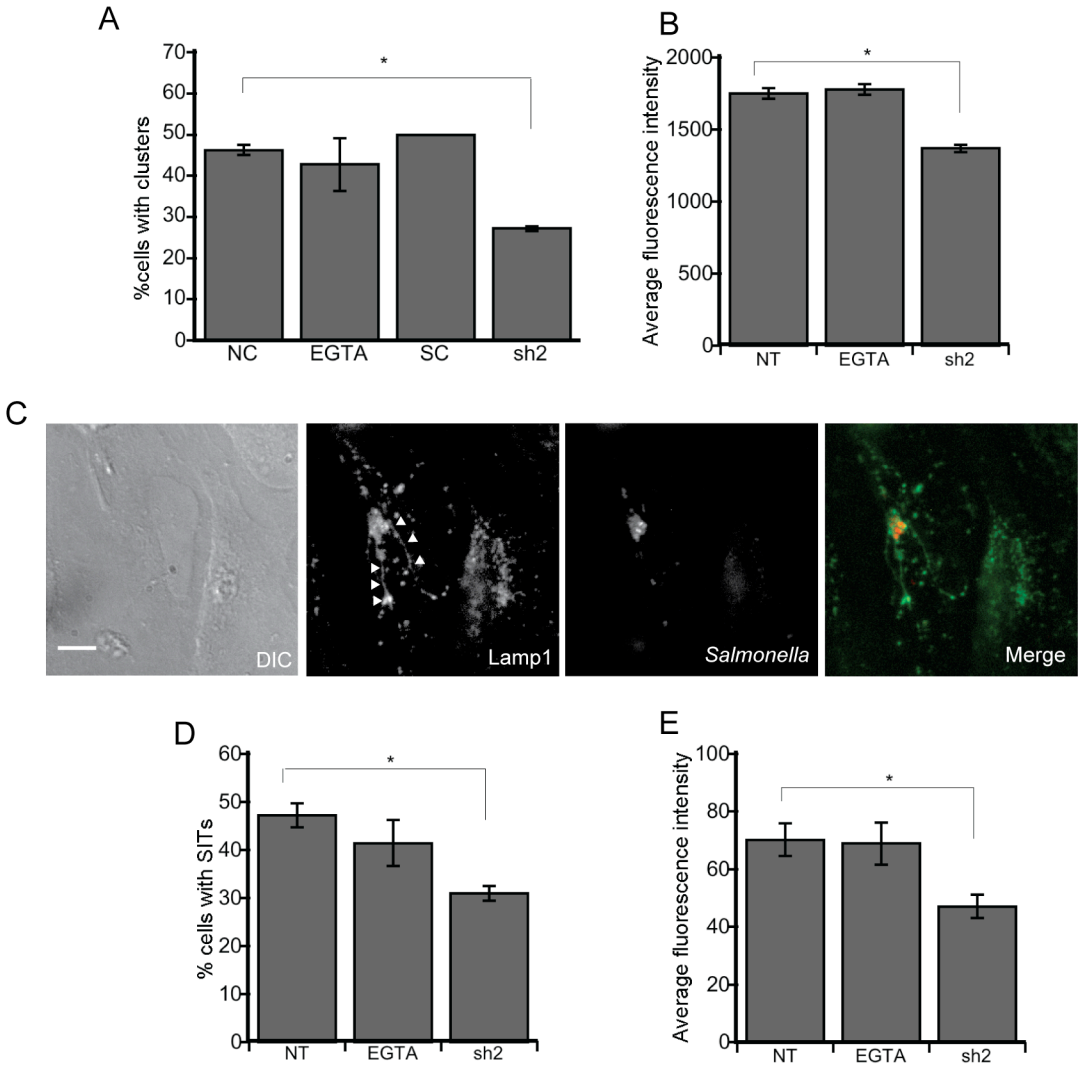

Figure 3.6 TRPM7 is required for *Salmonella* replication and survival. (A) Percent of invaded cells containing clusters of *Salmonella* 6 hours post-invasion. Asterisk indicates $P < 0.04$. Clusters were calculated in > 100 cells per triplicate. (B) Average mKate fluorescence intensity of *Salmonella* containing the SPI-2 reporter (see Experimental Procedures). Asterisk indicates $P < 0.05$. For each treatment, n > 60 per triplicate. (C) Illustration of the Lamp1 assay. Cells invaded with mCherry labeled *Salmonella* (middle left) were fixed and treated with an AlexaFluor 350 conjugated secondary antibody to label Lamp1 (middle). The overlay shows relative locations of Lamp1 and *Salmonella* (right). Scale bar is 10 μm. (D) Percent of invaded cells having SITs. Asterisk indicates $P < 0.003$. SITs were counted for > 50 cells per triplicate. (E) The average Lamp1 fluorescence intensity at sites of *Salmonella* clusters. Asterisk indicates $P < 0.04$. Lamp1 recruitment was calculated in > 100 cells per triplicate. Error bars represent SEM. NT, no treatment. SC, scrambled control. sh2, shRNA2. M.O.I. = 50 for all experiments.

address relative transcription of SPI-2 effectors. This assay revealed TRPM7 knockdown resulted in a reduction in SPI-2 induction, as measured by the average mKate fluorescence intensity in individual *Salmonella* (**Figure 3.6B**), suggesting TRPM7 is necessary for proper initiation of SPI-2 effector transcription.

During SCV maturation, late endosomal and lysosomal proteins are recruited to the SCV membrane to avoid host cell mediated degradation [5,6]. In addition, SITs, a membrane tubule network that is also enriched in lysosomal proteins, begins to extend from the SCV [26]. These SITs play an important but poorly defined role in infection. We therefore examined the presence of lysosomal-associated membrane protein 1 (Lamp1) to establish the formation of SITs as well as quantify the amount of Lamp1 recruitment to the SCV. Cells treated as above were infected with *Salmonella* and stained for Lamp1 6 hours post-infection. At this time point, SIT formation and Lamp1 recruitment to sites of *Salmonella* clusters could be clearly seen (**Figure 3.6C**). The number of invaded cells with well-formed SITs was similar for untreated and EGTA treated cells, and consistent with previously published results for HeLa cells invaded with *Salmonella* [26] (**Figure 3.6D**). Knockdown of TRPM7, however, reduced SIT formation in cells by one-third, suggesting SCVs lacking TRPM7 channels are unable to fully mature. TRPM7 knockdown also led to a significant decrease in total Lamp1 recruitment (**Figure 3.6E**). This result implies loss of TRPM7 leads to a defect in recruitment of late endosomal and lysosomal proteins to the SCV during maturation making them less likely to escape degradation. Taken together, these results suggest replication is impaired in HeLa cells lacking TRPM7 and further emphasize the importance of TRPM7 in *Salmonella* survival and infection.

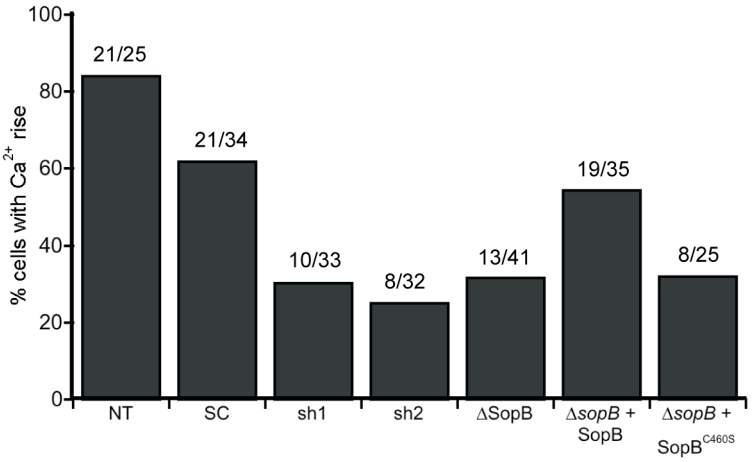

Figure 3.7 SopB phosphatase activity gates TRPM7 activation. Percent of cells having a Ca^{2+} response upon invasion by *Salmonella* after treatment with shRNA or knockout of SopB. The C462S mutant of SopB is catalytically inactive toward phosphoinositides. NT, no treatment. SC, scrambled control. sh1, shRNA1. sh2, shRNA2.

3.2.5 *Salmonella* effector SopB facilitates TRPM7 activation

Given that activation of TRPM7 Ca^{2+} channels at the initiation of invasion appears to contribute to *Salmonella* pathogenesis, we examined whether a *Salmonella* effector could contribute to this flux. The exact mechanism of TRPM7 activation is not well understood, though it has been proposed to be initiated by membrane movement [17,29], and there is evidence of its activation by phosphoinositides [30,31]. In addition to causing a drastic rearrangement of membranes upon invasion, *Salmonella* effectors have also been shown to modulate phosphoinositide concentration and distribution inside cells [3,12]. In particular, the effector SopB is a phosphoinositide phosphatase that, in conjunction with three other *Salmonella* effectors, facilitates host cell membrane ruffling and early SCV biogenesis [12-15,32]. We therefore examined the possibility that SopB modulation of phosphoinositides enables activation of TRPM7 upon invasion. To examine its connection to the Ca^{2+} influx, we created a *Salmonella* strain lacking the *sopB* gene (Δ*sopB*) and examined its effects on the Ca^{2+} response seen during early invasion. Δ*sopB* displayed a reduction in the percentage of cells exhibiting a Ca^{2+} response compared to cells invaded with wild-type *Salmonella* (32 % vs. 83 %), similar to reductions seen upon TRPM7 knockdown (**Figure 3.7**). Reconstitution of SopB in the Δ*sopB* strain increased the percent of cells responding to 54 %, though this was still below wild type levels. It is possible that reconstitution of the SopB protein was not up to wild-type levels in these *Salmonella*. To determine if the phosphatase activity of SopB was responsible for the Ca^{2+} response through TRPM7, cells were infected with *Salmonella* carrying a phosphatase-inactive SopB ($SopB^{C462S}$), which contains a mutation in its catalytic domain. This strain resulted in 32 % of cells displaying Ca^{2+} influx upon invasion, phenocopying the results for Δ*sopB*. These results implicate the

Salmonella effector SopB in TRPM7 activation, and suggest the TRPM7 Ca^{2+} channel may be regulated by phosphoinositides.

3.3 Discussion

Salmonella effectors are able to modulate a number of cellular pathways upon secretion into host cells. Previous work has shown *Salmonella* invasion causes an increase in intracellular Ca^{2+} and alteration of phosphoinositide pools, which enable invasion and membrane closure [7-10]. In this study, we further characterized the nature and effect of this relationship between invasion and Ca^{2+} and demonstrated an ability of the *Salmonella* effector SopB to initiate Ca^{2+} influx through TRPM7 channels in a manner dependent on its phosphatase activity. This influx positively regulates efficiency of invasion, allowing more bacteria to invade each cell, while bacterial replication remains unaffected. However, *Salmonella* replication and SCV maturation are dependent on TRPM7 channel expression in cells. This work further enhances current understandings of effector modulation of host cell signaling pathways.

A rise in intracellular Ca^{2+} during bacterial infection of a host cell has been detected for a number of pathogens in addition to *Salmonella*, including *Shigella*[33] and enteropathogenic *E. coli* (EPEC)[34,35]. In all cases, the increase in cytosolic Ca^{2+} has been found to be dependent on the TTSS and required for entry into the host, similar to the results for *Salmonella* seen herein, though different pathogens may use different mechanisms to elevate intracellular Ca^{2+}. By examining Ca^{2+} transients at the single cell level, we found that in addition to a general rise in intracellular Ca^{2+}, there is also a localized Ca^{2+} response occurring at the site of *Salmonella* invasion. Given the numerous Ca^{2+} dependent pathways in a cell, this localized Ca^{2+} influx could activate any of a number of downstream signaling systems. Previous studies have suggested the

bacteria-induced Ca^{2+} rise is necessary not only for efficient invasion, but also evading degradation[36] and enabling actin reorganization induced upon bacteria and host cell interaction[37]. Our observations on the extensions of ruffles and increased uptake of extracellular fluid in the absence of Ca^{2+} fits with a model in which Ca^{2+} influx regulates actin in membrane ruffling, ensuring its timely and efficient closure upon bacterial uptake. In addition, we suspect that without proper membrane closure, SCVs are more likely to fuse with lysosomes, aligning with previous observations linking the intracellular Ca^{2+} rise with increased invasion efficiency and formation of the macropinosome [10]. We therefore suspect the Ca^{2+} influx observed during early stages of invasion (< 1 hour) is essential in setting up the early SCV to ensure its integrity for further maturation and replication of *Salmonella*.

Despite a number of examples documenting an increase in cytosolic Ca^{2+} upon invasion by *Salmonella*, the molecular mechanism for this rise has remained uncharacterized. In this work, we have found the localized Ca^{2+} influx occurs through TRPM7 channels in the plasma membrane, and is facilitated in part by the phosphatase activity of the *Salmonella* effector SopB. The role of SopB in *Salmonella* invasion of cells is multifaceted, contributing to membrane ruffling, early SCV formation, and even SCV maturation [3,12-15,32], as it is not degraded for some time after its initial secretion into cells[38]. SopB has an indirect effect on invasion, as it modulates the concentrations and distributions of phosphoinositide pools, which alters availability of signaling second messengers in the cell[3,12]. This is intriguing, as it implicates phosphoinositides in TRPM7 gating. TRPM7 has been suggested to be activated by membrane stretch and swelling, as well as by phosphoinositides, though the exact mechanism remains controversial[17,29,30,39]. We therefore speculate that phosphoinositide products of SopB phosphatase activity regulate Ca^{2+} influx through TRPM7, which may contribute to membrane sealing and SCV biogenesis. In fact,

this fits with previous reports on the contribution of the phosphatase activity of SopB in SCV formation and maturation[3,14,15]. As knockout of SopB did not completely abrogate the Ca^{2+} response, it is possible that multiple mechanisms or effectors contribute to the Ca^{2+} influx, and this remains to be investigated. However, the implication that SopB is able to gate TRPM7 through its phosphatase activity adds further support to TRPM7 gating by phosphoinositides, enhancing understandings about this channel itself.

In addition to enabling the Ca^{2+} influx during invasion, TRPM7 was also found to be essential for maintaining replication of *Salmonella* in the host. Upon maturation of the SCV, a low concentration of Mg^{2+} is maintained within the environment of the vacuole, allowing induction of SPI-2 effectors necessary for replication [23,25,28]. These effectors set up the SCV and thus the intracellular niche of *Salmonella*, enabling recruitment of late endosomal and early lysosomal proteins to evade degradation, formation of SITs, and replication of bacteria [5,6,26]. As TRPM7 is proposed to be a Mg^{2+} transporter as well as a Ca^{2+} channel [19,40], we speculate that formation of the macropinosome results in inclusion of TRPM7 channels, which may then facilitate Mg^{2+} transport in the SCV. This idea is supported by the observation that knockdown of TRPM7 reduced SPI-2 induction, Lamp1 recruitment to the SCV, and *Salmonella* replication. Without TRPM7, the SCV may lack the optimal balance of Mg^{2+}, impairing the ability of SPI-2 effector transcription and resulting in the decrease in replication, recruitment of Lamp1, and SIT formation. Thus, TRPM7 may participate both as the molecular mechanism of Ca^{2+} influx and as a facilitator of *Salmonella* infection of cells by setting up the intracellular niche necessary for replication. Future studies on Mg^{2+} concentrations within the SCV and their dependence on TRPM7 would be essential in establishing this relationship.

In conclusion, we show *Salmonella* regulate invasion efficiency by gating TRPM7 Ca^{2+} transport. In addition, the TRPM7 channel enables SCV maturation in a manner that could be dependent on its potential Mg^{2+} gating capabilities. Our proposed function of Ca^{2+} and TRPM7 in *Salmonella* invasion and replication is outlined in **Figure 3.8**. The findings in this study characterize the connection between Ca^{2+} and *Salmonella* invasion and give a novel function to SopB as a regulator of TRPM7, supporting TRPM7 gating through phosphoinositides.

3.4 Acknowledgements

We would like to thank the following sources for financial support: University of Colorado Signaling and Cell Cycle Regulation Training Grant (NIH T32 GM08759) to J. E. M., NIH GM084027 to A. E. P., and the University of Colorado.

3.5 Experimental Procedures

Cell culture and transfection. HeLa cells were cultured in DMEM supplemented with 10% (v/v) FBS and 1% (v/v) penicillin and streptomycin and grown at 37 °C in 5% CO_2. For transfections, cells were plated at 60-80% confluency in the appropriate tissue culture dishes one day prior to transfection. After 24 h, the appropriate DNA was transfected into cells using TransIT (Mirus) and manufacturer recommended protocols. All assays and microscopy were performed 72 h post-transfection.

Cloning and constructs. For TRPM7 knockdown, short-hairpin RNAs (shRNA) were designed based on previously published siRNA sequences [17]. The shRNA1 and shRNA2 primer sets were designed with BamHI and XhoI overhangs (IDTDNA) and annealed together by heating a 1:1 ratio of the primers at 95 °C for 5 minutes followed by cooling 1 °C per minute to

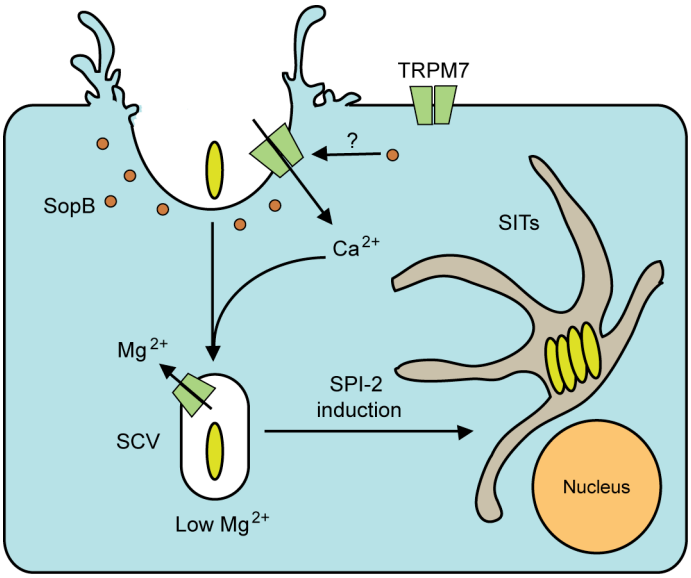

Figure 3.8 Schematic of TRPM7 activation by SopB in invasion. Upon infection of a host cell, the *Salmonella* effector SopB activates membrane ruffling and TRPM7, causing an influx of Ca^{2+} into the cell through this channel. *Salmonella* are then engulfed through macropinocytosis and TRPM7 channels on the developing SCV help maintain the required environment for replication and survival of bacteria.

25 °C. Resulting shRNA peptides were ligated into an FG12 vector (provided by Dr. Xuedong Liu, University of Colorado-Boulder) digested with BamHI and XhoI. This vector contains a GFP selection marker to enable identification of transfected cells. Reconstitution of TRPM7 in cells treated with the shRNA, was accomplished with a C-terminally modified TRPM7 insensitive to shRNA2. Mouse TRPM7 was amplified and ligated into a pRex-IRES-mCherry_nuc vector (modified from pRex_IRES_GFP1.1 from Dr. Xuedong Liu, University of Colorado-Boulder) between BamHI and NotI restriction sites. This construct encodes an internal ribosomal entry site between the TRPM7 and nuclear-localized mCherry gene, enabling the selection of TRPM7-expressing cells on the basis of nuclear fluorescence.

Knockdown of TrpM7 using shRNA. HeLa cells were transfected with empty FG12-GFP vector, vector containing shRNA complementary to the TRPM7 ion channel allele (shRNA1 and shRNA2), or scrambled control shRNA 72 h prior to experimentation to ensure maximal knockdown of the TRPM7 ion channel. For all studies, only GFP positive cells were examined. Confirmation of protein and RNA knockdown was performed using Western blotting and RT-PCR, respectively.

Western blotting and RT-PCR. HeLa cells were plated on a 10-cm dish and transfected as described 72 h prior to performing Western blotting or RT-PCR. Cells were sorted on a fluorescence activated cell sorter in order to enrich the GFP positive population. For Western blotting, sorted cells were lysed in STEN buffer (50mM Tris-HCl, pH 7.6, 150mM NaCl, 2mM EDTA, 1% TritonX-100, 0.2% NP-40, and protease inhibitor cocktail from Roche) for 20 minutes. Protein concentration was measured using the BCA Protein Assay Kit (Pierce) and 5 mg protein was loaded onto a 4 – 20% Tris-HCl gradient gel (Pierce). Proteins were transferred onto PVDF membranes and probed using the primary antibodies anti-TRPM7 (Novus

Biologicals) and anti-β-actin (Sigma). Detection of proteins was accomplished using Rabbit anti-Goat or Rabbit anti-Mouse (Zymed) HRP-conjugated secondary antibody, respectively.

For RT-PCR, total RNA was extracted from cells using an RNeasy Mini Kit (Qiagen) and manufacturer recommended protocols. Reverse transcription was then performed using the Omniscript Reverse Transcription Kit (Qiagen), with a random 6-mer primer, and the reaction was run for 1 h at 37 °C. A total of 5 μl of the RT reaction was used to PCR amplify a ~500 bp fragment of TRPM7 and GADPH C-terminal ends.

Instrumentation for fluorescence microscope. For imaging experiments, cells were washed and placed in Hank's Balanced Salt Solution with HEPES (20mM HEPES, 1X HBSS (Gibco), and 2g/L D-glucose, pH 7.2) or Ca^{2+}-free HHBSS (20mM HEPES, 1X HBSS without Ca^{2+}, Mg^{2+}, or sodium bicarbonate, 2g/L D-glucose, 490μM $MgCl_2$, 450μM $MgSO_4$, pH 7.2). Imaging experiments were conducted at room temperature (25 ºC). Fluorescence imaging was performed on an Axiovert 200M wide-field microscope (Zeiss) equipped with a Lambda 10-3 filter changer (Sutter Instruments) and Cascade 512B camera (Photometrics). Images were acquired using METAFLUOR software (Universal Imaging). Experiments were performed using a 1.3 NA 40X objective (Zeiss) using either 1X or 1.6X optovar. The filter combinations used were as follows: Fura-2: 340/26 (excitation), 380/10 (excitation), 535/40 (emission), 455 (dichroic); Cascade Blue: 390/22 (excitation), 470/24 (emission), 455 (dichroic); AlexaFluor 350: 340/26 (excitation), 470/24 (emission), 455 (dichroic); GFP: 480/20 (excitation), 510/20 (emission), 495 (dichroic); mCherry: 577/20 (excitation), 630/60 (emission), 595 (dichroic).

Salmonella strains. Salmonella Typhimurium strain SL1344 carrying the previously described constitutive mCherry red fluorescent protein vector (pAmCh) was used for most infection experiments [41]. *Salmonella* strains carrying a null mutation in the TTSS effector SopB

(ΔSopB) were created using recombination exchanges with the kanamycin resistance gene as previously described [42]. Gene deletions and insertions were confirmed by PCR using flanking gene specific primers. SopB null *Salmonella* reconstituted with the C462S mutation were obtained from Dr. John Brumell [43].

Calcium imaging. Cells were plated on 3.5-cm glass bottom dishes and transfected with 1 μg shRNA or empty vector DNA as described. In order to examine Ca^{2+}, cells were stained with 5μM Fura-2-AM and 3μM Pluronic® F-127 (Invitrogen) for 45 minutes at room temperature. After 10 minute incubation in 1 mL HHBSS to cleave the AM-ester, cells were placed in a fresh 1 mL aliquot of HHBSS for imaging. The SL1344 mCherry strain was grown under SPI-1 invasion inducing conditions and used to infect HeLa cells at a multiplicity of infection (MOI) of 50. Images were acquired every 15 s. Ca^{2+} responses were measured as an increase in the Fura-2 ratio (340/380) above resting levels after background subtraction.

Invasion and Replication Assays. HeLa cells were seeded into 12-well plates containing glass coverslips. Cells were transfected with 500 ng/well DNA as described above. HeLa cells transfected with empty vector were either treated with EGTA (2 mM) in Ca^{2+}-free HHBSS or regular HHBSS. Cells were infected at MOI = 50 as described. Infections were allowed to proceed for 15 minutes at 37 °C with 5% CO_2 prior to removal of extracellular bacteria. Remaining extracellular bacteria were treated with 100 μg × mL^{-1} gentamycin (Sigma) and cells were incubated for an additional 45 minutes. Infected HeLa cells were either fixed with 3.7% formaldehyde at 1 hour post-infection or aspirated and overlaid with 10 μg × mL^{-1} gentamycin and incubated at 37 °C with 5% CO_2 for an additional 5 hours (6 hours post-infection time point) prior to fixation. Coverslips from each treatment were then mounted for microscopic analysis. Only those HeLa cells expressing GFP were scored for infection and replication. The red

fluorescent protein marker mCherry was used to score intracellular bacteria. For invasion assays, individual bacteria were counted in each cell and multiple invasions were assigned based on location of bacteria relative to the nucleus. Only bacteria on opposite sides of the nucleus were counted as being two separate invasions. All treatments (e.g. shRNA or EGTA) were performed in triplicate for both time points (1 and 6 hours post-infection).

Dextran internalization assay. Cells plated onto 3.5cm imaging dishes were transfected as above and infected with an MOI = 50 as described. Infections proceeded at 37 °C for 25 minutes in the presence of Cascade Blue dextran (Invitrogen) before washing *Salmonella* out. Images of invaded cells were acquired for each condition and all treatments were done in triplicate. Regions of dextran taken up into cells were measured for average fluorescence intensity using ImageJ (NIH).

FM4-64 Membrane assay. Cells plated on 3.5 cm dishes were stained with FM4-64 for 1 minute before treatment with *Salmonella* at an MOI = 50 as above, in HHBSS or HHBSS supplemented with 2 mM EGTA. Cells were imaged for ~1 hour at a 15 second time interval. Length of ruffles 37 minutes post invasion were analyzed at their widest point using ImageJ.

Salmonella Pathogenicity Island-2 (SPI-2) Reporter Assay. The SPI-2 reporter plasmid was generated by cloning the promoter of the SPI-2 regulated gene *sseA* (P_{sseA}: 450-bp fragment SPI-2 promoter) [44] into the HindIII and XhoI sites of vector pACYC177. The fluorescent reporter gene *mKate2* [45] was cloned downstream of the SPI-2 regulated promoter (P_{sseA}) using the putative ribosomal binding site from the *sseA* gene and XhoI restriction ends. The SPI-2 reporter plasmid was then introduced into *Salmonella* Typhimurium SL1344 by electroporation and tested for induction of fluorescence under *in vitro* SPI-2 induction conditions (LPM: low phosphate/Mg^{2+} media) [46]. SL1344 bacteria carrying the SPI-2 reporter plasmid displayed no

detectable mKate2 fluorescence under *in vitro* SPI-1 (invasion) inducing conditions, an environmental stimulus known to repress expression of SPI-2 regulated genes. However, upon *in vitro* stimulation of the SPI-2 regulon (LPM media), robust fluorescence was observed in bulk and by fluorescence microscopy in SL1344 strains carrying the SPI-2 reporter plasmid. Invasion assays were performed as described above using the SL1344 SPI-2 reporter strain. Treatments (e.g. shRNA knock-down of TRPM7, etc.) were performed in triplicate. After six hours of infection, cells were fixed and processed for fluorescence microscopy analysis. Intracellular bacterial fluorescence (SPI-2 regulated mKate2) was quantified using ImageJ (NIH) by selecting regions of interest and extracting the average fluorescent intensity of each bacterium. Greater than 60 individual bacteria were quantified per replicate for each treatment (total $n \geq 180$).

Salmonella Induced Tubules and Lamp-1 Recruitment Assay. HeLa cells in 12-well plates on glass coverslips were transfected 24 h prior to infection with mCherry expressing SL1344 bacteria as described. After 6 hours of infection, HeLa cells were fixed and processed for immunofluorescence using a mouse anti-Lamp1 antibody (H4A3; Santa Cruz Biotechnology) and rabbit anti-Mouse AlexaFluor 350 secondary antibody (Invitrogen). Coverslips were mounted to glass slides and infected HeLa cells were scored for the appearance of one or more SITs. Additionally, the recruitment of Lamp1 to the SCV, a measure of SCV maturation, was quantified by measuring the average background subtracted intensity of Lamp1 (AlexaFluor 350 channel) for each SCV. All treatments were performed in triplicate and > 50 or > 100 SCVs were scored and quantified for SITs and LAMP-1 recruitment, respectively.

Statistical analysis. Statistical analysis on data was performed using Kaleidagraph 4.0 (Synergy Software). Data are represented as the mean ± SEM or ± SD, as indicated. Differences

between the means were compared using an ANOVA with Student-Newman-Keuls post-hoc test to determine statistical significance ($P < 0.05$).

3.6 References

1 Hansen-Wester, I. & Hensel, M. *Salmonella* pathogenicity islands encoding type III secretion systems. *Microbes Infect* **3**, 549-559, (2001).

2 Zhou, D., Mooseker, M. S. & Galan, J. E. Role of the S. typhimurium actin-binding protein SipA in bacterial internalization. *Science* **283**, 2092-2095, (1999).

3 Zhou, D., Chen, L. M., Hernandez, L., Shears, S. B. & Galan, J. E. A *Salmonella* inositol polyphosphatase acts in conjunction with other bacterial effectors to promote host cell actin cytoskeleton rearrangements and bacterial internalization. *Mol Microbiol* **39**, 248-259, (2001).

4 Fu, Y. & Galan, J. E. A *Salmonella* protein antagonizes Rac-1 and Cdc42 to mediate host-cell recovery after bacterial invasion. *Nature* **401**, 293-297, (1999).

5 Garcia-del Portillo, F., Zwick, M. B., Leung, K. Y. & Finlay, B. B. Intracellular replication of *Salmonella* within epithelial cells is associated with filamentous structures containing lysosomal membrane glycoproteins. *Infect Agents Dis* **2**, 227-231, (1993).

6 Steele-Mortimer, O., Meresse, S., Gorvel, J. P., Toh, B. H. & Finlay, B. B. Biogenesis of *Salmonella* typhimurium-containing vacuoles in epithelial cells involves interactions with the early endocytic pathway. *Cell Microbiol* **1**, 33-49, (1999).

7 Ruschkowski, S., Rosenshine, I. & Finlay, B. B. *Salmonella* typhimurium induces an inositol phosphate flux in infected epithelial cells. *FEMS Microbiol Lett* **74**, 121-126, (1992).

8 Pace, J. L. & Galan, J. E. Measurement of free intracellular calcium levels in epithelial cells as consequence of bacterial invasion. *Methods Enzymol* **236**, 482-490, (1994).

9 Pace, J., Hayman, M. J. & Galan, J. E. Signal transduction and invasion of epithelial cells by S. typhimurium. *Cell* **72**, 505-514, (1993).

10 Roy, D. *et al.* A process for controlling intracellular bacterial infections induced by membrane injury. *Science* **304**, 1515-1518, (2004).

11 Berridge, M. J., Bootman, M. D. & Roderick, H. L. Calcium signalling: dynamics, homeostasis and remodelling. *Nat Rev Mol Cell Biol* **4**, 517-529, (2003).

12 Terebiznik, M. R. *et al.* Elimination of host cell PtdIns(4,5)P(2) by bacterial SigD promotes membrane fission during invasion by *Salmonella*. *Nat Cell Biol* **4**, 766-773, (2002).

13 Mallo, G. V. *et al.* SopB promotes phosphatidylinositol 3-phosphate formation on *Salmonella* vacuoles by recruiting Rab5 and Vps34. *J Cell Biol* **182**, 741-752, (2008).

14 Hernandez, L. D., Hueffer, K., Wenk, M. R. & Galan, J. E. *Salmonella* modulates vesicular traffic by altering phosphoinositide metabolism. *Science* **304**, 1805-1807, (2004).

15 Bakowski, M. A. *et al.* The phosphoinositide phosphatase SopB manipulates membrane surface charge and trafficking of the *Salmonella*-containing vacuole. *Cell Host Microbe* **7**, 453-462, (2010).

16 Sukhan, A., Kubori, T., Wilson, J. & Galan, J. E. Genetic analysis of assembly of the *Salmonella* enterica serovar Typhimurium type III secretion-associated needle complex. *J Bacteriol* **183**, 1159-1167, (2001).

17 Wei, C. *et al.* Calcium flickers steer cell migration. *Nature* **457**, 901-905, (2009).

18 Nadler, M. J. *et al.* LTRPC7 is a Mg.ATP-regulated divalent cation channel required for cell viability. *Nature* **411**, 590-595, (2001).

19 Schmitz, C. *et al.* Regulation of vertebrate cellular Mg^{2+} homeostasis by TRPM7. *Cell* **114**, 191-200, (2003).

20 Nilius, B., Owsianik, G., Voets, T. & Peters, J. A. Transient receptor potential cation channels in disease. *Physiol Rev* **87**, 165-217, (2007).

21 Reddy, A., Caler, E. V. & Andrews, N. W. Plasma membrane repair is mediated by $Ca(^{2+})$-regulated exocytosis of lysosomes. *Cell* **106**, 157-169, (2001).

22 Idone, V. *et al.* Repair of injured plasma membrane by rapid Ca^{2+}-dependent endocytosis. *J Cell Biol* **180**, 905-914, (2008).

23 Groisman, E. A. The pleiotropic two-component regulatory system PhoP-PhoQ. *J Bacteriol* **183**, 1835-1842, (2001).

24 Rathman, M., Sjaastad, M. D. & Falkow, S. Acidification of phagosomes containing *Salmonella* typhimurium in murine macrophages. *Infect Immun* **64**, 2765-2773, (1996).

25 Zaharik, M. L. *et al.* The *Salmonella* enterica serovar typhimurium divalent cation transport systems MntH and SitABCD are essential for virulence in an Nramp1G169 murine typhoid model. *Infect Immun* **72**, 5522-5525, (2004).

26 Birmingham, C. L., Jiang, X., Ohlson, M. B., Miller, S. I. & Brumell, J. H. *Salmonella*-induced filament formation is a dynamic phenotype induced by rapidly replicating *Salmonella* enterica serovar typhimurium in epithelial cells. *Infect Immun* **73**, 1204-1208, (2005).

27 Drecktrah, D., Knodler, L. A., Howe, D. & Steele-Mortimer, O. *Salmonella* trafficking is defined by continuous dynamic interactions with the endolysosomal system. *Traffic* **8**, 212-225, (2007).

28 Zaharik, M. L., Vallance, B. A., Puente, J. L., Gros, P. & Finlay, B. B. Host-pathogen interactions: Host resistance factor Nramp1 up-regulates the expression of *Salmonella* pathogenicity island-2 virulence genes. *Proc Natl Acad Sci U S A* **99**, 15705-15710, (2002).

29 Numata, T., Shimizu, T. & Okada, Y. TRPM7 is a stretch- and swelling-activated cation channel involved in volume regulation in human epithelial cells. *Am J Physiol Cell Physiol* **292**, C460-467, (2007).

30 Runnels, L. W., Yue, L. & Clapham, D. E. The TRPM7 channel is inactivated by PIP(2) hydrolysis. *Nat Cell Biol* **4**, 329-336, (2002).

31 Kozak, J. A., Matsushita, M., Nairn, A. C. & Cahalan, M. D. Charge screening by internal pH and polyvalent cations as a mechanism for activation, inhibition, and rundown of TRPM7/MIC channels. *J Gen Physiol* **126**, 499-514, (2005).

32 Mason, D. *et al.* Alteration of epithelial structure and function associated with PtdIns(4,5)P2 degradation by a bacterial phosphatase. *J Gen Physiol* **129**, 267-283, (2007).

33 Tran Van Nhieu, G. *et al.* Connexin-dependent inter-cellular communication increases invasion and dissemination of Shigella in epithelial cells. *Nat Cell Biol* **5**, 720-726, (2003).

34 Dytoc, M., Fedorko, L. & Sherman, P. M. Signal transduction in human epithelial cells infected with attaching and effacing Escherichia coli in vitro. *Gastroenterology* **106**, 1150-1161, (1994).

35 Foubister, V., Rosenshine, I. & Finlay, B. B. A diarrheal pathogen, enteropathogenic Escherichia coli (EPEC), triggers a flux of inositol phosphates in infected epithelial cells. *J Exp Med* **179**, 993-998, (1994).

36 Majeed, M., Gustafsson, M., Kihlstrom, E. & Stendahl, O. Roles of Ca^{2+} and F-actin in intracellular aggregation of Chlamydia trachomatis in eucaryotic cells. *Infect Immun* **61**, 1406-1414, (1993).

37 Brown, M. D., Bry, L., Li, Z. & Sacks, D. B. Actin pedestal formation by enteropathogenic Escherichia coli is regulated by IQGAP1, calcium, and calmodulin. *J Biol Chem* **283**, 35212-35222, (2008).

38 Knodler, L. A., Winfree, S., Drecktrah, D., Ireland, R. & Steele-Mortimer, O. Ubiquitination of the bacterial inositol phosphatase, SopB, regulates its biological activity at the plasma membrane. *Cell Microbiol* **11**, 1652-1670, (2009).

39 Rohacs, T. & Nilius, B. Regulation of transient receptor potential (TRP) channels by phosphoinositides. *Pflugers Arch* **455**, 157-168, (2007).

40 Ryazanova, L. V. *et al.* TRPM7 is essential for $Mg(^{2+})$ homeostasis in mammals. *Nat Commun* **1**, 109, (2010).

41 Van Engelenburg, S. B. & Palmer, A. E. Quantification of real-time *Salmonella* effector type III secretion kinetics reveals differential secretion rates for SopE2 and SptP. *Chem Biol* **15**, 619-628, (2008).

42 Datsenko, K. A. & Wanner, B. L. One-step inactivation of chromosomal genes in Escherichia coli K-12 using PCR products. *Proc Natl Acad Sci U S A* **97**, 6640-6645, (2000).

43 Marcus, S. L., Wenk, M. R., Steele-Mortimer, O. & Finlay, B. B. A synaptojanin-homologous region of *Salmonella* typhimurium SigD is essential for inositol phosphatase activity and Akt activation. *FEBS Lett* **494**, 201-207, (2001).

44 Hansen-Wester, I., Stecher, B. & Hensel, M. Type III secretion of *Salmonella* enterica serovar Typhimurium translocated effectors and SseFG. *Infect Immun* **70**, 1403-1409, (2002).

45 Shcherbo, D. *et al.* Far-red fluorescent tags for protein imaging in living tissues. *Biochem J* **418**, 567-574, (2009).

46 Coombes, B. K., Brown, N. F., Valdez, Y., Brumell, J. H. & Finlay, B. B. Expression and secretion of *Salmonella* pathogenicity island-2 virulence genes in response to

acidification exhibit differential requirements of a functional type III secretion apparatus and SsaL. *J Biol Chem* **279**, 49804-49815, (2004).

Chapter 4

The protein *MICU1* regulates mitochondrial Ca^{2+} uptake

Fabiana Perocchi, Vishal M. Gohil, Hany S. Girgis, X. Robert Bao, Janet E. McCombs, Amy E. Palmer, and Vamsi K. Mootha

Adapted from *Nature* **467:** 291-296 (2010)

4.1 Introduction

Mitochondria play an essential role in cellular Ca^{2+} homeostasis. When cytosolic levels of Ca^{2+} reach micromolar concentrations, Ca^{2+} is taken up into the organelle, shaping the cytosolic Ca^{2+} signals and oscillations that control a diverse array of cellular processes[1,2]. Mitochondrial Ca^{2+} uptake has been well defined, and functional characterization of this uptake has established a mitochondrial "uniporter", which transports Ca^{2+} into the mitochondrial matrix, is dependent on membrane potential, and is regulated by high levels of cytosolic calcium[3,4]. Many studies to date have firmly established the physiological relevance of this uptake through the use of genetically encoded Ca^{2+} indicators (GECIs) targeted to the mitochondria[5-7].

In addition to shaping cytosolic Ca^{2+} signals, mitochondrial Ca^{2+} stimulates ATP production[8-10], while excessive Ca^{2+} uptake leads to cell death and contributes to pathogenesis[11]. Although the biophysical properties of mitochondrial Ca^{2+} uptake have been extensively characterized[12-14], the identity of the proteins involved in forming the uniporter has remained elusive, making it difficult to investigate how uptake impacts development and disease[14,15]. By identifying the molecular makeup of the uniporter, small molecules could be designed to target the specific proteins involved, enabling more rigorous studies of mitochondrial Ca^{2+} and its dysregulation in disease. The numerous studies on uniporter function have established that it must localize to the inner membrane of the mitochondria[3,4], be expressed in most mammalian tissues[16], and have homologues in both vertebrates and kinetoplastids, where classically defined mitochondrial Ca^{2+} uniporter activity is evolutionarily conserved[16-18].

An RNA interference (RNAi) screen of proteins meeting the above criteria identified mitochondrial Ca^{2+} uptake 1 (*MICU1*) as a potential candidate for regulating mitochondrial Ca^{2+}. In order to determine its impact on Ca^{2+} homeostasis and mitochondrial uptake, MICU1 was

knocked down in cells using short hairpin RNA (shRNA) and the Ca^{2+} phenotype was measured using GECIs targeted to various regions of the cell. Levels of Ca^{2+} in the mitochondria, cytosol, and ER were measured and store operated Ca^{2+} entry (SOCE) was examined to determine the full impact of MICU1 on Ca^{2+} homeostasis.

4.2 Results

4.2.1 Identification of *MICU1* by the Mootha lab at Harvard Medical School

In order to identify proteins required for Ca^{2+} uptake into the mitochondria, an RNAi screen was employed (see Methods). Candidate proteins were pulled from the proteomic inventory MitoCarta, which contains 1,098 mouse mitochondrial proteins from 14 tissues. Of these proteins, 1,013 have been mapped to the human genome[19], 18 of which localize to the mitochondrial inner membrane[20,21], are expressed in the majority of mammalian tissues, and are conserved in kinetoplastids[19]. Analysis of the narrowed down list of proteins involved targeting four to five shRNAs to 13 of the genes in HeLa cells containing mitochondria-targeted aequorin[5] (see Methods). Aequorin emits light in response to increases in Ca^{2+} and is influenced by both the $[Ca^{2+}]$ in the mitochondrial matrix as well as by cell viability. To elicit a Ca^{2+} response, cells were treated with histamine, which stimulates inositol-1,4,5- trisphosphate (IP_3)-induced Ca^{2+} release from internal stores into the cytosol that is then taken up into the mitochondria. This uptake results in a Ca^{2+} peak in mitochondria ($[Ca^{2+}]_{mito}$) before slowly decreasing as it is removed from the mitochondria[22].

Plotting the luminescence of aequorin against cell viability for each shRNA in the RNAi screen identified those shRNAs that abrogated the Ca^{2+} response in mitochondria regardless of their effect on cell number. While most of the shRNAs tested had no effect on mitochondrial

Ca^{2+} transport, one showed a dramatic decrease in Ca^{2+} uptake while having little effect on cell viability (**Figure 4.1A**). This shRNA, dubbed sh1-*MICU1*, targeted the poorly characterized gene *CBARA1*, now referred to as mitochondrial Ca^{2+} uptake-1 (*MICU1*), indicating the importance of this gene in Ca^{2+} uptake. In order to exclude off-target effects of sh1-*MICU1* on the observed phenotype, sh1-insensitive MICU1 was reconstituted into cells, and uptake into the mitochondria was restored (**Figure 4.1B**). These data suggest silencing of *MICU1* contributes to the attenuation of Ca^{2+} uptake into the mitochondria, stressing an important role for MICU1 in the mitochondrial Ca^{2+} transport machinery.

4.2.2 Effect of *MICU1* on Ca^{2+} homeostasis

In order to determine how knockdown of *MICU1* affected mitochondrial Ca^{2+} homeostasis, we transfected a mitochondria-targeted fluorescence resonance energy transfer (FRET)-based reporter (4mtD3cpv) into control cells (pLKO.1) and cells stably expressing sh1-*MICU1*[7,23]. Resting levels of Ca^{2+} in mitochondria were compared, as was Ca^{2+} uptake into the organelle. After establishing a baseline, cells were either treated with histamine to induce IP_3-regulated release from internal stores, or thapsigargin, which inhibits the sarco-endoplasmic reticulum Ca^{2+} ATPase (SERCA) pump to deplete internal stores and activate SOCE. Supporting its role in uniporter function, resting levels of Ca^{2+} in the mitochondria of pLKO.1 cells were higher than those of sh1-*MICU1* treated cells (**Table 4.1**), suggesting sh1-*MICU1* cells are unable to normally regulate uptake of Ca^{2+}. As expected from the RNAi screen, both histamine and thapsigargin treated control cells showed transient increases in $[Ca^{2+}]_{mito}$ while the response in sh1-*MICU1* cells was abrogated. Representative traces of the responses in these cells are shown in **Figure 4.2A** and **B**, courtesy of Dr. Amy Palmer. These data further implicate MICU1 in the regulation of mitochondrial Ca^{2+} uniporter function in HeLa cells.

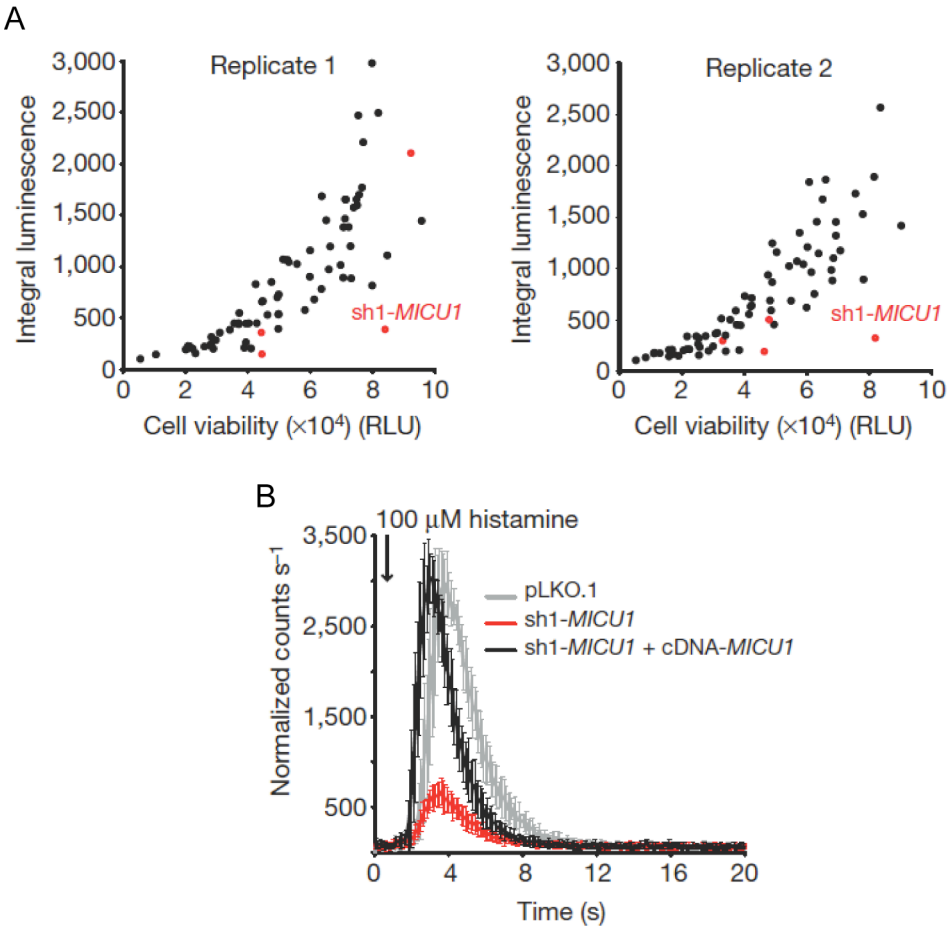

Figure 4.1 Targeted RNAi screen for mitochondrial Ca^{2+} uptake. (A) Results of the targeted RNAi screen for 13 of the 18 top candidate genes. Each point represents one RNAi hairpin expressed in HeLa cells stably expressing mitochondrial aequorin. Mitochondrial Ca^{2+} uptake, reported as the integral luminescence over 30s following 100 µM histamine stimulation, is plotted as a function of cell viability (relative luminescence units, RLU). RNAi hairpins targeting *MICU1* are shown in red. (B) cDNA rescue of the sh1-*MICU1* mitochondrial Ca^{2+} phenotype. Kinetic traces of mitochondrial Ca^{2+} uptake normalized to cell number are shown for control cells, *MICU1*-silenced cells and rescue cells (mean ± s.d., n = 3). Figure recreated from original publication.

Table 4.1. Intracellular Ca^{2+} measurements*

Ca^{2+} measurement	pLKO.1	sh1-*MICU1*	*P*-value§
Resting $[Ca^{2+}]_{mito}$	0.21 + 0.08 μM (n = 30)	0.04 + 0.01 μM (n = 25)	< 0.0001
Resting $[Ca^{2+}]_{cyto}$	0.10 + 0.06 μM (n = 38)	0.08 + 0.06 μM (n = 40)	0.10
Resting $[Ca^{2+}]_{ER}$†	0.69 + 0.12 (n = 18)	0.68 + 0.09 (n = 22)	0.99
SOCE amplitude‡	0.78 + 0.18 (n = 21)	0.76 + 0.08 (n = 21)	0.67

* Table recreated from original publication.

† Data are reported as ΔR ($R - R_{min}$), where R is the FRET ratio.

‡ Store operated calcium entry (SOCE). Data are reported as a fraction of the maximum value, $(R_{SOCE} - R_{min})/(R_{max} - R_{min})$.

§ *P*-values correspond to a two-sided Student's *t*-test with unequal variance for resting $[Ca^{2+}]_{cyto}$, resting $[Ca^{2+}]_{ER}$ and SOCE. For resting $[Ca^{2+}]_{mito}$, the *P*-value corresponds to one-way ANOVA.

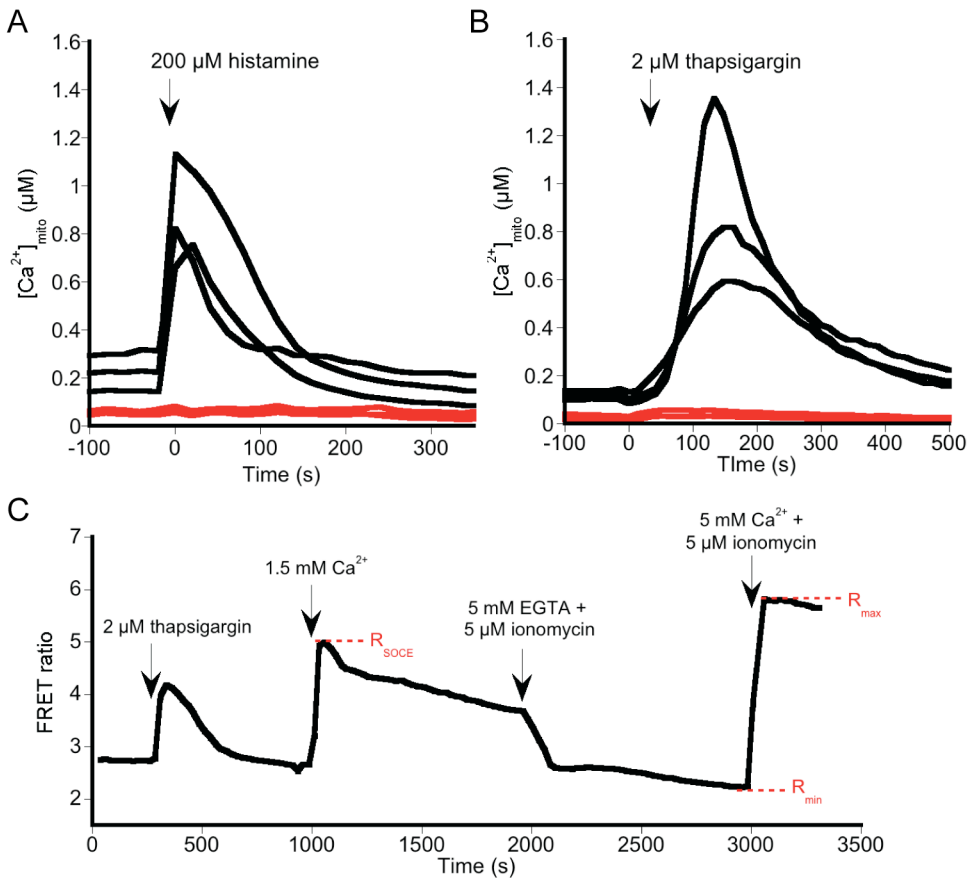

Figure 4.2 Measurements of mitochondrial Ca^{2+} uptake in single cells. (A) Mitochondrial Ca^{2+} dynamics in single HeLa cells measured by FRET following treatment with histamine. Traces are representative of $n = 20$ control and $n = 12$ sh1-*MICU1* cells. Black, control. Red, sh1-*MICU1*. (B) Similar measurements in HeLa cells after stimulation with thapsigargin. Traces are representative of $n = 15$ control and $n = 11$ sh1-*MICU1* cells. Results for *A* and *B* courtesy of Dr. Amy Palmer. (C) Example of an SOCE experiment. Cells transfected with a cytosolic Ca^{2+} FRET sensor are treated with thapsigargin in the absence of Ca^{2+} before adding excess extracellular Ca^{2+} to induce SOCE. The sensor is then calibrated to find the R_{min} and R_{max}. SOCE is calculated as $(R_{SOCE} - R_{min})/(R_{max} - R_{min})$.

Though MICU1 is necessary for Ca^{2+} uptake into mitochondria, it is possible its role in Ca^{2+} homeostasis is not limited to this organelle. To investigate this further, various aspects of Ca^{2+} homeostasis were compared for each cell type, including resting ER and cytosolic calcium concentrations and the SOCE response (**Table 4.1**). To examine ER levels, cells were transfected with the ER-targeted FRET-based reporter D1ER[24], and resting ratios (R) were measured before depleting the ER of Ca^{2+} with thapsigargin and EGTA to measure the minimum ratio (R_{min}). This level, reported as $R - R_{min}$, was no different for pLKO.1 and sh1-*MICU1* cells (0.69 ± 0.12 and 0.68 ± 0.09, respectively). For cytosolic Ca^{2+} concentration measurements, the FRET-based calcium sensor D3cpv was used. Similar to ER levels, no difference was observed between the two cell types, with Ca^{2+} concentrations of 0.10 ± 0.06 μM for pLKO.1 and 0.08 ± 0.06 μM for sh1-*MICU1* cells. Finally, SOCE was measured by treating D3cpv transfected cells with thapsigargin in Ca^{2+}-free buffer before adding back extracellular Ca^{2+} (**Figure 4.2C**). A comparison of the maximum ratio of the SOCE-induced Ca^{2+} peak ($R_{SOCE} - R_{min}$) to the maximum ratio upon treatment with excess Ca^{2+} ($R_{max} - R_{min}$) also revealed no differences between control and sh1-*MICU1* cells. Overall, MICU1 appears to have a specific role in mitochondrial Ca^{2+} uptake without affecting other aspects of cellular Ca^{2+} homeostasis.

4.2.3 Characterization of *MICU1* knockdown in additional cell lines

After establishing a role for MICU1 in HeLa cells, we next examined whether it regulates mitochondrial Ca^{2+} uptake in HEK293 cells and MCF-7 cells. Similar to the HeLa experiments, sh1-*MICU1* was stably expressed in both the above cell lines and cells were transfected with 4mtD3cpv to establish any effects on the uptake of Ca^{2+} into mitochondria upon treatment with thapsigargin. Results from these studies were inconclusive, as no or minute responses were seen in control MCF-7 and HEK293 cells (**Figure 4.3A** and **B**, respectively), despite the fact that

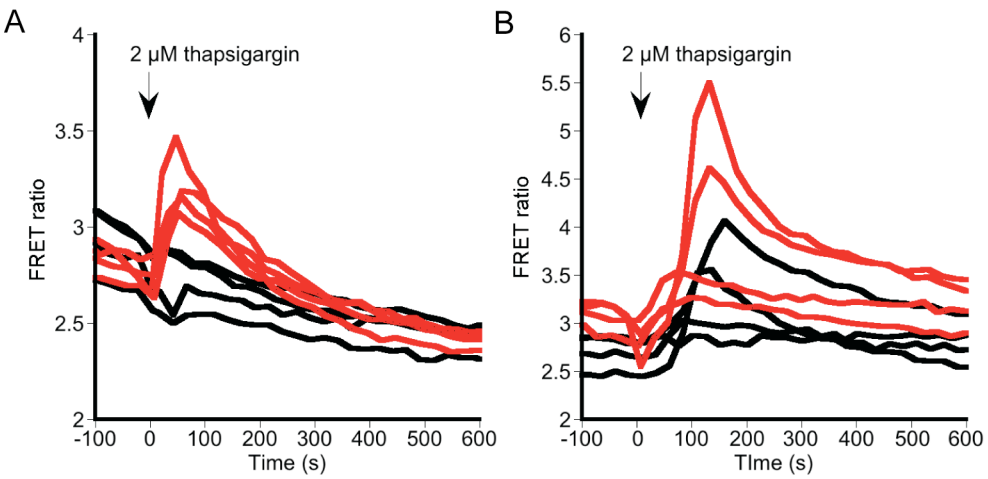

Figure 4.3 Measurements of mitochondrial Ca^{2+} uptake in MCF-7 and HEK293 cells. (A) Mitochondrial Ca^{2+} dynamics in single MCF-7 cells measured by FRET following treatment with thapsigargin. Traces are representative of $n = 20$ control and $n = 23$ sh1-*MICU1* cells. Black, control. Red, sh1-*MICU1*. (B) Similar measurements in HEK293 cells. Traces are representative of $n = 11$ control and $n = 10$ sh1-*MICU1* cells. Black, control. Red, sh1-*MICU1*.

previous studies have shown that upon Ca^{2+} release from intracellular stores in both cell types there is a robust uptake of Ca^{2+} into mitochondria[25]. In contrast, sh1-*MICU1* expressing cells responded with an uptake in Ca^{2+}, contrary to the observations in HeLa cells (**Figure 4.3A,B**). It is possible that MICU1 has no regulatory function in mitochondrial Ca^{2+} for these cell types and instead, alternative mechanisms may exist to confer tissue-specific control of Ca^{2+} homeostasis[26,27]. However, *MICU1* knockdown in these cells was only 60 – 80% compared to > 90% in the HeLa cells (data not shown). Thus, without extensive knockdown of the MICU1 protein, the ability of mitochondria to take up Ca^{2+} may not be abolished. In addition, there could be multiple proteins working in concert with MICU1 to regulate mitochondrial Ca^{2+} uptake that may be able to compensate for its absence in these cells.

4.3 Discussion

The uptake of Ca^{2+} into mitochondria has been extensively characterized, with many studies examining the relevance of the Ca^{2+} uptake in cellular Ca^{2+} homeostasis[12,13]. However, none of the molecular components required for uptake have been found. Evaluating the contribution of mitochondrial Ca^{2+} uptake to intact cell physiology, growth and development has been hampered by the lack of specific and direct inhibitors[15]. This study identified MICU1 as an essential regulator of mitochondrial Ca^{2+} uptake, suggesting it plays a key role in uniporter function. Importantly, MICU1 localizes to mitochondria and knocking it down attenuates Ca^{2+} uptake. While multiple mechanisms for Ca^{2+} uptake into mitochondria may exist, this study has established a specific target for examining Ca^{2+} uptake in disease and pathogenesis.

Though it is clear MICU1 controls Ca^{2+} uptake, the mechanisms through which it does so remain unclear. One possibility is it could constitute a pore-forming channel subunit. However,

as it has only one predicted membrane-spanning domain, it is unlikely to do so as a monomer. Additionally, it may be involved in buffering Ca^{2+} in the mitochondria, with its impact on uptake being only secondary. A third option is it may act as a sensor for Ca^{2+} via two canonical EF hands located within the protein, gating the activity of a partner channel. These EF hands are essential for mitochondrial Ca^{2+} uptake as mutation of both EF hands diminishes Ca^{2+} uptake into the mitochondria upon histamine stimulation (data not shown). Regardless of the mechanism, the identification of MICU1 should facilitate the full molecular characterization of the mitochondrial Ca^{2+} uptake machinery, and pave the way for understanding and targeting mitochondrial Ca^{2+} uptake in normal physiology and disease.

4.4 Experimental Procedures

RNA interference screen. A library of shRNA lentiviral particles targeting the 13 candidate genes and negative controls were purchased from the Broad Institute's RNAi Consortium. Two independent screens were performed. Briefly, 15,000 mt-AEQ HeLa cells were seeded in a 96-well plate (PerkinElmer catalog no. 6005181). After 12 h the media was replaced with DMEM supplemented with 10% FBS and 8 μg ml^{-1} polybrene (Sigma catalog no. H9268). Infection was performed by addition of 20 μl of gene-specific shRNA lentivirus suspension to each well followed by 30 min of centrifugation at 800*g* at 37 ˚C. Cells were washed three times with regular growth media and returned to 37 ˚C at 5% CO_2. Twenty-four hours after infection, infected cells were selected in growth media supplemented with 2 μg ml^{-1} puromycin. Luminescence-based measurements of mitochondrial Ca^{2+} and cell number were performed 6 days after infection. Cell number and viability were assayed by CellTiter-Glo Luminescent Viability assay (Promega catalog no. G7571).

cDNA rescue experiments. A version of *MICU1* cDNA resistant to sh1-*MICU1* knockdown was *de novo* synthesized (Blue Heron Biotechnology) and cloned into a pENTR221 vector, ready for use in the Gateway cloning system (Invitrogen). The cDNA harbored eight synonymous mutations in the codons complementary to sh1-*MICU1*. Procedures and reagents for virus production and infection have been previously published[28]. Twenty-four hours after infection sh1-*MICU1* knockdown cells expressing sh1-*MICU*1-resistant cDNAs were selected with 2 μg ml^{-1} puromycin (Sigma P9620) and 10 μg ml^{-1} blasticidin (Invitrogen A11139).

Luminescence measurement of mitochondrial Ca^{2+}. Measurements of mitochondrial Ca^{2+} were performed upon both histamine and thapsigargin treatment as described previously[22,29]. Light emission was measured in a luminescence counter (MicroBeta^2 LumiJET Microplate Counter PerkinElmer) at 469 nm every 0.1 s.

FRET-based measurement of mitochondrial, cytosolic and ER Ca^{2+}. Cytosolic, mitochondrial and ER Ca^{2+} levels were measured using the D3cpv, 4mtD3cpv and D1ER Ca^{2+} sensors, respectively[7,24]. Briefly, cells were seeded on 3.5-cm imaging dishes, transiently transfected using TransIT (Mirus) according to manufacturer's protocol, and imaged 48 h after transfection. Imaging experiments were performed on an Axiovert 200M inverted fluorescence microscope (Zeiss) with a Cascade 512B CCD camera (Roper scientific), and equipped with CFP (430/24 excitation, 455 dichroic, 470/24 emission), YFP (495/10 excitation, 515 dichroic, 535/25 emission) and FRET (430/24 excitation, 455 dichroic, 535/25 emission) filters controlled by a Lambda 10-3 filter changer (Sutter Instruments) and analyzed using Metafluor software (Universal Imaging). Details on the microscope, sensor calibration and conversion of FRET ratios (including protocol for obtaining R_{min} and R_{max}) into Ca^{2+} concentrations have been

published[23]. Statistical significance was evaluated using either Student's t-test or two sample ANOVA.

4.5 References

1 Jouaville, L. S., Ichas, F., Holmuhamedov, E. L., Camacho, P. & Lechleiter, J. D. Synchronization of calcium waves by mitochondrial substrates in Xenopus laevis oocytes. *Nature* **377**, 438-441, (1995).

2 Kaftan, E. J., Xu, T., Abercrombie, R. F. & Hille, B. Mitochondria shape hormonally induced cytoplasmic calcium oscillations and modulate exocytosis. *J Biol Chem* **275**, 25465-25470, (2000).

3 Deluca, H. F. & Engstrom, G. W. Calcium uptake by rat kidney mitochondria. *Proc Natl Acad Sci U S A* **47**, 1744-1750, (1961).

4 Vasington, F. D. & Murphy, J. V. Ca ion uptake by rat kidney mitochondria and its dependence on respiration and phosphorylation. *J Biol Chem* **237**, 2670-2677, (1962).

5 Rizzuto, R., Simpson, A. W., Brini, M. & Pozzan, T. Rapid changes of mitochondrial Ca2+ revealed by specifically targeted recombinant aequorin. *Nature* **358**, 325-327, (1992).

6 Filippin, L., Magalhães, P. J., Di Benedetto, G., Colella, M. & Pozzan, T. Stable interactions between mitochondria and endoplasmic reticulum allow rapid accumulation of calcium in a subpopulation of mitochondria. *J Biol Chem* **278**, 39224-39234, (2003).

7 Palmer, A. E. *et al.* Ca2+ indicators based on computationally redesigned calmodulin-peptide pairs. *Chem Biol* **13**, 521-530, (2006).

8 Denton, R. M. & McCormack, J. G. The role of calcium in the regulation of mitochondrial metabolism. *Biochem Soc Trans* **8**, 266-268, (1980).

9 Hajnóczky, G., Robb-Gaspers, L. D., Seitz, M. B. & Thomas, A. P. Decoding of cytosolic calcium oscillations in the mitochondria. *Cell* **82**, 415-424, (1995).

10 Balaban, R. S. The role of Ca(2+) signaling in the coordination of mitochondrial ATP production with cardiac work. *Biochim Biophys Acta* **1787**, 1334-1341, (2009).

11 Bernardi, P. & Rasola, A. Calcium and cell death: the mitochondrial connection. *Subcell Biochem* **45**, 481-506, (2007).

12 Gunter, K. K. & Gunter, T. E. Transport of calcium by mitochondria. *J Bioenerg Biomembr* **26**, 471-485, (1994).

13 Kirichok, Y., Krapivinsky, G. & Clapham, D. E. The mitochondrial calcium uniporter is a highly selective ion channel. *Nature* **427**, 360-364, (2004).

14 Santo-Domingo, J. & Demaurex, N. Calcium uptake mechanisms of mitochondria. *Biochim Biophys Acta* **1797**, 907-912, (2010).

15 Hajnóczky, G. *et al.* Mitochondrial calcium signalling and cell death: approaches for assessing the role of mitochondrial Ca2+ uptake in apoptosis. *Cell Calcium* **40**, 553-560, (2006).

16 Carafoli, E. & Lehninger, A. L. A survey of the interaction of calcium ions with mitochondria from different tissues and species. *Biochem J* **122**, 681-690, (1971).

17 Docampo, R. & Vercesi, A. E. Ca2+ transport by coupled Trypanosoma cruzi mitochondria in situ. *J Biol Chem* **264**, 108-111, (1989).

18 Vercesi, A. E. & Docampo, R. Ca2+ transport by digitonin-permeabilized Leishmania donovani. Effects of Ca2+, pentamidine and WR-6026 on mitochondrial membrane potential in situ. *Biochem J* **284 (Pt 2)**, 463-467, (1992).

19 Pagliarini, D. J. *et al.* A mitochondrial protein compendium elucidates complex I disease biology. *Cell* **134**, 112-123, (2008).

20 Da Cruz, S. *et al.* Proteomic analysis of the mouse liver mitochondrial inner membrane. *J Biol Chem* **278**, 41566-41571, (2003).

21 McDonald, T. *et al.* Expanding the subproteome of the inner mitochondria using protein separation technologies: one- and two-dimensional liquid chromatography and two-dimensional gel electrophoresis. *Mol Cell Proteomics* **5**, 2392-2411, (2006).

22 Brini, M., Pinton, P., Pozzan, T. & Rizzuto, R. Targeted recombinant aequorins: tools for monitoring [Ca2+] in the various compartments of a living cell. *Microsc Res Tech* **46**, 380-389, (1999).

23 Palmer, A. E. & Tsien, R. Y. Measuring calcium signaling using genetically targetable fluorescent indicators. *Nat Protoc* **1**, 1057-1065, (2006).

24 Palmer, A. E., Jin, C., Reed, J. C. & Tsien, R. Y. Bcl-2-mediated alterations in endoplasmic reticulum Ca2+ analyzed with an improved genetically encoded fluorescent sensor. *Proc Natl Acad Sci USA* **101**, 17404-17409, (2004).

25 Berridge, M. J., Lipp, P. & Bootman, M. D. The versatility and universality of calcium signalling. *Nat Rev Mol Cell Biol* **1**, 11-21, (2000).

26 Lawrie, A. M., Rizzuto, R., Pozzan, T. & Simpson, A. W. A role for calcium influx in the regulation of mitochondrial calcium in endothelial cells. *J Biol Chem* **271**, 10753-10759, (1996).

27 Favaron, M. & Bernardi, P. Tissue-specific modulation of the mitochondrial calcium uniporter by magnesium ions. *FEBS Lett* **183**, 260-264, (1985).

28 Moffat, J. *et al.* A lentiviral RNAi library for human and mouse genes applied to an arrayed viral high-content screen. *Cell* **124**, 1283-1298, (2006).

29 Glitsch, M. D., Bakowski, D. & Parekh, A. B. Store-operated Ca2+ entry depends on mitochondrial Ca2+ uptake. *EMBO J* **21**, 6744-6754, (2002).

Chapter 5

Conclusions and Future Directions

5.1 Conclusions

The complexity and versatility of the Ca^{2+} signaling system makes Ca^{2+} an inherently difficult second messenger to study in live cells. However, due to its dysregulation in many disorders and pathogeneses, it is vital to establish methods for examining effects of disease on Ca^{2+} homeostasis and vice versa. In the work summarized here, regulation of Ca^{2+} homeostasis was characterized through the use of a variety of Ca^{2+} indicators, including 1) an endoplasmic reticulum (ER) targeted genetically encoded Ca^{2+} indicator (GECI) that helped clarify dysregulation in organellar Ca^{2+} due to mutations in the Alzheimer's disease (AD) associated protein presenillin-1 (PS1); 2) the small molecule dye Fura-2, which illuminated modulations in Ca^{2+} homeostasis by *Salmonella* invasion; and 3) both cytosolic and mitochondrial targeted GECIs to establish ways the newly discovered mitochondrial Ca^{2+} uptake 1 (MICU1) protein in mitochondria membranes regulated Ca^{2+}. These studies exemplify the versatility of the various Ca^{2+} indicators and their usefulness for examining the multifaceted process of Ca^{2+} signaling.

A number of studies have implicated PS1 in ER Ca^{2+} homeostasis[1-3]. However, most of these studies have relied on Ca^{2+} indicators that inferred ER Ca^{2+} alterations using cytosolic sensors instead of monitoring Ca^{2+} within the organelle itself. Some attempts to directly measure ER Ca^{2+} were done using MagFura-2, which is not specifically targeted to the ER, or ER-targeted aequorin, which can misrepresent Ca^{2+} levels due to the need to deplete the ER of Ca^{2+} before it is reloaded. As previous work has implicated PS1 in regulating the sarco/endoplasmic reticulum Ca^{2+} ATPase (SERCA) pump responsible for ER Ca^{2+} uptake[3], this function of PS1 could affect reloading of ER stores when it is mutated, skewing results of the Ca^{2+} homeostasis in such cells. Our study therefore utilized the ER-targeted cameleon D1ER[4] to more directly examine the effects of seven PS1 mutations on resting ER levels without extensive perturbation

to the cellular environment. In addition, Ca^{2+} transients released through the inositol-1,4,5-trisphosphate receptor (IP_3R) were measured using Fura-2. We found that mutations in PS1 differentially affected cellular Ca^{2+} homeostasis, as only M233V and A409T decreased ER Ca^{2+} concentrations while none of the mutations exhibited an increase. These two mutants also exhibited dysregulation in IP_3R Ca^{2+} release. Overall, our results suggested PS1 is able to regulate both SERCA and IP_3R, supporting previously published data[2,3]. Its modulation of multiple proteins is likely an effect of both PS1 itself as well as its catalytic activity as an aspartyl protease[5]. In fact, inhibition of its protease activity resulted in raising the resting levels of ER Ca^{2+} for both M233V and A409T to wild-type concentrations, suggesting ER Ca^{2+} load is regulated by a substrate of PS1 and not necessarily PS1 itself. However, previous reports have shown PS1 is able to directly interact with and modulate the IP_3R[2], so its functions in altering Ca^{2+} signaling are not solely due to its substrate products. This study demonstrated a useful method for using GECIs to directly examine the effects of PS1 mutations on ER Ca^{2+} without causing measureable perturbation to cells.

Switching gears, we next investigated the role of Ca^{2+} in bacterial pathogenesis. In order to interpret rapid Ca^{2+} transients in the cytosol of cells, we used Fura-2 to investigate fluctuations in Ca^{2+} during *Salmonella* invasion. Invasion of host cells by *Salmonella* causes a definite, though poorly characterized, rise in cytosolic Ca^{2+}. Since *Salmonella* are able to hijack a number of known signaling pathways, it seems likely that the highly ubiquitous Ca^{2+} signaling system would also be affected by this pathogen. Application of Fura-2 enabled us to observe changes in Ca^{2+} in live cells during the initial phase of infection, providing real time monitoring of the effects of invasion on Ca^{2+} homeostasis. We initially found that invasion-induced membrane ruffling led to a localized increase in Ca^{2+} at sites of invasion in the membrane. This increase

was caused by influx of Ca^{2+} through the transient receptor potential melastatin 7 (TRPM7) channel and regulated by the *Salmonella* effector SopB, a phosphoinositide phosphatase. Given the role of SopB in mediating early *Salmonella* containing vacuole (SCV) biogenesis[6-8] and the importance of Ca^{2+} influx for membrane closure[9], we suspect SopB induces Ca^{2+} influx to ensure membrane sealing in order to form the SCV, a necessary step for the replication and thus pathogenesis of *Salmonella*[10-14]. Indeed, invasion efficiency was reduced in the absence of a Ca^{2+} influx, supporting the idea that formation of the early SCV was compromised. TRPM7 was also vital to maintenance of replication. Upon knockdown of the channel, *Salmonella* pathogenicity island (SPI)-2 effector transcription decreased and replication was reduced, suggesting TRPM7 facilitates maturation of the SCV and thus survival of *Salmonella* in cells. This study uncovered a previously uncharacterized pathway in the mode of *Salmonella* infection.

In addition to detecting alterations in Ca^{2+} homeostasis in disease and pathogenesis, the use of Ca^{2+} indicators is also functional in characterizing the regulation of Ca^{2+} by certain proteins or organelles in normal cells. Through the use of a mitochondrial targeted GECI, we were able to characterize the regulation of Ca^{2+} uptake into mitochondria by a newly identified protein. Despite decades of research into cellular Ca^{2+} homeostasis, Ca^{2+} regulation in mitochondria remains poorly understood. While the role of mitochondria in Ca^{2+}homeostasis has been firmly established[15,16], knowledge of the molecular mechanisms of Ca^{2+} transport is lacking. In the collaborative study discussed in Chapter 4, a mitochondrial membrane protein identified as MICU1 was shown to regulate uptake of Ca^{2+} into the organelle. By transfecting cells with the cameleon 4mtD3cpv[17], we found that knockdown of this protein prevented the majority of mitochondrial Ca^{2+} uptake upon cytosolic rises induced by either the SERCA pump inhibitor thapsigargin, or histamine, which causes release of Ca^{2+} out of the ER through the IP_3R.

In addition, MICU1 was found to specifically affect mitochondrial Ca^{2+}, as Ca^{2+} uptake through store operated Ca^{2+} channels was not affected by MICU1 knockdown. This work characterized for the first time the involvement of a specific protein in the function of the mitochondrial uniporter, and use of a specifically targeted Ca^{2+} indicator was essential in defining its function.

5.2 Future directions

5.2.1 Characterizing PS1 regulation of ER Ca^{2+}

PS1 appears to have multiple roles within a cell, including serving as a regulator of Ca^{2+}-related proteins such as SERCA[3] and IP_3R[2], as well as an aspartyl protease with a number of substrates[5]. Examination of how ER Ca^{2+} is regulated by each of these functions is essential. Previous studies have shown interaction between PS1 and the IP_3R[2] as well as SERCA[3], though the full extent of their interaction and mechanisms of regulation are not well understood. In addition, our work illustrated the catalytic activity of PS1 is able to influence levels of Ca^{2+} in the ER. Therefore, determining substrates of PS1 responsible for this dysregulation is necessary to establish a mechanism for the protein in Ca^{2+} regulation. In addition, defining how interactions between PS1 and IP_3R or SERCA are able to modulate Ca^{2+} levels and release could provide important insights into how this protein normally functions in cells. For example, finding regions of PS1 that specifically interact with other Ca^{2+} regulatory proteins may shed light onto whether PS1 is able to gate Ca^{2+} influx or efflux, or whether it can act as a switch in channel activity.

Our work on PS1 mutations in Ca^{2+} dysregulation also highlighted a dysfunction in Ca^{2+} release from the ER through the IP_3R. In diseased cells, this could lead to altered Ca^{2+} transients which would affect regulation of any of a number of downstream pathways, possibly resulting in the cellular dyshomeostasis seen in disease. Therefore, examining effects of mutant PS1 on activation of gene transcription, apoptosis, or cell morphology could lead to mechanisms by

which mutant PS1 causes AD onset. By investigating these different aspects of dysregulation, much can be learned about AD in general. Little is known about mechanism of disease onset, and thus elucidating pathways to neurodegeneration is essential to finding effective therapeutics for treatment of AD.

5.2.2 Identifying the role of TRPM7 and Ca^{2+} in *Salmonella* pathogenesis

The work in Chapter 3 illustrates the importance of TRPM7 in SCV maturation and *Salmonella* replication. Given the role of Mg^{2+} in initiating SPI-2 effector transcription[18-20] and the potential function of TRPM7 in maintaining cellular Mg^{2+} homeostasis[21], we hypothesize TRPM7 is present on the SCV after macropinocytosis, where it might be able to regulate the low Mg^{2+} concentration required for SCV maturation. Therefore, future work should focus on verification of TRPM7 in SCV membranes, as this is an essential first step in linking it to maturation of the SCV. In addition, assessment of whether TRPM7 is able to influence the Mg^{2+} concentration within the SCV should be investigated. By establishing the exact mechanisms through which TRPM7 regulates *Salmonella* survival in cells, more can be understood about the mode of *Salmonella* infection, potentially uncovering targets for therapeutics.

Our studies also found a link between the phosphatase activity of SopB and activation of TRPM7, supporting previous work implicating phosphoinositides in TRPM7 regulation[22,23]. Therefore, ascertaining the pathway through which TRPM7 is gated in this manner would be fundamental to both determining how *Salmonella* can manipulate cell signaling pathways as well as clarifying the poorly understood method of TRPM7 gating. Establishing this mechanism could provide a number of targets for further research into treating *Salmonella* infections in whole organisms.

Given our proposal of the presence of TRPM7 on the SCV during replication, and its necessity for maturation of the SCV, it would be interesting to see how its activity is regulated in the SCV. SopB is known to subsist in cells for long periods of time after secretion into cells[24]. It also facilitates early SCV biogenesis, ensuring the development of an intracellular niche for *Salmonella*[10-14]. Given its role in TRPM7 activation for Ca^{2+} gating, it is possible SopB is able to gate TRPM7 in the SCV, allowing release of Mg^{2+} from inside the SCV. Establishing the exact role of SopB, or any other effectors, 2 – 4 hours post invasion could provide new insights into how *Salmonella* are able to evade host cell degradation machinery to thrive for infection of an organism.

5.2.3 Establishing the mitochondrial Ca^{2+} transport systems

The characterization of a novel protein in regulating transport of Ca^{2+} into the mitochondria is fundamental in furthering the current understanding of mitochondrial involvement in Ca^{2+} handling and its dysregulation in disease. However, many questions persist regarding the exact molecular mechanisms governing mitochondrial Ca^{2+} uptake. While MICU1 is irrefutably essential to this process, it has only one transmembrane domain, and so likely does not form a channel on its own. Identification of additional proteins that interact with MICU1 to facilitate Ca^{2+} transport across the membrane is essential for further characterization of mitochondrial Ca^{2+} handling. In addition, the exact mechanism by which MICU1 itself regulates Ca^{2+} influx is still unknown. Two canonical EF hands present in the protein are known to be necessary for Ca^{2+} transport. However, whether these act as a buffer of mitochondrial Ca^{2+} or a sensor for channel gating remains unknown. Therefore, what aspect these EF hand regions play in uniporter function should be examined.

Through the use of available Ca^{2+} indicators, we have examined multiple facets of cellular Ca^{2+} regulation in normal cells as well as in disease and pathogenesis. This research has uncovered previously unknown functions of Ca^{2+} transients as well as provided greater understanding of Ca^{2+} regulation by various proteins. The studies highlighted here demonstrate the utility of such sensors and illustrate important insights Ca^{2+} indicators can provide when examining disease and pathogenesis.

5.3 References

1 Tu, H. *et al.* Presenilins form ER Ca^{2+} leak channels, a function disrupted by familial Alzheimer's disease-linked mutations. *Cell* **126**, 981-993, (2006).

2 Cheung, K. H. *et al.* Mechanism of Ca^{2+} disruption in Alzheimer's disease by presenilin regulation of InsP3 receptor channel gating. *Neuron* **58**, 871-883, (2008).

3 Green, K. N. *et al.* SERCA pump activity is physiologically regulated by presenilin and regulates amyloid beta production. *J Cell Biol* **181**, 1107-1116, (2008).

4 Palmer, A. E., Jin, C., Reed, J. C. & Tsien, R. Y. Bcl-2-mediated alterations in endoplasmic reticulum Ca^{2+} analyzed with an improved genetically encoded fluorescent sensor. *Proc Natl Acad Sci USA* **101**, 17404-17409, (2004).

5 Duff, K. *et al.* Increased amyloid-beta42(43) in brains of mice expressing mutant presenilin 1. *Nature* **383**, 710-713, (1996).

6 Garcia-del Portillo, F., Zwick, M. B., Leung, K. Y. & Finlay, B. B. Intracellular replication of *Salmonella* within epithelial cells is associated with filamentous structures containing lysosomal membrane glycoproteins. *Infect Agents Dis* **2**, 227-231, (1993).

7 Birmingham, C. L., Jiang, X., Ohlson, M. B., Miller, S. I. & Brumell, J. H. *Salmonella*-induced filament formation is a dynamic phenotype induced by rapidly replicating *Salmonella* enterica serovar typhimurium in epithelial cells. *Infect Immun* **73**, 1204-1208, (2005).

8 Steele-Mortimer, O., Meresse, S., Gorvel, J. P., Toh, B. H. & Finlay, B. B. Biogenesis of *Salmonella* typhimurium-containing vacuoles in epithelial cells involves interactions with the early endocytic pathway. *Cell Microbiol* **1**, 33-49, (1999).

9 Roy, D. *et al.* A process for controlling intracellular bacterial infections induced by membrane injury. *Science* **304**, 1515-1518, (2004).

10 Bakowski, M. A. *et al.* The phosphoinositide phosphatase SopB manipulates membrane surface charge and trafficking of the *Salmonella*-containing vacuole. *Cell Host Microbe* **7**, 453-462, (2010).

11 Hernandez, L. D., Hueffer, K., Wenk, M. R. & Galan, J. E. *Salmonella* modulates vesicular traffic by altering phosphoinositide metabolism. *Science* **304**, 1805-1807, (2004).

12 Mallo, G. V. *et al.* SopB promotes phosphatidylinositol 3-phosphate formation on *Salmonella* vacuoles by recruiting Rab5 and Vps34. *J Cell Biol* **182**, 741-752, (2008).

13 Mason, D. *et al.* Alteration of epithelial structure and function associated with PtdIns(4,5)P2 degradation by a bacterial phosphatase. *J Gen Physiol* **129**, 267-283, (2007).

14 Terebiznik, M. R. *et al.* Elimination of host cell PtdIns(4,5)P(2) by bacterial SigD promotes membrane fission during invasion by *Salmonella*. *Nat Cell Biol* **4**, 766-773, (2002).

15 Jouaville, L. S., Ichas, F., Holmuhamedov, E. L., Camacho, P. & Lechleiter, J. D. Synchronization of calcium waves by mitochondrial substrates in Xenopus laevis oocytes. *Nature* **377**, 438-441, (1995).

16 Kaftan, E. J., Xu, T., Abercrombie, R. F. & Hille, B. Mitochondria shape hormonally induced cytoplasmic calcium oscillations and modulate exocytosis. *J Biol Chem* **275**, 25465-25470, (2000).

17 Palmer, A. E. *et al.* Ca^{2+} indicators based on computationally redesigned calmodulin-peptide pairs. *Chem Biol* **13**, 521-530, (2006).

18 Groisman, E. A. The pleiotropic two-component regulatory system PhoP-PhoQ. *J Bacteriol* **183**, 1835-1842, (2001).

19 Zaharik, M. L. *et al.* The *Salmonella* enterica serovar typhimurium divalent cation transport systems MntH and SitABCD are essential for virulence in an Nramp1G169 murine typhoid model. *Infect Immun* **72**, 5522-5525, (2004).

20 Zaharik, M. L., Vallance, B. A., Puente, J. L., Gros, P. & Finlay, B. B. Host-pathogen interactions: Host resistance factor Nramp1 up-regulates the expression of *Salmonella* pathogenicity island-2 virulence genes. *Proc Natl Acad Sci U S A* **99**, 15705-15710, (2002).

21 Schmitz, C. *et al.* Regulation of vertebrate cellular Mg^{2+} homeostasis by TRPM7. *Cell* **114**, 191-200, (2003).

22 Runnels, L. W., Yue, L. & Clapham, D. E. The TRPM7 channel is inactivated by PIP(2) hydrolysis. *Nat Cell Biol* **4**, 329-336, (2002).

23 Kozak, J. A., Matsushita, M., Nairn, A. C. & Cahalan, M. D. Charge screening by internal pH and polyvalent cations as a mechanism for activation, inhibition, and rundown of TRPM7/MIC channels. *J Gen Physiol* **126**, 499-514, (2005).

24 Knodler, L. A., Winfree, S., Drecktrah, D., Ireland, R. & Steele-Mortimer, O. Ubiquitination of the bacterial inositol phosphatase, SopB, regulates its biological activity at the plasma membrane. *Cell Microbiol* **11**, 1652-1670, (2009).

Appendix A

Appendix to Chapter 2 on the effects of PS1 mutations on STIM2 localization and ER Ca^{2+} release

A.1 Basal STIM2 localization is altered by PS1

To further investigate the effect of PS1 on basic homeostatic mechanisms of ER Ca^{2+}, we used a probe consisting of STIM2 tagged with YFP[1]. STIM2 is a single transmembrane ER protein that detects basal ER Ca^{2+} levels. Upon small decreases in $[Ca^{2+}]_{ER}$, STIM2 translocates to the plasma membrane (PM), forming ER-PM junctions and causing an influx of extracellular Ca^{2+} through membrane channels [1,2]. **Figure A.1A** displays representative images of STIM2-YFP fluorescence in WT vs. DKO cells, respectively. Under basal conditions, the majority of DKO cells displayed ER-localized fluorescence, whereas the distribution in WT cells was more punctate, suggesting that at rest, WT cells contain some preformed ER-PM junctions. Thus, WT cells are closer to the Ca^{2+} activation threshold of STIM2 than DKO cells, consistent with the lower level of $[Ca^{2+}]_{ER}$ in WT cells discussed in Chapter 2. These results suggest STIM2 localization might be an indicator of $[Ca^{2+}]_{ER}$ levels. Indeed, for the PS1 variants tested, the percentage of cells with pre-formed ER-PM junctions directly correlates with the $[Ca^{2+}]_{ER}$ levels determined using the D1ER probe (**Figure A.1B**). M233V and A409T, which exhibited the lowest levels of Ca^{2+} in the ER under resting conditions, had the greatest percentage of pre-formed ER-PM junctions. Interestingly, DKO cells expressing the V94M mutation, which had $[Ca^{2+}]_{ER}$ levels slightly higher than WT, yielded significantly less pre-formed ER-PM junctions than WT cells, further suggesting these cells may contain higher levels of Ca^{2+} within the ER.

A.2 Release of ER Ca^{2+} into the cytosol

As discussed in Chapter 2, direct monitoring of $[Ca^{2+}]_{ER}$ revealed that mutations in PS1 differentially affect levels of Ca^{2+} within the ER and can alter the rate at which Ca^{2+} leaks out of the ER. Therefore, we monitored the release of Ca^{2+} from the ER into the cytosol using the

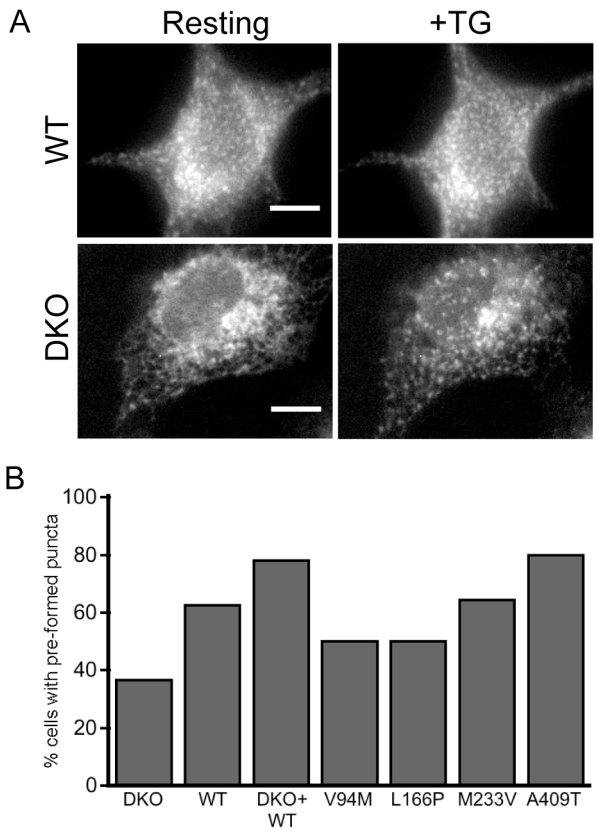

Figure A.1 Basal STIM2 localization is altered by PS1. (A) Representative fluorescence images showing STIM2-YFP localization in WT and DKO cells, before and after treatment with 4μM thapsigargin. Scale-bar is 10μm. (B) Bar graph comparing the percentage of cells with pre-formed ER-PM junctions. DKO: n = 86, 3 experiments; WT: n = 39, 2 experiments; DKO + WT: n = 62, 2 experiments; DKO + V94M: n = 71, 2 experiments; DKO + L166P: n = 26, 1 experiment; DKO + M233V: n = 25, 1 experiment; DKO + A409T: n = 29, 2 experiments. Error bars indicate SEM. Asterisk: $P < 0.01$, unpaired t-test.

small molecule dye Fura-2. Treatment with thapsigargin caused an initial rise in cytosolic Ca^{2+} as it leaks out of the ER, followed by a subsequent decrease in Ca^{2+} as homeostatic mechanisms return cytosolic levels to basal conditions by exporting Ca^{2+} out of the cell through plasma membrane pumps (**Figure A.2A**). After thapsigargin treatment, the Fura-2 probe was calibrated in order to convert fluorescence ratios to Ca^{2+} concentrations.

Under resting conditions (i.e. prior to treatment with thapsigargin) DKO cells exhibited significantly higher cytosolic Ca^{2+} levels than WT cells (**Figure A.2B**, $P < 0.0005$). This is consistent with our results in Chapter 2 showing that PS1 affected SERCA activity and a previous study which suggested that because the SERCA pump is more active in WT cells it is better able to maintain low cytosolic levels [3]. Surprisingly, DKO + WT exhibited a higher resting cytosolic level than WT cells. This is the only Ca^{2+} phenotype where the WT differed significantly from the WT + DKO and it is not clear why these two conditions yield a slight difference in resting cytosolic Ca^{2+}. All PS1 mutants were compared to DKO + WT to directly assess the impact of the mutation in the same genetic background. For the PS1 mutants, only the L166P variant of PS1 displayed a higher level of Ca^{2+} in the cytosol compared to WT cells, while all other mutations tested had no effect on resting levels of cytosolic Ca^{2+} (**Figure A.2**).

To compare Ca^{2+} release with the level of Ca^{2+} inside the ER store, we calculated the area under the thapsigargin-induced curve. Cells containing PS1 (both WT and DKO + WT) exhibited a much lower level of Ca^{2+} release than cells without PS1 (DKO cells), consistent with the reduction of Ca^{2+} within the ER in PS1 containing cells. Two PS1 mutations resulted in enhanced release compared to WT. V94M, which has higher ER Ca^{2+} levels based on the combined D1ER and STIM2 results, showed a significant increase in ER Ca^{2+} release; and

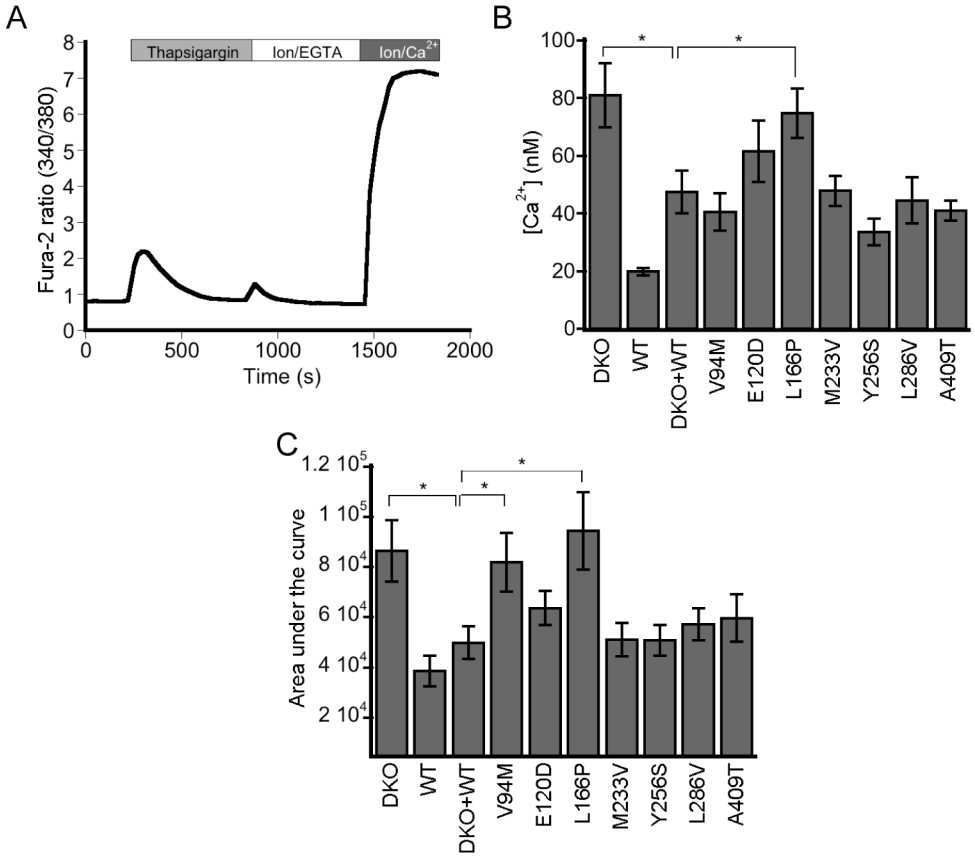

Figure A.2 Release of Ca^{2+} from the ER. (A) Representative data from time course experiment. Cells were treated with thapsigargin to release Ca^{2+} from intracellular stores before calibrating the Fura-2 probe with EGTA (R_{min}) followed by excess Ca^{2+} (R_{max}). (B) Resting cytosolic Ca^{2+} levels. Fura-2 ratios were converted to [Ca^{2+}] as described in Methods. (C) Ca^{2+} released into the cytosol upon treatment with thapsigargin. Data are represented as the area under the thapsigargin-induced curve. Error bars indicate SEM. Asterisk: $P < 0.05$, unpaired t-test. WT: n = 20; DKO, DKO + WT, L166P: n = 10; V94M: n = 14; E120D: n = 15; M233V: n = 9; Y256S: n = 12; L286V, A409T: n = 11.

L166P exhibited greater Ca^{2+} release despite showing no difference in the amount of Ca^{2+} within the ER. Interestingly, although M233V and A409T have lower ER Ca^{2+} levels at rest, they exhibit the same Ca^{2+} release as the WT, suggesting enhanced release for these mutants. These data not only highlight the discrepancy between ER Ca^{2+} load and release, implicating a role for PS1 in regulating ER Ca^{2+} release, but also indicate that some mutations in PS1 enhance Ca^{2+} leak from ER stores. We did not detect any mutations that lead to diminished release.

A.3 References

1 Brandman, O., Liou, J., Park, W. S. & Meyer, T. STIM2 is a feedback regulator that stabilizes basal cytosolic and endoplasmic reticulum Ca^{2+} levels. *Cell* 131, 1327-1339, doi:S0092-8674(07)01543-7 [pii]10.1016/j.cell.2007.11.039 (2007).

2 Liou, J. *et al.* STIM is a Ca^{2+} sensor essential for Ca^{2+}-store-depletion-triggered Ca^{2+} influx. *Curr Biol* 15, 1235-1241 (2005).

3 Green, K. N. *et al.* SERCA pump activity is physiologically regulated by presenilin and regulates amyloid beta production. *The Journal of cell biology* 181, 1107-1116 (2008).